Molecular Modelling of Stimuli Responsive Gate Effects in Flexible Metal Organic Frameworks

This thesis is submitted to

University College London

in partial fulfilment of the requirements for the Degree of

Doctor of Philosophy

by

Benjamin Tam

Supervisors: Dr Ozgur Yazaydin and Dr Michail Stamatakis

Department of Chemical Engineering

2018

Declaration

I, Benjamin Tam confirm that the work presented in this thesis is my own. Where information has been derived from other sources, I confirm that this has been indicated in the thesis.

Benjamin Tam

Abstract

Metal-Organic Frameworks (MOFs) are new remarkable nano-porous materials that exhibit exceptional thermal and chemical stabilities. They have a broad range of applications ranging from, not limited to, gas storage/separation, molecular separations, sensor, catalysis, drug delivery and removal of toxic chemicals and detoxification of warfare agents. The properties of the materials are highly dependent on the nature of the atomic interactions and structural arrangement of the crystallise material. This thesis focused on the MOFs that respond to stimuli where the structure will undergo reversible transformation in which it can lead to remarkable sorption properties that enhance the material performance.

The selected MOFs, ZIF-8 and Mg-MOF-74 were studied in this thesis. The materials were evaluated at atomistic and quantum levels. Here, we proposed a new theoretical concept regarding controlling molecular movements by implanting molecular machines in Mg-MOF-74. We designed the molecular machines to respond to external electric field and the machines are anchored within the one-dimensional pore channel of Mg-MOF-74. The pore opening and closing was simultaneously controlled by the induced electric field; thus, the flow directions of methane can be controlled at molecular level.

Moreover, this thesis moved onto the study regarding mechanical ‘gate’ opening movements in ZIF-8 which are stimulated by introduction of water molecules to the system. First, we examined with water models response in ZIF-8. Five types of different water models and six different ZIF-8 force fields were chosen and simulated with Grand Canonical Monte Carlo method. We found that the simulated adsorption isotherms are significant diverse in relation to water models. Afterward, we mimicked experimental water adsorption set up through the use of a graphene piston in molecular dynamics simulation. Here, we demonstrated through the use of water that we witnessed experimental ‘gate’ effect. However, we also found that current atomics force fields in literature were unable to replicate the adsorption isotherm at experimental conditions, resulting in the development and modifications for new force field that tune to water responses in ZIF-8.

Impact Statement

As the ever desires and growth of human populations, there have been needs to search for new materials to improve current technology. For the growth in material efficiency, understanding at atomistic level is essential. In recent years, there have been strong focuses on nano-technology mechanical functions to improve the performance of materials. These studies can be performed with very expensive and state-of-the-art equipment. However, with the ever increasing computational power, nano-materials functionality can be predicted with an excellent degree of accuracy and fraction of the expenses.

In recent decades MOFs are one of the emerging nano-technology that have been widely investigated. These hybrid inorganic/organic crystalline porous materials can be adapted and designed for a wide range of applications, and they are considered as potential materials to replace zeolites and other porous materials. In particular, these materials have the ability to make atomistic movement over induced stimuli. Thus, in this thesis, we first focused on the development of a novel concept regarding controlling the molecular movement with electric field. We implanted dipolar molecular gates within Mg-MOF-74, which can perform like a butterfly valve and control the flow direction of fluids across the MOFs. Moreover, we chose to study the 'gate' effect within MOFs, due to its saloon-door-like movement and it enhanced the mixture separation ability. ZIF-8 was found to perform such movements and have the ability to selectively separate many gas mixtures. We further proposed study regarding inducing the gate movement through introduction to water molecules as a stimulus. Therefore, from the

understanding of the underlying atomistic movement, we will assuredly extend the use of MOFs for new applications.

Acknowledgements

First of all, I would like to express my deep gratitude towards my supervisor Dr. Ozgur Yazaydin, for his continuous support and guidance throughout my PhD. I am truly grateful for all the opportunities he has offered and build me up to a self-efficient learner. Thank you so much for the opportunity to work in the group.

I also would like to give thanks to my second supervisor Dr Michail Stamatakis for the eye-opening PhD transfer viva that I received; the examination has helped me with the writing of this thesis.

I would like to give thanks to all my colleagues for their support and guidance throughout my PhD. In particular, special thanks towards my dear friends, Dr. Isil Akpinar, Aydin Ozcan and Dr. Sada Namsani for stepping beyond requirements to help me to finish this PhD and for their personal friendships have helped me through the ups and down in the years. I would also like to mention Dr. Naghmeh Saeidi Bidokthi, Kai Bin Yu and Turan Selman Erkal who were a great support in the group.

Furthermore, my sincere thanks to Tran, Evita, Elnaz, Zeynap, Dai, Teng, Din, Marietta, Abeer, Victor, Marti, Illaria, Veselina, Connor, Richard, Elliot, Tom and Charles for their help and support in my personal life. In particular to mention my best friend, Zi Wei Leong, his constant communications has been uplifting through this time, also my thanks extended to Danny Tam and Nicky Wong for their emotional support. Furthermore, I would like to mention Elena Tsolaki, for the mischiefs and adventure that we been through. Not a single regret and those memory definitely the highlights of my PhD.

Also special thanks to the UCL STaEPP department for offering the opportunity for me to teach in Hong Kong University of Science, Technology and Central University of Technology and many more opportunities in the future. In particular, I am very grateful to Naomi, Carla, Joe, Alan, Adam, Kate and Emanuela as working with them had been a pleasure.

I am very grateful for my parents and my sister, their continuous encouragement, concern and care have been a great contribution to my PhD. I thank them for their patience and support and love. Without them, I would not have finished my PhD.

I would also like to dedicate my thesis to my late cat, who sadly passed away during the final month of my PhD. He was my comfort and my love, always gave warmth whenever I needed it. He will be forever missed and always have that place in my heart. May god rest his soul.

And finally, most important of all, I would like thank the almighty God who gave me strength and relentless determination to finish my PhD.

Publications

1. **B. Tam**, O. Yazaydin, “Design of Electric Field Controlled Molecular Gates Mounted on Metal-Organic Frameworks”, Journal of Materials Chemistry A, 2017, 5, 8690 – 8696
2. M. Erkartal, U. Erklic, **B. Tam**, H. Usta, O. Yazaydin, J. T. Hupp, O. K. Farha, U. San, “From 2-methylimidazole to 1,2,3-triazole: a topological transformation of ZIF-8 and ZIF-67 by post-synthetic modification”, Chemistry Communications., 2017, 53, 2028 – 2031
3. A. Bulut, Y. Zorlu, M. Wörle, A. Çetinkaya, H. Kurt, **B. Tam**, A. Ö. Yazaydın, J. Beckmann, G. Yücesan, “Short Naphthalene Organophosphonate Linkers to Microporous Frameworks”, Chem. Select, 2017, 2, 7050 – 7053
4. S. S. Nair, N. Illyaskutty, **B. Tam**, O. Yazaydin, C. Wöll, H. Kohler, H. Gliemann, “Membrane based sieving and reduced humidity cross-response for ZIF-8 and ZnO – A combined experimental and theoretical approach”, (Manuscript in preparation)
5. **B. Tam,** O. Yazaydin, “Grand Canonical Monte Carlo simulations of various water models in Zeolitic Imidazole Framework-8” (Manuscript in preparation)
6. **B. Tam,** O. Yazaydin, “Molecular dynamic simulations of water intrusion in flexible ZIF-8” (Manuscript in preparation)

Contents

List of Figures

Abbreviation

Abbreviation	Meaning
AMBER	Assisted Model Building with Energy Refinement
BET	Brunauer–Emmett–Teller
BDC	Benzenedicarboxulate
BMI	Barrier Height Imagining
CFC MC	Continuous Fractional Component Monte Carlo
DFT	Density Functional Theory
EDTA	Ethylenediaminetetraacetic acid
GCMC	Grand Canonical Monte Carlo
LJ	Lennard Jones
NMR	Nuclear Magnetic Resonance
MC	Monte Carlo
MD	Molecular Dynamics
MIM	Mechanically Interlocked Molecules
MMM	Mix Matrix Membrane
MOF	Metal Organic Framework
MORF	Metal Organic Rotaxane Framework

PMB	Para-methoxybenzyl
PMF	Potential Mean Force
STM	Scanning Tunnelling Microscope
SPC	Soft Porous Crystal
SPC/E	Extended Simple Point Charge Model
TFA	Trifluoroacetic acid
UFF	Universal Force Field
UV	Ultraviolet
VdW	Van der Waal
ZIF	Zeolitic Imidazole Framework

<u>This page has been left blank intentionally</u>

1 Introduction

MOFs, also known as porous coordination polymers, are an emerging class of crystalline porous materials with high degree of symmetry. These are nano-porous structures made from self-assembly of organic linkers and metal ions or metal oxide cluster into high symmetry crystalline structures (Figure 1.1). The materials have high adsorption affinity for gaseous species, which is similar to natural occurring zeolite, yet MOFs have greater flexibilities as the size and shape of the pore can be tuned by the variation in organic linker and metal nodes. Thus, these porous materials can offer beyond the limitations of zeolites.(1)

These materials were known in the early 1980s, however stable crystallise structures are only formulated in the late decade of 1990s by Yaghi and colleagues.(2) Chemical and thermal robustness are the key features of MOFs that capture industrial interests, in particular high concentration of ions lead to applications in catalysis and gas storage/separation. Thus, MOFs are considered potential materials to challenge the current position of porous materials (zeolite).(3-10)

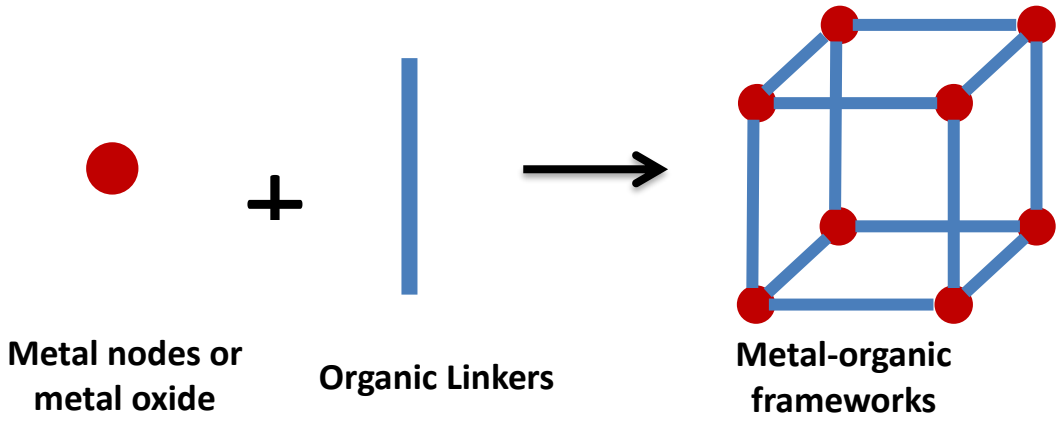

Figure 1.1 – Visual representations of metal-organic frameworks

During the last decade, from the perspective of global climate and clean energy, the research of porous materials have evidently shifted from capture and store gas molecules (H_2, CH_4, and CO_2)(3, 5, 11-13) to applications such as sensors,(14-16) drug carriers,(17-20) filters,(21-24) energy storage.(25-28) Experimentalists often require sieving through many promising organic linkers and test assorted MOFs through trial and errors. Thus, these processes are often expensive and time consuming as over 70,000 MOFs have been recorded in crystal data bank (Figure 1.2).(2, 29) Furthermore, the large entries are often unchecked due to the limited resources to thoroughly test each structure integrity, pore volume size or any other physical properties, therefore, leading to the current data susceptible to inconsistent result.(30, 31)

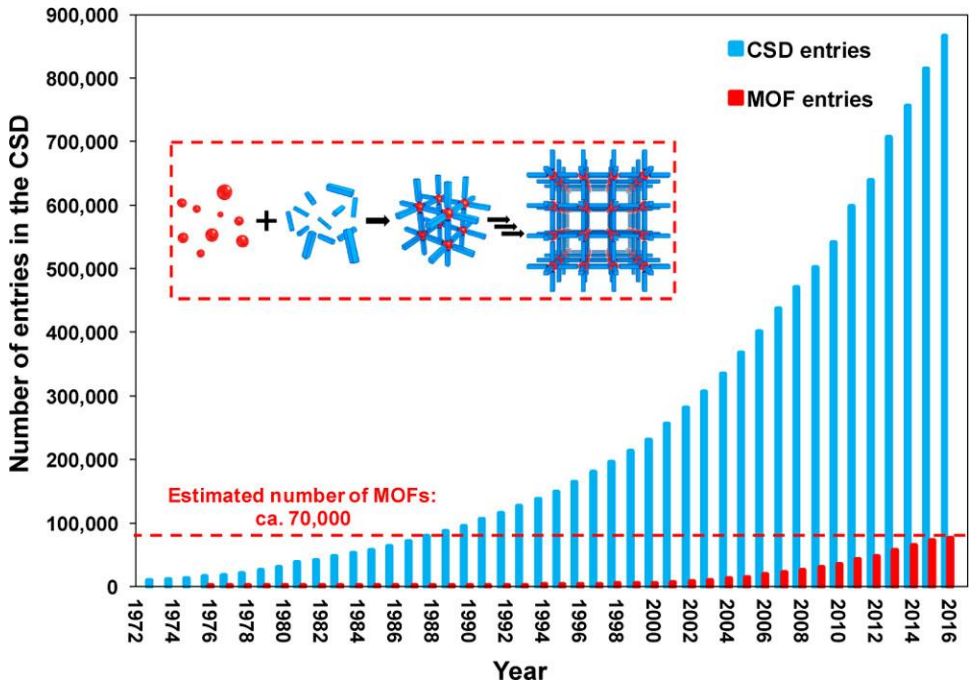

Figure 1.2 – Growth of the Cambridge Structure Database and MOF entries since 1972. The inset shows the MOF self-assembly process from building blocks: metals (red spheres) and organic ligands (blue struts). Adapted with permission from Moghadam *et al.*, 2017. Copyright (2017) American Chemical Society.

To address these issues, MOF community has turned toward computational simulations in order to give an insight of the structural chemistry. Data such as adsorption isotherm, surface area, pore volume, heat of adsorptions can easily be obtained through molecular simulations (12, 32-40) and the speed of evaluation are only limited by computational power. Therefore, many have combined molecular simulation with experimental in order to validate their respective results.(33, 34, 41, 42)

Herein, this thesis focuses on the so called “third-generation” functional MOFs where the dynamics of the flexible structure can change the functionality of the material.(43) These MOFs have non-rigid structure and undergo reversible structural transformation in response to stimuli.(35, 44-47) A prominent examples of MOFs structural transformation is the so called ‘breathing’ effect. The structures respond to external stimuli (e.g. guest molecule adsorption/desorption)(1, 44, 45) and have drastic alterations to the unit cell pore volume. This leads to the change of capacity within the MOFs. Likewise, ‘Gate’ effect is another example of structural transformation. The linker is induced by stimuli and rotated on it axis while retaining the original crystalline geometry. The rotation is somewhat comparable to “saloon-door” opening and can expose to a restricted pore space within the MOFs. The reported MOFs with this property are duly exploited for applications such as separation by size and shape, as the flexibility gives the structure a sieve-like functionality.(7, 33, 47) In both structural transformation examples, the structure will revert to the original dimension once the stimuli is removed from the system.

As strong interests in flexible MOFs research were building up from 1990s, another area of research was gaining momentum is molecular machines. In 2016, Jean-Pierre Sauvage, Sir J. Stoddart and Bernard L. Feringa were awarded Nobel Prize for their development and contributions to the molecular chemistry. Their joint award was granted based on their work in manufacture synthetic supramolecular structure; where the molecular components can control and perform a repeatable physical task under the effect of stimuli. The machines are controlled through the responses to various stimuli, such as chemical,(48-51) photon,(52-56) electric field(57-59) and used as a fuel to power the physical motion. Their idea brought forward a novel research pathway where precise molecular movement is manipulated and enhanced; in such that the chemical reactions,(49, 60) sensing,(56, 61-63) chemical transportation[59, 64, 65] and many more functionalities are controlled at molecular level.(56, 62-64, 66-69) Since the directional displacement at molecular scale is comparable to the movement of a macro machines; these supramolecular structures are given the name as “molecular machines”.

Propelled by the advancement in both synthetic MOFs and inspired by the stimuli control in molecular machines, the interest in this thesis will focus on molecular simulations study of MOFs that undergo structure transformation under the effect of stimuli. The study further promotes the understanding structure phenomena in molecular scales. Additionally, only few research groups have successfully demonstrated the possibility to combine both molecular structures and provided a new application pathway for the combine complex.(70-72) Thus, building upon the underexplore idea, stimuli responsive molecular machines with MOFs acting as a host will further conceptually explored.

1.1 Porous Adsorbent Materials

In this section, the general classifications of nano-porous materials and general industrial adsorbent materials are covered.

1.1.1 Porous Materials

Due to the large surface area and the potential of interacting with molecules, throughout the bulk material, strong interests are widely received for porous materials. In particular, industries are interested in adsorption,(3, 5, 12, 34, 73, 74) separation,(7, 34, 74, 75) ion exchange,(76-79) catalysis(80-83) and toxic removal(84-88) where porous materials are widely used.

International Union of Pure and Applied Chemistry (IUPAC) categorise porous material based on the diameter of the pore.(89) Pores with diameter in the range less than 2 nm are categorised as ‘micropores’. In between 2 nm to 50 nm pore diameter, those are known as ‘mesopores’. Whereas the pore diameter is beyond 50 nm, it is known as ‘macropore’.(89) Within the range between 1 to 100 nm, it is within the subgroup ‘nanoporous materials’. Both porous and nanoporous material materials can be either organic or inorganics by its composition and constituents. Here, I am going to give a brief introduction to the well-known porous material, zeolite, activated carbon and metal-organic-frameworks.

Zeolites are a well-known inorganic crystalline aluminosilcates porous material with interconnected pores range from 4 – 13 nm.(90) Some of these materials are naturally occurring; thus, it can be excavated from ground. However, these materials consist of uniform pore size; this brings advantage as well as drawback which dependent on the practice. The consistent pore size distribution can be used

for applications such as sieving and separating molecules by size.(91) At the same time, the separation ability is limited by the pore size distribution and only selective mixture can be separated.

Activated carbon is an organic porous structure; it is composed of many different pore sizes and known as amorphous porous materials. The material is prepared through pyrolysis of carbon-rich materials (i.e. coal, wood char). They possess high surfaces area, porosity and adsorption capability, but a major drawback is poor selectivity and the efficiency is dependent on the type of carbon.(92)

MOFs are nano-porous material developed during 1990s, it is a new class of hybrid crystalline porous material. The structure of MOFs combines organic linkers with inorganic metals or metal nodes. MOFs are well-defined structures and contain larger internal surface area.(41) The advantage of MOFs is the highly tuneable pore size and surface area by changing the metal ions and/or the organic linker. Furthermore, they also offer high selectivity in comparison to zeolite and activated carbon due to the interaction between the adsorbate and the metal ions. Further discussion of MOFs will be given in Chapter 2.

2 Literature Review

In this chapter, a general background on MOFs functionalities and potential applications. Specific focus will be on flexible porous materials, also known as "soft porous crystals", where the material will respond to physical and chemical stimuli. Furthermore, their future potential in smart material applications is explained.

2.1 Metal-Organic Frameworks (MOFs)

Metal-organic frameworks (MOFs) are a class of advanced crystalline materials with large empty cavities and strong affinities to many gaseous molecules. It is formed by self-assembly of metal ions and organic ligands through coordination bonds. On a nanoscale level, MOFs had shown the elegance and mastery in chemistry synthesis. Theoretically, plentiful MOFs materials can be synthesised by interchange organic linkers and metal ions. Through combination of various inorganic and organic components one could adjust the shape and pore size. There are judicious choice of multidentate linkers, such as polycarboxylates, phosphonates, sulfonates, amines, imidazolates, pyridyl and phenolates can be used to design MOFs.(93)

Although MOFs existed since 1980s, the first few MOFs structure collapsed once solvent was evacuated from the pores. However, in 1990s, Yaghi *et al.*(94) were first to synthesise a robust 3D crystalline structure known as MOF-5 (IRMOF-1), with surface area reaching 3631 m^2 g^{-1}.(95) It is formed by 1,4-benzenedicarboxulate (BDC) coordinated with Zn_4O octahedral metal clusters, which the unit form a cubic framework Figure 2.1 with the formula of

$Zn_4O(BDC)_3 \cdot (DMF)_8(C_6H_5Cl)$. Whereas, the nearest competitive zeolites (zeolite Y) and activated carbon surface area reach up to 1000 m^2 g^{-1} and 3500 m^2 g^{-1}, respectively.(29, 95) Just of late, the apparent theoretical limit surface areas of MOFs can reach up to 10,000 m^2 g^{-1}.(96)

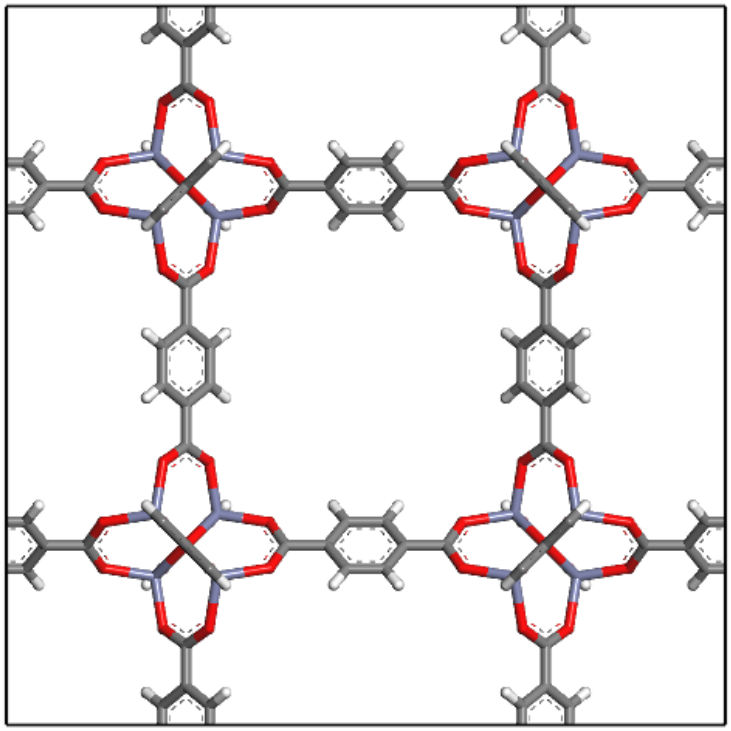

Figure 2.1 – Structure of IRMOR-1 (MOF-5). ZnO_4 tetrahedral formed a coordinate bond with benzenetricarboxylate linkers. The pore diameters ~ 1.2 nm while the pore aperture around ~0.8 nm. Carbon, hydrogen, oxygen and zinc are represented by grey, white, red and purple respectively

Another well-known group of MOFs are called Zeolitic Imidazolate Frameworks (ZIFs).(97) There are a wide range of interests in ZIFs as these materials have properties similar to zeolite; permanent porosity, uniform pore size, high stability and framework diversity. (97-99) The porous cage cavities are interconnected by small windows which permits gas separation by shape and size.(7, 100) It is formed by bivalent transition metals coordinate with organic ligands and assembles to tetrahedral units. The surface area can reach up to 2000 m^2 g^{-1} and pore volume

~0.663 cm^3 g^{-1}.(97) ZIFs exhibited similar functionalities to zeolite.(8) One comparable similarity is the imidazole linkers have a prefer orientation (M – IM – M) close to 145 degrees and similar to the connectivity orientation that can be found in zeolites (Si – O – Si units) (Figure 2.2). Thus during the self-assemble, the ZIFs can form structure that resemble to the zeolite topology.

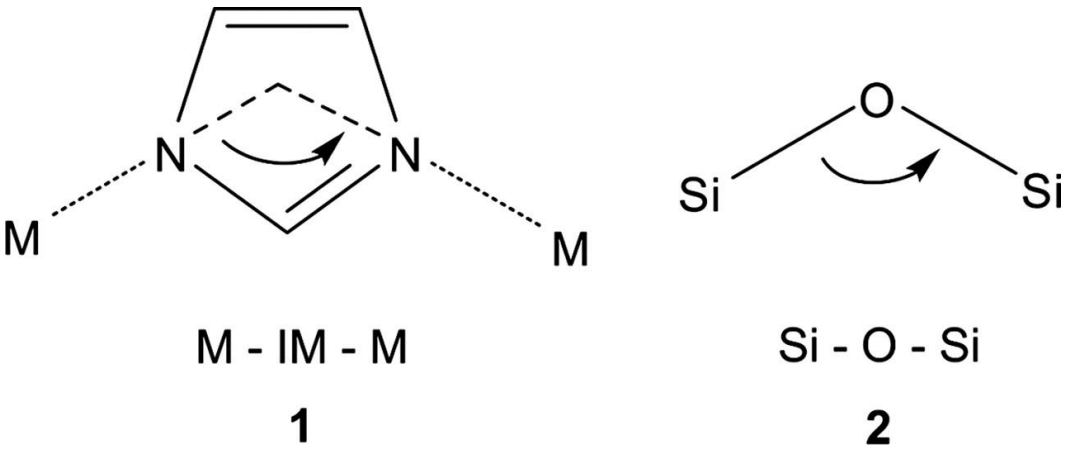

Figure 2.2 – The bridging Imidazole linkers, IM (left) with metal, M which have similar angle orientation to zeolite (right). Adapted with permission from Park *et al.*, 2006. Copyright (2006) National Academy of Science

ZIFs stand above the zeolite in terms of varieties in structure chemistry. Herein, imidazole can lose a proton and form co-ordinate bond with various metal ions (Fe(II), Cu(II), Co(II), Zn(II)… etc.), and self-assemble into structure with high crystalline and symmetry. High concentration of transition metal ions would be integrated and lined within the pores, thus desirably, offers the ability for many catalytic applications.(101) Electronic and steric properties can be manipulated according to the organic linkers' functionalisation,(4, 102) incidentally resulted in the possibility to create numerus applications for ZIFs.

Another example to show the flexibility of ZIFs is one could fine tune the porous material through modification to the imidazolate linkers. In such that the

hydrophobicity and molecular selectivity can change, leading to the design of different adsorption properties. This makes ZIFs ideal materials for gas storage and separation applications.(7, 14, 103) These materials have a strong interest to oil industries as it is useful for screening small hydrocarbon molecules, such as separating ethylene/ethane,(7) as the tradition cryogenic distillation is an energy intensive process.

2.2 Stimuli Responsive MOFs

As general descriptions and applications for MOFs were introduced in the former/previous chapter, we are interested in a subset of MOFs that can respond to physical and chemical stimuli and undergo a reversible physical structural transformation. These types of MOFs are known as flexible MOFs or Soft Porous Crystals (SPCs); they have an underlying coordinative network with cooperative structure transformability to give physical alteration and extra degree of functionality for MOFs. This mechanical property is associated with anisotropic elastic behaviour of the materials. Fundamentally, all stimuli dependent phenomena are related to structural flexibility and the change can lead to the phenomena such as increased adsorption capacity,(28, 44) entrapped and released molecules(104-107) and separation molecules by size.(2, 75, 100, 108, 109)

The conceptual and potential applications of flexible framework were recognised at very early stage in 1990s. Envisioned of the applications are greatly diverse, but currently the main investigated applications focus on gas separation or gas sensor. The visions for responsive flexible MOFs are not restricted to the adsorptive – host interactions, it can also be designed to be activated by other physical stimuli, such as thermal, light, electric field or electrical.(110-115)

With adsorptive gas separation, ideally, high selectivity and capacity are desirable for efficient separation. Flexible framework in principle can adapt and combine these two requirements, in which it can sieve through multi-component mixture as well as providing storage to one component. Here, the engineering challenge is to design a flexible MOF in a way where only one specific interaction dominates the pore opening response for a target adsorptive.

Herein, the first prominent example of the reverse structure transformation to discuss is the so-called 'breathing' MOFs, where the unit cell volumes are drastically changed upon external stimuli. Figure 2.3 is an example of MOF that can be transformed from closed pore (cp) or narrow pore (np) to large pore (lp) or open pore form, and vice versa. Here, the stimuli are the adsorbates where it intruded into the MIL-53 (Materiaux Institute Lavoisier - 53).(116) With different adsorbate stimuli, the pore can either be at open or close channel state. Ghoufi *et al.* demonstrated the 'breathing' effect in MIL-53 (Cr) can also be induced through the application of electric field.(117) This effectively transformed the structure without the needs of adsorbate.

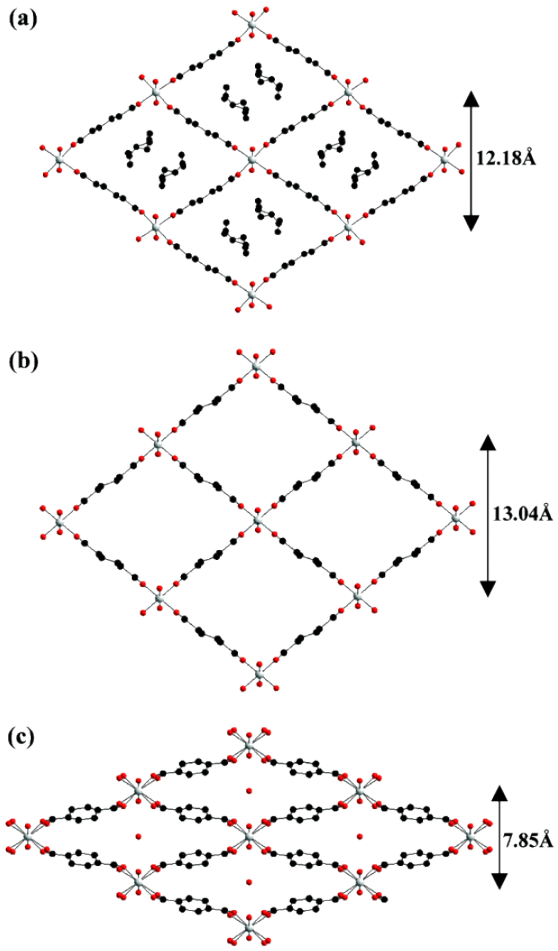

Figure 2.3 – Visual representations of breathing effect of MIL-53 a) with DMF within the pore, b) vacuum and c) with water molecules within the pore. Adapted with permission from Chen *et al.*, 2013. Copyright (2013) American Chemical Society.

Another special feature in SPCs and also a prominent example of structure distortion is 'gate' opening effect. In broad-term, gate opening occurs are due to the linkers ability to rotate upon its crystallographic position,(118) thus, exposing the empty cavity or changing the cell volume to accommodate different size of molecules into the framework. Frequently, the linkers' rotations are induced by adsorptive approaching to the framework. As chapter 2.1 gave an introduction to ZIFs, there are many reports on ZIFs can accommodated molecules bigger than the pore aperture size based on their crystallographic data.(1, 26, 119-123) Gate

mechanism can be exploited in the direction of efficient separation(108, 124) and entrapment/storage of adsorptive particles.(9, 18)

Some MOFs not only show adsorptive stimuli induced transformation, but also show stress induced reversible deformation. ZIF-8 is such an example where the high pressure forced a complete reversible phase transition.(33) Moggach *et al.* performed in situ single X-ray diffraction with increasing pressure and showed that the unit cell volume increased from 4900.5 $Å^3$ to 4999.6 $Å^3$, up to a pressure of 0.18 GPa.(125)

Remarkably, ZIF-8 also goes through phase transformation by electric field.(114) Knebel *et al*. revealed that non-destructive and reversible way to control gas transportation through a ZIF-8 membrane with the exposure of 500 V mm^{-1}. The unit cell dimension transited from a cubic to monoclinic and triclinic polymorphs. Knebel implicitly referred that with a sufficiently strong electric field, complete linker alignment could be achieved. For instance, ZIF-7 and ZIF-11 are good candidates to test further due to their well-known dipolar moment property within linkers,(25) sequentially will have greater response to the electric fields. Additionally, Knebel's experiment expanded to HKUST-1, a non-soft porous crystal, and shown electric field cannot induce structural change in rigid framework. The author demonstrated electric field can only influence MOFs that displays inherit flexibility. This accruement is huge as there are many known MOFs do behave as SPCs and polar molecules can easily be functionalised within the framework.

Photoresponsivity is another pronounced area of research for stimuli responsive MOFs. It is well understood that some organics molecules change their

conformation or structure upon interaction with light. In most cases, the MOFs are functionalised with azobenzene group, and upon the exposure of light, the conformation changes from trans to cis isomerisation, thus accompanying with the change of accessible pore volume.(112) Yanai *et al.* demonstrated the embedded azobenzene in the flexible host compound, $[Zn_2(terephthalate)_2(triethylenediamine)]_n$ (Figure 2.4) can transform the structure through the emission of 365 nm wavelength of light.(126) The azobenzene conformed from trans to cis and this accompany with phase changes in the MOF. The change exposed the cavity behind the azobenzene and allowed N_2 molecules to enter into the empty cavity. Similarly, Brown *et al.* embedded azobenzene upon the linkers of IRMOF-74-III where upon the emission of the light, the pore aperture increased from 8.3 Å to 10.3 Å.(113) Thus, by the emission of light, molecular movements can precisely control and lead to the possibility of applications such as encapsulation and molecule separation by size.

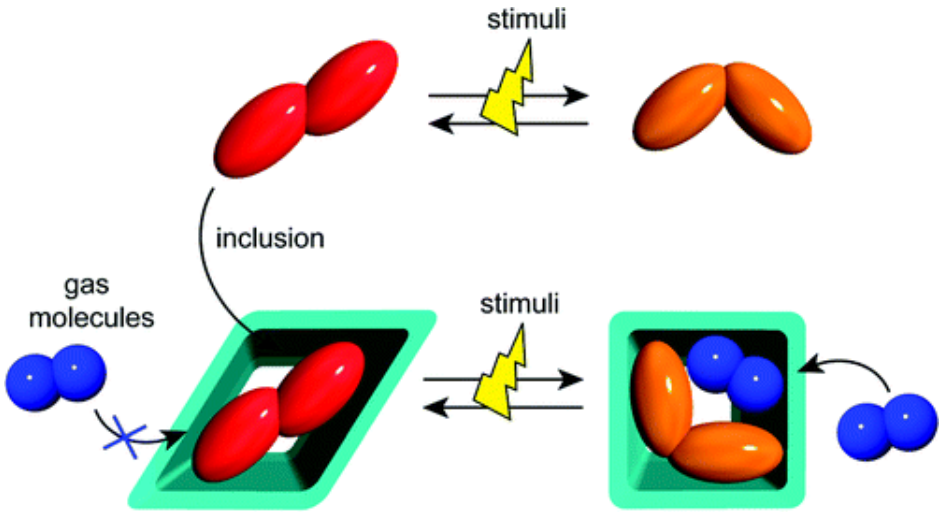

Figure 2.4 – Schematic illustration of the concept of guest-to-host structural transmission. Red and orange objects represent trans-AB and cis-AB, respectively. The conformational change in the guest molecule by external stimuli triggers a structural transformation of the crystalline host framework. Adapted with permission from Yani *et al.*, 2012. Copyright (2012) American Chemical Society.

Essentially the transformation from crystal-to-crystal or crystal-to-amorphous is a phase transition. However, only hundreds crystalline structures in the Cambridge structural database exhibit this effect or related stimuli responsive property. Even so, only few MOFs have been systematically studied for the flexibility; in which current literatures mostly concentrated on MIL-53,(28, 44, 116, 117, 127, 128) MIL-88,(129-131) paddle-wheel based pillar frameworks(132-134) and ZIF-8.(9, 105, 114, 135)

3 Thesis Aim and Outline

3.1 Scope of the Thesis

Gas storage, molecular separation and energy storage are one of the potential areas of development in MOFs community. To reduce wastages and contributions to global warming, it is utmost important to find effective materials as the demand for efficient and low-cost devices ever increasing. Thus, there is a strong push to the advancement in the development of MOFs (41, 136) as it can provide multitude of benefits, such as low cost, low energy requirements, mixture separation and storage of greenhouse gas.(5, 12, 137-141) Wastage during synthesis can be reduced if one understood interactions at atomistic level. Therefore, based on fundamental theories and characteristic of atoms one could conceptually design materials to match the purpose of the application.

In this direction, we are to conceptually combine molecular machines and host it within MOFs to create a novel material, in particular we focused on Mg-MOF-74 and a molecular turnstile design that was influenced by Horinek *et al.*(142) and Seldenthuis *et al.*(58) The molecular machines are designed to respond to electric field and we are to demonstrate the designed complex can conceptually utilised for gas storage applications.

Consequently, to gain further understanding of structural flexible and stimuli responsive MOF at atomistic scale, we dedicated our attention to ZIF – 8 and investigate the effect of water model to the structural framework. Here, we further explore the hydrophobicity of ZIF – 8 and systematically study different structural force field within the MOF community.

3.2 Objectives of the Thesis

The objectives of the thesis are given as follows:

1. Verify suitable MOFs for hosting molecular machines
2. Combine molecular machines and MOFs in order to form a new complex that is controlled through the use of electric field.
3. Demonstrate the concept of using electric field as a stimulus to control adsorption in MOFs
4. Clarify different water models effect within ZIF-8 by using Monte Carlo and CFC MC methods.
5. Replicate experimental water intrusion set up in molecular simulation, where using water as a stimulus and induce 'gate' opening in ZIF-8 through graphene piston MD simulations.
6. Comparison study of water responses in various known flexible force field for ZIF-8

3.3 Outline of the Thesis

Through the literature descriptions and the theories that were mentioned above, the outline of the thesis to deliver the following:

Chapter 4 will explain a general concept of Molecular Dynamics (MD), Monte Carlo (MC) and Density Functional Theory (DFT). MD and MC methods required an accurate force field to account for the interactions of the materials, therefore a general description of common force fields is described. DFT were used to calculate the interactions between adsorbate – adsorbent.

Chapter 5 aims to conceptually demonstrate the possibility of controlling a dipolar molecular machine within the host Mg-MOF-74 by electric field; thus leading the proposition to utilise the concept of flow direction and sorption control in molecular scale. We simulated the theoretical design through the combination of Molecular Dynamics (MD) and Density Functional Theory (DFT). It is demonstrated the control of the methane flow direction by using electric field. Finally, the designed complex was proposed to be applicable for industrial purposes such as gas storage and loading of pharmaceutical molecules.

Chapter 6 concentrates on studying the experimental phenomena that were described in chapter 2.2, where the ZIF-8 'gate' effect and water adsorption were not thoroughly investigated computationally. The investigation will first involve a comparison study with current six existential force fields and probe with water TIP4P model. Secondly, five different water models will be compared and the interaction between the adsorbate and adsorbent will be investigated. This will give an insight regarding the effect of water model and the adsorbent and provide a general reference to future computational simulation for hydrophobic MOFs. This investigation will involve Monte Carlo (MC) and Continuous Fractional Component Monte Carlo (CFC MC).

Chapter 7 focuses on the 'gate' effects in ZIF-8 and replicates experiment set up in molecular simulation. We are to simulate a non-equilibrium MD for ZIF-8 structure by utilising a graphene piston in order to provide a directional pressure. Multiple force fields description of ZIF-8 that found in literature is tested with three different water models.

Chapter 8 concludes the main results in this thesis and a future scope is given for the further advancements to the work that was presented.

Chapter 9 contains the appendix and supplementary information for the thesis.

4 Theory and Simulation methods

In the following sections, I am going to give a brief insight of the techniques that were used throughout this thesis. Firstly, an introductory theory regarding to adsorption will be given. Then due to the fact that the systems we investigated are in molecular scales, thus techniques such as Molecular Dynamics (MD), Monte Carlos (MC) and Density Functional Theory (DFT) are used to explain the phenomena that occurred in experiments. The reasoning for using each technique will become apparent in the following sub-chapters.

4.1 Adsorption

In this section, I am going to introduce the basic of adsorption theory and give a general background for the phenomena that is observed when gas is introduced into porous material. Each type of isotherm will be explained and how it is related to the structural properties of any MOFs.

4.1.1 Introduction to Adsorption Theory

Adsorption is the process for the adhesion of atoms, ions or molecules from gas or liquid onto a surface, resulting accumulation of the substance at interface between two phases, such as gas/solid or liquid/solid. Adsorption physical mechanisms are split into two categories: physisorption and chemisorption. Physisorption occurred when a solid surface held the substrates by Van der Waal (VdW) forces and electrostatic forces without modification to the molecule chemistry, whereas chemisorption forms a chemical bond with the substrates resulting change in the molecule properties.(143) In general, transition from physisorption to chemisorption occurs when heat of adsorption beyond the region of 50 kJ mol^{-1}.

Prior to the adsorption of species upon the solid interface, the species are known as ‘adsorptive’. As adsorption occurs at the interface, the species become ‘adsorbate’ and it is adsorbed onto the solid substrate known as ‘adsorbent’. Here, the key parameter for adsorbate adsorption capacity dependent on surface area, accessible pore and defects within the adsorbent.(144-146) A promising adsorbent should have large surface area that is accessible to the adsorbates. Microporous materials with a large internal surface area are regards as promising adsorbents, with the pore network allows transport of adsorbate to the interior.(147) Defects comes in various form, such as pore blockage, missing linkers, functionalisation of the surface which can trigger an increase or decrease in adsorption capacity.(144, 146, 148, 149)

4.1.2 Langmuir Isotherm Model

Langmuir Isotherm Model is the most common and simplest model for adsorption isotherm; this model can be applied to both physisorption as well as chemisorption. The model quantified the adsorbed amounts of adsorbates on an adsorbent. Here, the theory relies on four basic assumptions:

- Molecules are adsorbed at well-defined localised sites on the homogenous adsorbent surface
- Each active site can only adsorb one adsorbate
- Energetically equivalent for all sites
- No interaction between neighbouring adsorbate

Based on the assumption mentioned, Langmuir model describe a single molecular later (monolayer) adsorption on the adsorbent surface and gives a constant adsorbate capacity. Molecules are assumed in contact with the adsorbent surface in monolayer adsorption. (Figure 4.1)

Figure 4.1 – Schematic illustration of monolayer adsorption

4.1.3 Freundlich Adsorption Isotherm

Freundlich Isotherm Model is an empirical model that represents adsorption - multilayer adsorption process with non-uniform energy distribution heat of adsorption and affinities. Due to multiple layers of molecules, not all adsorbates are in contact with the adsorbent surface. The adsorption heat and affinities are due to interactions between the adsorbate, adsorbent surface and functional group on the adsorbent surface.

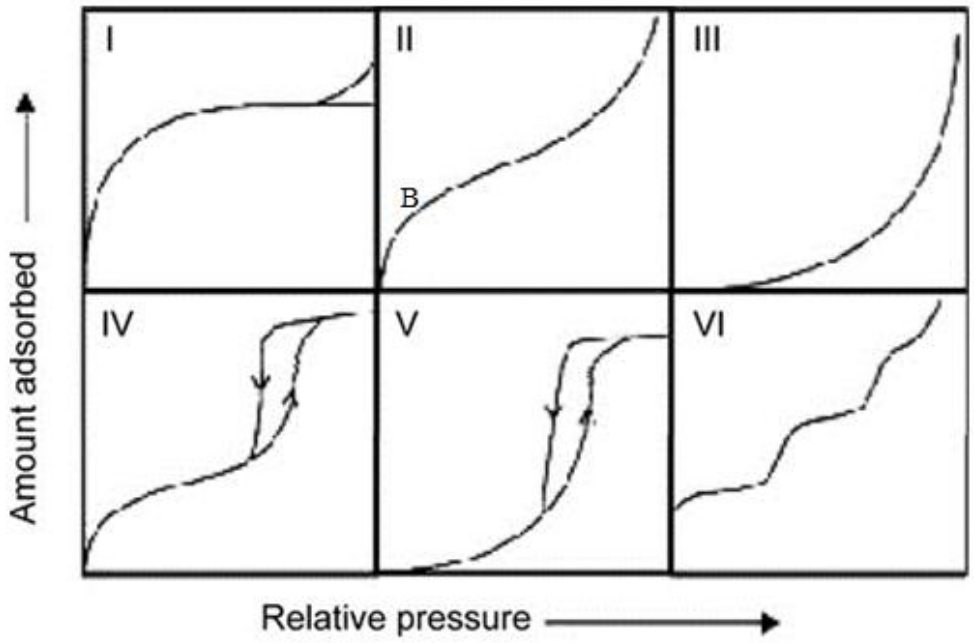

Figure 4.2 – IUPAC adsorption isotherms classification with x and y axis represents the increasing pressure and adsorbed quantity, respectively. Reprinted with permission from Q-R Fang *et al.*, Inorganic Chemistry. Copyright Taylor & Francis Group.

Information regarding the shape of the adsorption isotherm can deterministic specific adsorption phenomenon. International Union of Pure and Applied Chemistry (IUPAC) classified six types of sorption isotherm (Type I, II, III, IV, V, VI).(150) The isotherm is depicted at Figure 4.2. Type I isotherm expressed microporous and accessible micropores volume dominates the adsorbates uptake limitation at relatively high pressure. Type II isotherm are due to nonporous or macroporous unrestricted monolayers layer formations until at point B, where the point indicates the monolayer fully saturate and multiple layer adsorptions begin. Type III isotherms show the strong adsorbate-adsorbate interactions in comparison to adsorbent-adsorbate interactions. Type IV and V isotherm correspond to multilayer adsorption and followed by capillary condensation in mesoporous adsorbents. The initial part of type IV isotherm follows type II isotherm, however

the hysteresis loop attribute to the filling and emptying by capillary condensation in mesopores. Whereas type V is related to type III isotherm, in which the adsorbent-adsorbate interaction is weak but hysteresis loop is observed. Type VI isotherm represents stepwise layer by layer adsorption on a uniform surface. (Figure 4.3)

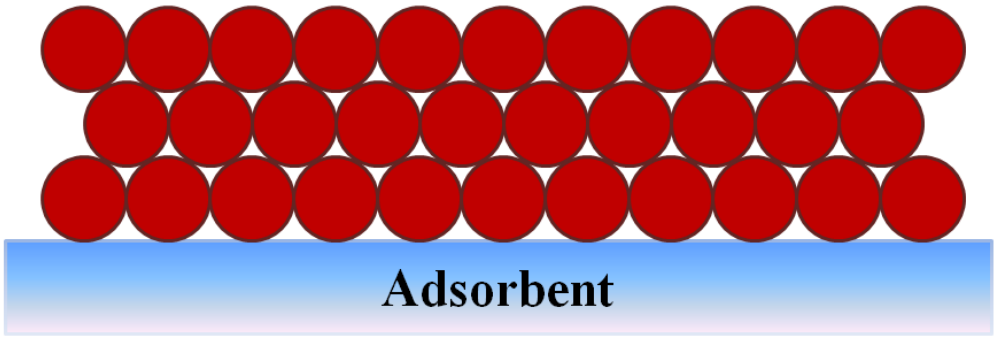

Figure 4.3 – Schematic representation of multi-layer adsorption

4.1.4 Metal Organic Frameworks Adsorption

Adsorption isotherm is an important tool for giving structure information inside the MOFs or any nano porous adsorbents. Information such as surface area and volume metric can be calculated through the data in adsorption isotherm. The relation between the adsorbate and the adsorbent can be given through the shape of the graph. Often, inert gaseous species such as nitrogen, argon are used to probe the framework.(151) For rigid porous materials, these adsorption isotherms are easily obtained through Monte Carlos (Chapter 4.2.2) simulations or obtained through experiment by the usage of Brunauer-Emmett-Teller (BET) machine. However, this thesis focused on flexible metal organic frameworks and the adsorption isotherms drastically change with structure deformation. Thus, the surface area and pore volume coincide with the transition of the structure. This transformation can

be induced by external stimuli, such as and not limited to, pressure, stress, adsorbate and any other external field.(152-155) MIL-53 is an example for exhibiting pore expansion and shrinkage caused by the present of adsorbed molecules or pressure, in particular these phase transition is known as “breathing effect”.(156) The transition caused the surface area change from ~1100 m^2 g^{-1} (narrow pore, NP) to ~1500 m^2 g^{-1}(large pore, LP). (157-159) Llewellyn et al. have shown the CH_4 and CO_2 produced different adsorption isotherm with different pore size of thee framework.(157, 160) The NP (hydrated) pore showed no adsorption for CH_4 whereas LP (anhydrated) has adverse effect (Figure 4.5). Bousquet et al. studied the transition of MIL-53 from LP to NP through molecular simulation (Figure 4.4).(161) The authors have shown the pore remained at LP metastable structure until 0.1 bar, then the structure exchange to NP until ~25 bar. Beyond 25 bar the structure reverted back from NP to LP due to pore being forcefully filled with the gaseous species. This breathing effect is not limited to MIL-53 and also be found in MOFs such as MIL-47 and MIL-101.(162-164)

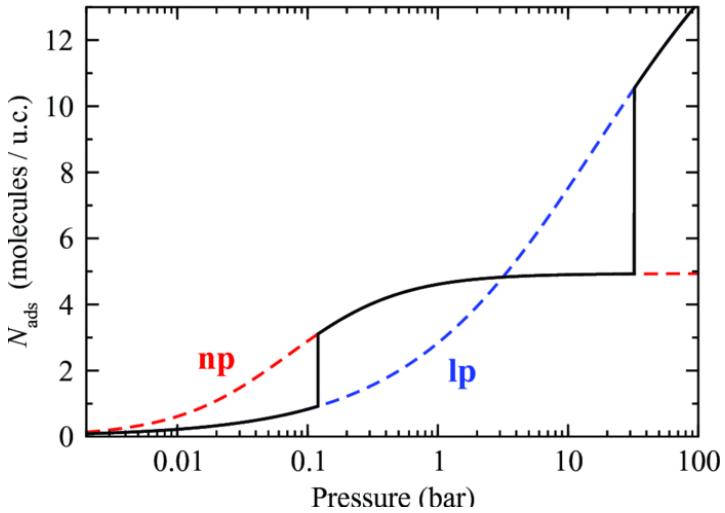

Figure 4.4 – Adsorption isotherms computed at T = 300 K with GCMC simulations in the np (dashed red) and lp (dashed blue) rigid structures. The full black line is a composite adsorption isotherm, featuring the breathing transitions calculated using an analytical model in the osmotic ensemble. Adapted with permission from Bousquet *et al.*, 2006. Copyright (2012) AIP Publishing

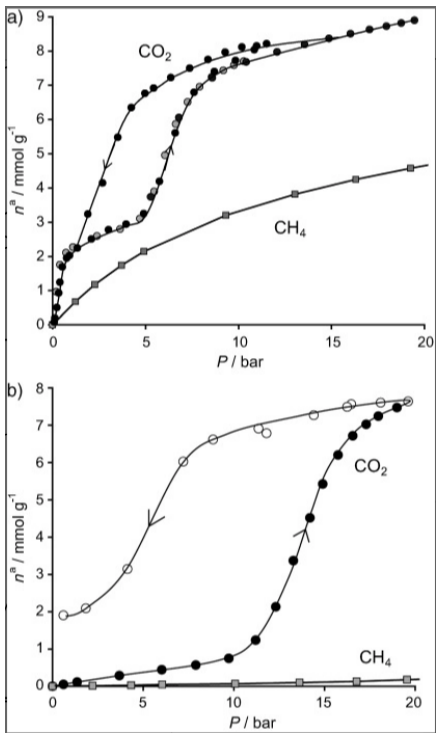

Figure 4.5 – Comparison of the adsorption isotherms of carbon dioxide and methane at 304 K on a) dehydrated and b) hydrated forms of MIL-53(Cr). Grey- and black-filled circles represent two different experiments. Adapted with permission from Llewellyn *et al.*, 2006. Copyright (2001) John Wiley and Sons

ZIF-8 is another well-known example of MOFs that can go through phase transition.(122, 165) Here, the MOF linkers rotated which accompany with the pore volume adjustment. Further information of flexible ZIF-8 will be further discussed in Chapter 7. The phase transitions change the surface area from 1270 m^2 g^{-1} to 1706 m^2 g^{-1}.(105) Fairen-Jimenez et al. compared and demonstrated in experimental and simulation study that the structure transformation change the adsorption curve ZIF-8.(33, 105) Zhang et al. identified 3 distinctive regions of ZIF-8 transition in Figure 4.7.(166) The authors have identified region I as High Loading (HL) structure (Figure 4.6 (b)) and region III as Low Loading (LL) (Figure 4.6(a)) and the transition period where it is a mixture of HL and LL pore and gives a distinctive adsorption curve.

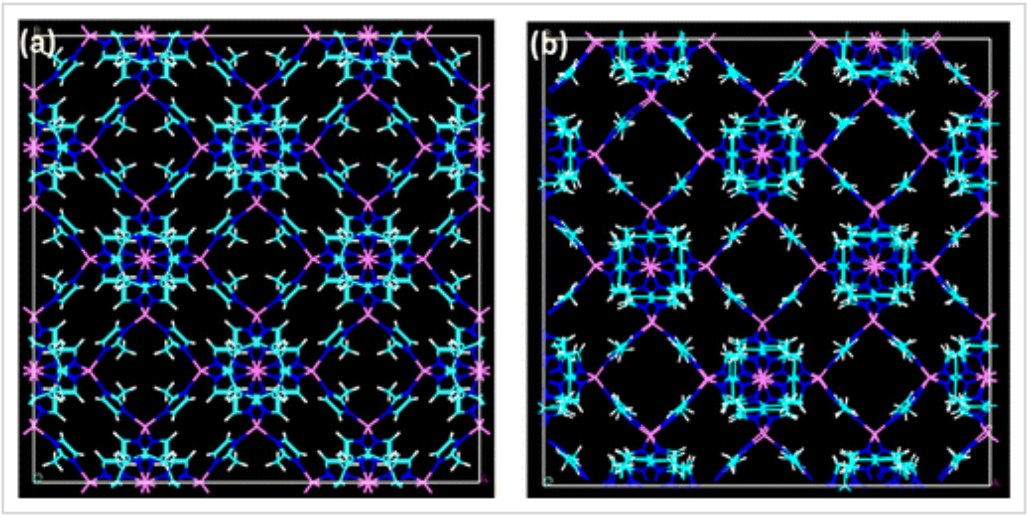

Figure 4.6 - ZIF-8 structures at (a) low loading (LL) and (b) high loading (HL) of N2 sorption. Adapted with permission from Zheng *et al.*, 2006. Copyright (2031) American Chemical Society.

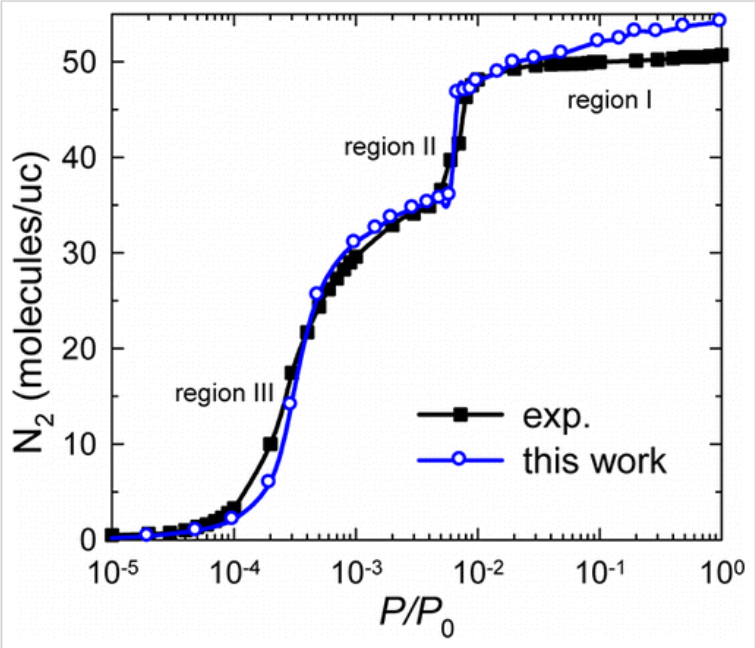

Figure 4.7 - N2 sorption in ZIF-8 at 77 K versus the pressure of bulk N2 (P0 = 1 bar) Adapted with permission from Zheng *et al.*, 2006. Copyright (2031) American Chemical Society.

However, sampling phase transition behaviours due to adsorption is not simple to simulate, as the difficulty lies in the sampling full phase space and the contributing large energy barrier from one phase to another. Resulting the probability of phase transition is greatly limited in molecular dynamic simulation. Hybrid Monte Carlo and Molecular Dynamic were utilised by Zhang et al.(166) and they were able to replicate experimental transition for N_2 adsorption. Another method to simulate flexible framework was approached by Coudert et al. through the usage of osmotic ensemble.(167) The osmotic ensemble method uses the free energy of the host framework and the adsorbates to calculate the probabilistic transition of the structure. Thus it was used to demonstrate the breathing effect in MOFs. Zang et al. further demonstrated the osmotic ensemble methods used in predicting structural transitions and adsorption in other nano porous materials.(168, 169)

The accuracy of adsorptive induced structure transformation by using osmotic ensemble comes at the cost of computational power. Dunne et al. simplified the breathing effect to a one dimensional problem and explored osmotic ensemble by using transfer matrix method to evaluate the breathing effect of MIL-53. The authors also further demonstrated their method can be used to deal with binary mixture in MIL-53(Al).(169, 170) However, the interests of the structure transformation usually lie with the metastable states of the structure. Thus, if the structure metastable states were known and crystallographic positions were given, Grand Canonical Monte Carlo (Chapter 4.2.2) method is sufficient for the generation of adsorption isotherms.

4.2 Molecular Modelling

Computational simulation is simply a tool for modelling a system by inputting a set of parameters to a pre-set algorithm and an output will be generated through a repeat cycle calculation. Herein, molecular modelling, it is referred to the ways of modelling the behaviour of a molecules and molecular system. This involves in several algorithms or simulation techniques; in which the methods will provide new understanding of the procedures for the simulation, thus, specific material design can be engineered, ranging from the scale of atoms, molecules to macroscopic level. The available computational methods take different time spans to perform the simulations depending on the sizes of the system. Figure 4.8 shows the time, length scale and the techniques can be used for simulating different systems size.

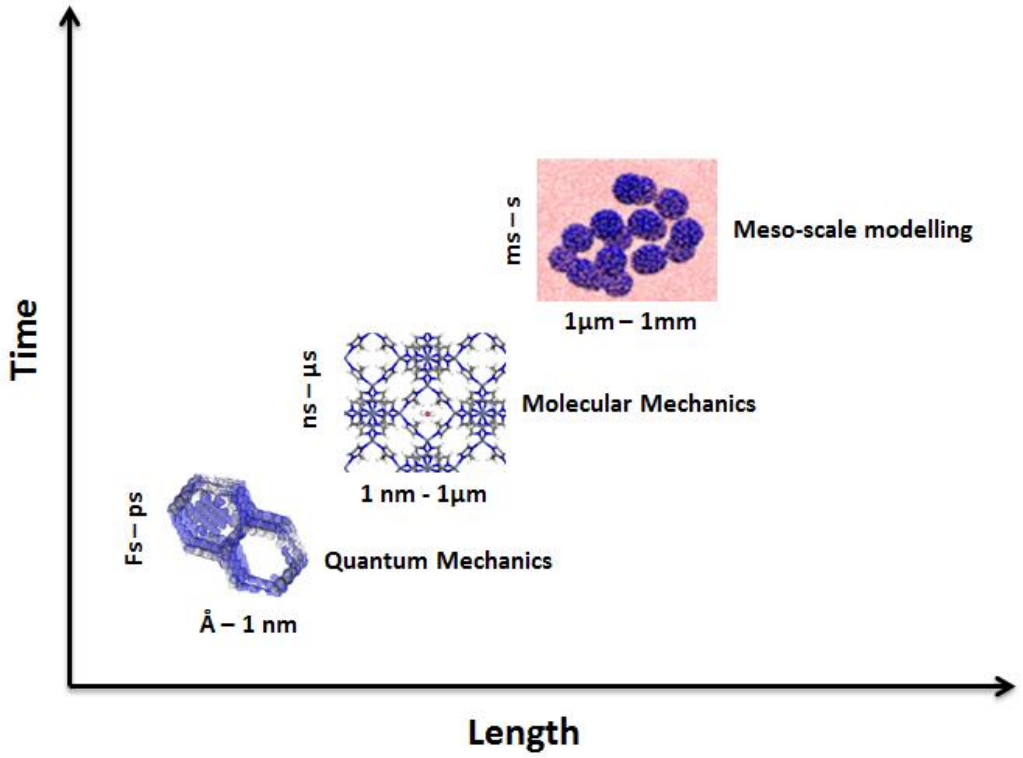

Figure 4.8 – A diagram to illustrate the time and length scales accessible by various simulation methods

4.2.1 Molecular Dynamics

Molecular Dynamics (MD) is a technique to observe transport and equilibrium properties in the many-body classical systems through computational simulation. In here, classical system is under the context where the nuclear motions obey the law of classical mechanics. Thus, the technique provides a good approximation for broad range of materials when sufficient intermolecular interaction information was delivered.

Simulation starts with a model system where N numbers of particles are prepared and Newton's equation of motion is solved until the properties of the system do not change with time. At equilibrium, one could perform actual measure to get the thermodynamic properties.

The basic of MD simulation starts with this set of instruction:

1) Parameters and specific conditions are set before the start of simulation (i.e. Initial temperature, particles, time steps… etc.)
2) Initial position and velocity are provided before initialising simulation
3) Forces acting upon the particles are calculated
4) Newton's equations of motion are integrated. This step and previous step are repeated until the system reaches the desired length of time
5) The average measurements are printed and the simulation stop

The most time-consuming part of the simulation is the force calculation, as there are N particles in the system, we must evaluate $\frac{N(N-1)}{2}$ pair distance. The force calculations are based on equation that are mentioned in chapter 4.3

Newtonian's law of motions is the fundamental basis of classical mechanics, in which momentum and positions of the nuclear are known. It is sufficient by using Newton's equation to understand MD. Here, Verlet algorithms are broadly used in molecular simulations, the derivation starts with simple Taylor expansion of particle coordinate, $r(t)$ in relation to time, t:

Equation 4.2.1

$$r(t+\Delta t) = r(t) + v(t)\Delta t + \frac{f(t)}{2m}\Delta t^2 + \frac{\Delta t^3}{3!}\dddot{r} + \cdots$$

Where $f(t)$ is the force applied onto the atom, m is the mass of the atoms and $v(t)$ is the velocity of the atoms. The co-ordinate from previous time step are given by:

Equation 4.2.2

$$r(t-\Delta t) = r(t) - v(t)\Delta t + \frac{f(t)}{2m}\Delta t^2 - \frac{\Delta t^3}{3!}\dddot{r} + \cdots$$

By summing the two equations together:

Equation 4.2.3

$$r(t+\Delta t) + r(t-\Delta t) = 2r(t) + \frac{f(t)}{m}\Delta(t^2)$$

Here, the new position can be calculated by simply rearrange the equation and by means of the previous location of the coordinate:

Equation 4.2.4

$$r(t+\Delta t) = 2r(t) - r(t-\Delta t) + \frac{f(t)}{m}\Delta(t^2)$$

The numerical derivation between $t+\Delta t$ and $t-\Delta t$, gives the velocity of the particle in the system:

$$r(t+\Delta t) - r(t-\Delta t) = 2v(t)\Delta t$$

Or

$$v(t) = \frac{r(t+\Delta t) - r(t-\Delta t)}{2\Delta t}$$

In MD simulation, the time evolution of the system is observed through using different ensemble. This thesis focused on canonical ensembles (NVT) and isobaric and isothermal ensemble (NPT). Both ensembles required to maintain the temperature and/or pressure of the system at the anticipated value. Thermostats and barostats are built within the simulation algorithm to maintain the temperature and the pressure of the system. Usually, the constant temperature is achieved by

coupling the velocity of the atoms to dynamical variables and the pressure is maintained by altering the box volume. Examples such as Nose-Hoover thermostat,(171) Berendsen barostats and thermostat,(172) Andersen thermostat(173) and Parrinello-Rahman barostats(174, 175) are commonly used in simulation for maintaining the temperature and the pressure..

4.2.2 Monte Carlo

Monte Carlo (MC) is another molecular simulation technique that uses probabilistic approach to sample a molecular system. The algorithm of MC is relatively simple as the core of most programs followed these rules:

1) Random selection of a particle and calculate its energy
2) Then randomly displace the particle and calculation the new energy
3) Accept the movement of the particle from old configuration to new configuration with the pre-set probabilities.
4) The steps are loop until satisfactory cycles are obtained.

This thesis focused on Grand-Canonical Monte Carlo (GCMC), where the temperature, volume and the chemical potential are fixed (μ, V, T ensemble). Here, the number of molecules can fluctuate in a way such that the chemical potential of the gas inside and outside the adsorbate are equal. This ensemble allows us to study the amount of gaseous molecules adsorption into MOFs.

To understand statistical mechanic basis for the GCMC, we must first understand the partition function of the N molecules interacting molecules:

Equation 4.2.5

$$Q(N,M,V,V_0,T) = \frac{V^N(V_0-V)^{M-N}}{\Lambda^{3M}N!\,(M-N)!}\int ds^{M-N}\int ds^N \exp[-\beta U(s^N)]$$

Where V is the volume and $M-N$ is the ideal gas molecules in volume V_0-V. Λ is the thermal de Broglie wavelength and it is determined through $\Lambda = \frac{h}{\sqrt{2\pi m k_b T}}$

The particle in the system can be varied, thus the equation becomes:

Equation 4.2.6

$$Q(M,V,V_0,T) = \frac{V^N(V_0-V)^{M-N}}{\Lambda^{3M}N!\,(M-N)!}\int ds^{M-N}\int ds^N \exp[-\beta U(s^N)]$$

For ideal gas, the integral over the reduced co-ordinate s^{M-N} becomes 1. Thus the probability density for a system with $M-N$ particles at reduced co-ordinates s^{M-N} in volume $V' \equiv V_0 - V$ and N particles at reduced coordinates s^N in volume, V^N:

Equation 4.2.7

$$\mathcal{N}(s^M;N) = \frac{V^N V'^{M-N}}{Q(M,V,V',T)\Lambda^{3M}N!\,(M-N)!}\exp[-\beta U(s^N)]$$

Here, as $M \to \infty$, $V' \to \infty$, $(M/V') = \rho$. The chemical potential of an ideal gas, μ is related to particle density, ρ by

Equation 4.2.8

$$\mu = k_B T ln\Lambda^3\rho$$

As $M/N \to \infty$, the partition function becomes:

Equation 4.2.9

$$Q(\mu, V, T) \equiv \sum_{N=0}^{\infty} \frac{\exp(\beta\mu N)\, V^N}{\Lambda^{3N} N!} \int ds^N \exp\left(-\beta U(s^N)\right)$$

And the probability density

Equation 4.2.10

$$\mathcal{N}_{\mu,V,T}(s^M; N) \propto \frac{\exp(\beta\mu N)\, V^N}{\Lambda^{3N} N!} \exp\left(-\beta U(s^N)\right)$$

So now, after core equation for GCMC simulation is derived, the simulation becomes like this:

1. Random particle is selected and a displacement is given to the particle. The move is accepted with the probability:

Equation 4.2.11

$$acc(s \to s') = \min\left(1, exp\left\{-\beta\left[U\left(s'^N\right) - U(s^N)\right]\right\}\right)$$

2. A particle is inserted or deleted following the acceptance probability:

For insertion and deletion are given respectively:

Equation 4.2.12

$$acc(N \to N+1) = \min\left[1, \frac{V}{\Lambda^3 (N+1)} exp\{\beta[\mu - U(s^{N+1}) + U(s^N)]\}\right]$$

Equation 4.2.13

$$acc(N \to N-1) = \min\left[1, \frac{\Lambda^3 N}{V} exp\{-\beta[\mu + U(s^{N-1}) - U(s^N)]\}\right]$$

4.3 Force Field

Force field is a set of equations and parameters that is used for calculating the potential energy of a system. It is not always possible to capture an accurate force field since this requires either specific experimental data or a large set of quantum mechanics calculation.

The force field is used in the calculation of the overall potential energy in the system. It is defined by 4 components (Equation 4.3.1):

Equation 4.3.1

$$\mathrm{U}(r^N) = \sum_{bond} k_{ij}\left(l_{ij} - l_{ij_0}\right)^2 + \sum_{angles} k_{ijk}\left(\theta_{ijk} - \theta_{ijk_0}\right)^2 + \sum_{Torsions} V_{ijkl}\left(1 + \cos\left(n\phi - \phi_{ijkl_0}\right)\right) + \sum_{i=1}^{N}\sum_{j=i+1}^{N}\left(4\varepsilon_{ij}\left(\left(\frac{\sigma_{ij}}{r_{ij}}\right)^{12} - \left(\frac{\sigma_{ij}}{r_{ij}}\right)^{6}\right) + \frac{q_i q_j}{4\pi\varepsilon_0 r_{ij}}\right)$$

Where $\mathrm{U}(r^N)$ represents the potential energy. The first term describes the potential energy of a bonded pairs and this increase with the deviation from the equilibrium bond length. The second term describes the sum of angles in the molecules; the third term is the torsions potential as the bond rotated. The last term is the potential energy of non-bonded term; this potential can be separated into an electrostatic term and Van der Waals term.

Equation 4.3.2

$$v(l) = k(l - l_0)^2$$

The first term, bond stretching, can be explained by using the harmonic potential equation (Equation 4.3.2) for computational simplification purpose. However, harmonic potential does not truly express the true resonant of the bond. There are other forms of the equation such as Morse curve to improve the accuracy of bond stretching or by increasing the number of Tayler series expansion terms; however, this will not be discussed further.

Equation 4.3.3

$$v(\theta) = k(\theta - \theta_0)^2$$

Angle bending energy $v(\theta)$ can be presented with harmonic potential (Equation 4.3.3). Many regards angle bending and bond stretching have "hard" degrees of freedom, in that a significant amount of energies are needed to cause structure deformation. Sequentially, substantial structure deformation energies contributed by torsional and non-bonded terms.

Equation 4.3.4

$$v(\omega) = \sum_{n=0} V(1 + \cos(n\phi - \phi_0))$$

Torsional/dihedral (Equation 4.3.4) term describes the existence of barriers to rotation about chemical bonds. It is fundamentally important to the structure properties as it favours energy at lowest state. V describes the 'barrier' height, the maximum energy position of the structure orientation, and can have multiple

maximum and minimal energy. This leads to multiple favourable positions that a structure can be achieved.

Non-bonded interactions separate into electrostatic interaction and other weak interaction (Van der Waals). Electrostatic interactions are properties depicted from electronegative elements; strong electronegative element attracts electrons from less electronegative element. Due to the uneven spread of electrons, unequal charge distributions are spread across a molecule and often represented through an electron density map. Thus one common approach to the spread of electrons is an arrangement of fractional point charges throughout the molecules. Electrostatic energy potential U_q is calculated through as a sum of interaction between two particles by using Coulomb's law:

Equation 4.3.5

$$\mathrm{U}_q = \sum_{i \neq j}^{N} \left(\frac{q_i q_j}{4\pi\varepsilon_0 r_{ij}} \right)$$

Where N represents the numbers of molecules, $q_i$and q_j represents the fractional point charge of molecules i and j, ε_0 is the permittivity of free space and $r_{ij}$is the distance between the two different charges.

Lennard – Jones potential is a model that approximates the weak force interaction (Van der Waals) between a pair of atoms or molecules:

Equation 4.3.6

$$U_{LJ} = 4\varepsilon \left[\left(\frac{\sigma_{ij}}{r_{ij}} \right)^{12} - \left(\frac{\sigma_{ij}}{r_{ij}} \right)^{6} \right]$$

ε is the potential well and σ_{ij} is the finite distance that the inter-particle potential is zero.

4.3.1 General Molecular Interaction Development

In the computational area of MOFs community, it is common to describe Van der Waal potential of individual atoms with a general force field, such as Universal Force Field (UFF), (176) AMBER,(177) DREIDING,(178) CHARMM(179) etc. as it is sufficient to describe most adsorption of neutral molecules. However, in the case where the molecules have a permanent dipole moment, it is important to take consideration of electrostatic charge potentials within the framework. Quantum mechanics are applied to calculate the electrostatic potential surface and point charge are assigned to the individual atoms on the framework. As mentioned in chapter 2.2, some MOFs respond to stimuli and undergo phase transition and the intramolecular force field were also derived from one of the mentioned general force field. In this thesis, we are to focus on UFF and AMBER force fields since they are widely used in the community, thus a brief review of each force field is given in the following paragraph.

A. K. Rappe developed Universal Force Field (UFF); the parameters are based on physical data such as the bonded distance and non-bonded distance.(176) This force field is created for generalising all common atoms and molecules. However, with this type of generalisation does not full capture specific system characteristics, therefore these inaccuracies could accumulate and resulting simulation deviated from experimental results. An improved version can be specifically designed for a group of molecules, example as such are UFF4MOF,(180) BTW-FF(181) and MOF-FF(182) are used to increase the accuracy in MOFs simulation. They

improved the force field by generating the metal ions parameters through QM calculations.

J. Wang et al(177) developed a General force field which is known as General AMBER Force Field (GAFF). The force field is designed for organic molecules specifically compatible for proteins and nucleic acids. Effectively this is related to MOFs as the linkers are made up of organic molecules. AMBER force field has been compared the force field parameters with various quantum methods and force field, such as Møller–Plesset perturbation theory (MP2) and CHARMM force field, and yields compatible results in both cases.(177)

4.4 Density Functional Theory (DFT)

DFT approach has been extensively used in scientific field for observing property of the material at quantum level. The method addresses important problems in widespread range of areas of research with high degree of accuracy and efficiency. DFT allows all properties to be determined and explained by using electron density, $\rho(\vec{r})$, which is a function of positional variable, $\vec{r} = r(x, y, z)$. In this section, a basic discussion of DFT concepts and its construction are presented.

Schrödinger equation describes the time independent form of the energy for a molecular system with the following equation:

$$H\Psi = E\Psi$$

Where H is the Hamiltonian, Ψ is wave function and E is energy. The Hamiltonian of a system contains information of N_M nuclei and N_e electrons. A very important aspect of quantum mechanics is the wavefunction; itself contains all information that can possibly be known about the quantum system at hand.

Equation 4.4.1

$$\Psi(\vec{x}_1, \dots, \vec{x}_N, \vec{R}_1, \dots, \vec{R}_M)$$

which stands for the wave function of the i'th state of the system. The wavefunction depends on the 3N spatial coordinates $\{\vec{r}_i\}$, the term $\{\vec{x}_i\}$ is a collective representation of N spin coordinates $\{\vec{s}_i\}$ of the electrons and the last term 3M spatial coordinates of the nuclei, $\{\vec{R}_M\}$. It is worth noting that the wavefunction Ψ is not observable, physical interpretation can only be associated with the square of the wave function in that

Equation 4.4.2

$$\left|\Psi(\vec{x}_1, \dots, \vec{x}_N, \vec{R}_1, \dots, \vec{R}_M)\right|^2 d\vec{x}_1, \dots, d\vec{x}_N$$

represents the probability that electrons (1, …, N) are found simultaneously in the volume/orbital $d\vec{x}_1, \dots, d\vec{x}_N$. This probability must not change if the coordinates of any two electrons are switched. However, because electrons are fermions with spin $= \frac{1}{2}$, the wavefunction have to be antisymmetric with interchangeable spatial and spin coordinates of any two electrons, (here i,j):

Equation 4.4.3

$$\Psi(\vec{x}_1, \dots, \vec{x}_i, \vec{x}_j, \dots, \vec{x}_N) = -\Psi(\vec{x}_1, \dots, \vec{x}_j, \vec{x}_i, \dots, \vec{x}_N)$$

and does not violated the quantum-mechanical generalisation of Pauli's exclusion principle (no two electrons can occupy the same state).

4.4.1 Kohn-Sham Approach

For many materials studies, it is apparent that the system will contain many atoms in order to obtain meaningful results, for each atom will contain N number of electrons and each electron position needed to be calculated. Therefore, the computational calculation is enormous. Furthermore, interaction between the electron-electron and electrons-nuclei are not independent and leads to many-body problem. Hohenberg-Kohn theorems allowed a construction of a rigorous many-body theory by utilising the electron density, $\rho(\vec{r})$. The framework of the ground state energy of an atomic or molecular system can be written as

Equation 4.4.4

$$E_0 = \min_{\rho \to N} \left(F[\rho] + \int \rho(\vec{r})\, \mathrm{V}_{Ne} d\vec{r} \right)$$

where $\int \rho(\vec{r})\, \mathrm{V}_{Ne} d\vec{r}$ is the energy due to external potential, it simply determined by the density and is independent to the wave function generating the density. The universal functional $F[\rho]$ contained the individual contributions of the kinetic energy, the classical Coulomb interaction and the non-classical portion due to self-interaction correction, exchange (i.e. antisymmetric) and electron correlation effects.

Equation 4.4.5

$$F[\rho(\vec{r})] = T[\rho(\vec{r})] + J[\rho(\vec{r})] + E_{ncl}[\rho(\vec{r})]$$

Where $T[\rho(\vec{r})]$ is the kinetic energy, $J[\rho(\vec{r})]$ is the classic coulomb interaction between electron-electron and nuclei-electron, and $E_{ncl}[\rho(\vec{r})]$ is non-classical energy portion due to self-interaction correction, exchange and electron correlation

effects. Only $J[\rho(\vec{r})]$ is known, while the other two contribution terms explicit form remains unknown.

Kohn-Sham equation gives a better formulation on the kinetic energy in comparison to Thomas – Fermi as the density is not dependent on coarse estimations $\int \rho^{\frac{5}{3}}(\vec{r})d\vec{r}$. Kohn-Sham introduces the followed separation of the functional, $F[\rho(\vec{r})]$:

Equation 4.4.6

$$F[\rho(\vec{r})] = T_s[\rho(\vec{r})] + J[\rho(\vec{r})] + E_{XC}[\rho(\vec{r})]$$

T_s is the exact kinetic energy of the non-interacting reference system and defined in Equation 4.4.7, $J[\rho(\vec{r})]$ is the classic coulomb interaction and $E_{XC}[\rho]$ is known as the exchange – correlation energy. Here, one must point out that the non-interacting kinetic energy is not equal to the true kinetic energy of the interacting system, $T_s \leq T$.

Equation 4.4.7

$$T_s = -\frac{1}{2}\sum_{i}^{N}\langle\varphi|\nabla^2|\varphi\rangle$$

Where φ is the spin orbital and ∇^2 is the Laplacian operator is defined as a sum of differential operators in Cartesian coordinates Equation 4.4.8:

Equation 4.4.8

$$\nabla^2 = \frac{\partial}{\partial x^2} + \frac{\partial}{\partial y^2} + \frac{\partial}{\partial z}$$

Hence exchange – correlation energy is defined by Equation 4.4.9:

Equation 4.4.9

$$E_{XC}[\rho] \equiv (T[\rho] - T_s[\rho]) + (E_{ee}[\rho] - J[\rho]) = T_c[\rho] + E_{ncl}[\rho]$$

Where T_c the residual is part of the true kinetic energy and $E_{ncl}[\rho]$ is the non-classical electrostatic contributions. Thus, one could look at $E_{XC}[\rho]$ is the functional which contains everything that is unknown. The term contains the non-classical effects of self-interaction correction, exchange and correlation and a portion belonging to the kinetic energy.

The expression for the energy of the interacting real system Equation 4.4.10 is formulated in the following order; exact kinetic energy of non-interacting reference system, electron-electron electrostatic energy, exchange-correlation energy and nuclear-electron electrostatic energy:

Equation 4.4.10

$$E[\rho(\vec{r})] = T_s[\rho] + J[\rho] + E_{XC}[\rho] + E_{Ne}[\rho]$$

$$= T_s[\rho] + \frac{1}{2}\int\int \frac{\rho(\vec{r}_1)\rho(\vec{r}_2)}{r_{12}} d\vec{r}_1 d\vec{r}_2 + E_{XC}[\rho] + \int V_{Ne}\rho(\vec{r}) d\vec{r}$$

$$= -\frac{1}{2}\sum_i^N \langle\varphi_i|\nabla^2|\varphi_i\rangle + \frac{1}{2}\sum_i^N\sum_j^N \int\int |\varphi_i(\vec{r}_1)|^2 \frac{1}{r_{12}} \left|\varphi_j(\vec{r}_2)\right|^2 d\vec{r}_1 d\vec{r}_2 + E_{XC}[\rho(\vec{r})]$$

$$- \sum_i^N \int \sum_{r_{1A}}^M \frac{Z_A}{r_{1A}} |\varphi_i(\vec{r}_1)|^2 d\vec{r}_1$$

Due to the fact that searching all eligible functions is obviously not possible, variational principle is applied to the equation above in order to minimise the energy and thus gives the equation:

Equation 4.4.11

$$\left(-\frac{1}{2}\nabla^2 + \left[\int \frac{\rho(\vec{r}_2)}{r_{12}} d\vec{r}_2 + V_{XC}(\vec{r}_1) - \sum_A^M \frac{Z_A}{r_{1A}}\right]\right)\varphi_i = \left(-\frac{1}{2}\nabla^2 + V_{eff}(\vec{r}_1)\right)\varphi_i$$

$$= \varepsilon_i \varphi_i$$

One must notice that $V_{XC}(\vec{r}_1)$ is still an unknown term. An expression is given to relate the exchange energy and density:

Equation 4.4.12

$$V_{XC} \equiv \frac{\delta E_{XC}}{\delta \rho}$$

The success of the DFT approached based on the exchange correlation functional. Different approximations $V_{XC}(\vec{r}_1)$ function has different DFT methods, like Local Density Approximation (LDA), Generalized Gradient Approximation and so on.

LDA method is based on the assumption of uniform electron gas, where all the electron density is constant throughout all space.

Equation 4.4.13

$$V_{xc}^{LDA}[\rho(r)] = \int \rho(r)\varepsilon_{xc}\big(\rho(r)\big)dr$$

$\varepsilon_{xc}\big(\rho(r)\big)$ is the density function of exchange correlation energy per electron in a uniform gas. GGA are still local approximation, however the spin of the electron and the gradient of the density at the local position are considered.

Equation 4.4.14

$$V_{xc}^{GGA}[\rho(r)] = \int \rho(r)\varepsilon_{xc}(\rho(r)\uparrow, \rho(r)\downarrow, \nabla\rho(r)\uparrow, \rho(r)\downarrow)\, dr$$

DFT functions are important to analyse the electronic structure of atoms and molecules. Here, in this thesis, we chose to use Perdew-Burke-Ernzerhof (PBE) hybrid functional(183) as it is accurate enough and computationally less expensive in comparison to other hybrid functional.

5 Design of Electric Field Controlled Molecular Gates Mounted on Metal-Organic Frameworks

In this study, we propose and computationally demonstrate the concept of electric field controlled molecular gates mounted on the open-metal coordination sites in MOF materials. The MOF-molecular gate complex functions by opening and closing under the effect of an electric field. Our design involves Mg-MOF-74, a MOF with hexagonal channels with open-metal coordination sites at each corner, and a multifunctional gate molecule with permanent dipole which anchors itself on the host MOF material and responds to changes in the direction of an electric field by rotating around its backbone which acts as an axle. By carrying out density functional theory (DFT) calculations and molecular dynamics (MD) simulations, we show that the MOF-molecular gate complex can be switched between two stable configurations, open and closed, by turning on and off an external electric field. We further show that the molecular gate can be controlled to block or allow the diffusion of methane molecules through the channels of the MOF like a nanoscale butterfly valve. Electric field controlled molecular gates mounted on MOFs can pave the way for new molecular machines and nanodevices which can store, deliver or select molecules on demand and with atomic precision.

5.1 Introduction

Molecular machines are supramolecular structures designed to transform external stimuli to coordinated collective mechanical movements which mimic those occurring at the macroscopic level.(184, 185) Examples of molecular machines are rotors,(186) switches,(56, 62, 63) gates,(106, 187) elevators,(188, 189) motors(56,

67-69) and tweezers,(66) most of which were inspired by nature.(190, 191) More sophisticated designs include molecular machines which can move objects 10,000 times greater than their mass(64) and a molecular car.(59, 65) In the mid-1990s, Bedard *et al.*(192) was the first to suggest the concept of electric field controlled molecular doorways by employing dipolar molecules. Later Zheng *et al.*(193) synthesized a molecular rotor and characterized its response to an electric field by scanning tunnelling microscopy and barrier height imaging. Horinek *et al.,*(142) Hsu *et al.*(194) and Seldenthuis *et al.*(58) reported molecular simulations of similar unidirectional rotational control of supramolecular machines by an electric field.

Another area developing rapidly, like molecular machines, and have harnessed great interest recently, is MOFs.(2, 41, 195-197) MOFs are inorganic-organic hybrid porous crystalline materials formed by the self-assembly of metal ions and organic ligands via coordination bonds. In principal, with a judicious choice of the inorganic and the organic building blocks it is possible to fine tune the pore size and shape and chemical functionality of MOFs.(198, 199) Thanks to such versatility MOFs have been investigated for a wide range of applications, such as separations,(200) gas storage,(11, 73) drug delivery,(41, 201, 202) sensors,(16, 41, 203) luminescence(203, 204) and catalyst.(101, 205, 206) Structural and chemical properties of MOFs can also be tuned by post-synthesis modification.(198, 207, 208) This is usually achieved by ligand functionalization or grafting molecules on open-metal coordination sites. The latter forms the basis of our study. By grafting ligands on open-metal coordination sites, majority of previous studies aimed at tuning the pore size and chemistry of MOFs for various separation and catalyst applications.(208-215) More recently, Stoddart and colleagues demonstrated the

idea of positioning redox-active molecular switches within MOFs by grafting them on the open-metal coordination sites.(51, 70)

Propelled by the advancement in both synthetic molecular machines and MOFs, here we propose to mount molecular gates on the open-metal sites of MOFs and control their opening and closing by utilizing changes in an electric field.[58, 192-194] The molecular gate consists of three basic features; anchors, a permanent dipole and an axle. The strong attraction provided by the open-metal coordination sites in MOFs provide anchoring points for the gate molecule and the permanent dipole allows the gate molecule to be influenced by an electric field and rotate around an axle to block or allow the diffusion of molecules in a channel. In our MOF-molecular gate design we first identified a MOF suitable for hosting a gate molecule. M-MOF-74 (M-CPO-27, M_2-dhtp) (M = Mg, Ni, Co, Zn, Mn, Fe)(86, 216, 217) materials have been studied for the adsorption of different species, including light gases and hydrocarbons.(5, 32, 40, 86, 137, 218-223)

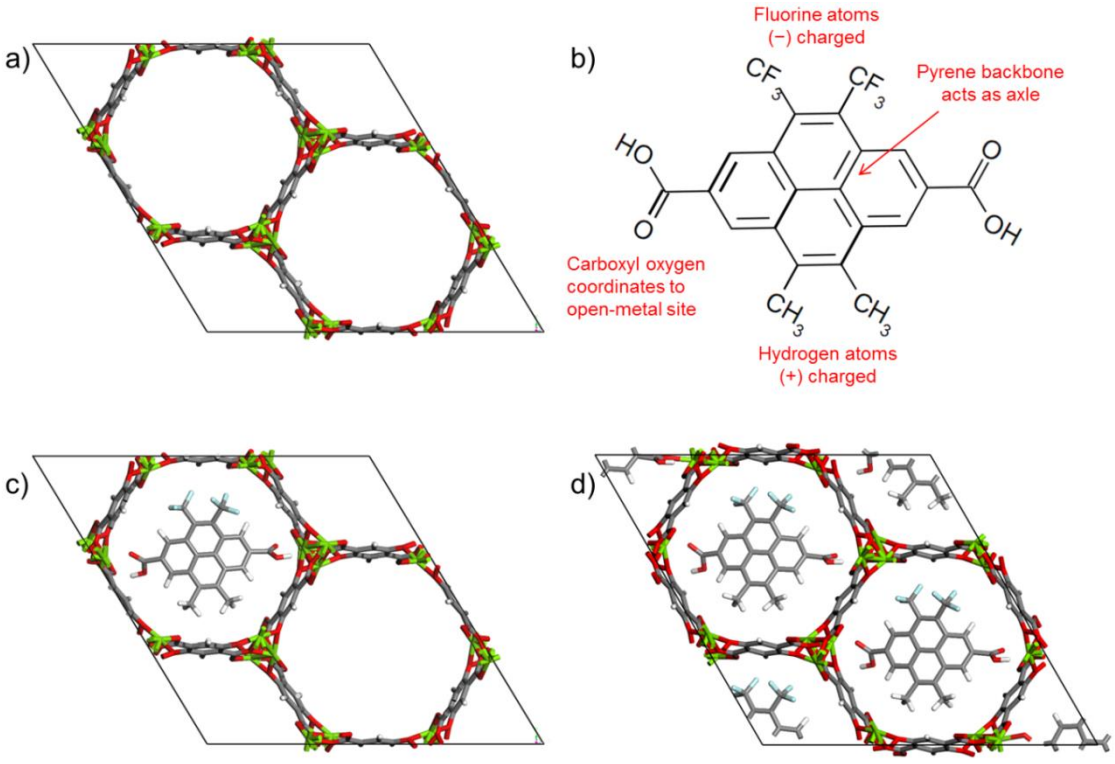

Figure – 5.1 a) Mg-MOF-74 unit cell, b) chemical structure of the gate molecule, 4,5-dimethyl -9,10-bis(triflоromethyl)pyrene-2,7-dicarboxylic acid,(224) c) a molecular gate placed in one of the Mg-MOF-74 channels, and d) MOF-molecular gate complex where all three channels of Mg-MOF-74 were occupied by the gate molecules. Carbon, oxygen, magnesium, fluorine and hydrogen are represented with grey, red, green, cyan and white, respectively.

M-MOF-74 is composed of 2,5-dihydroxyterephthalate ligands and one of the named metal ions, forming a structure with hexagonal one-dimensional channels which are about 12 Å in size and bear a high density of open-metal coordination sites. The open-metal sites facing one another in M-MOF-74 provide anchoring points in order to mount the gate molecules and its one-dimensional channels are ideal for the demonstration of the gating effect; i.e. closing or opening the pore. Of particular interest to us is Mg-MOF-74 (Figure – 5.1a) due to the strong binding energies reported for various adsorbates.(23, 139)

For the gate molecule, we considered 4,5-dimethyl-9,10-bis(triflоromethyl)pyrene-2,7-dicarboxylic acid (Figure – 5.1b). The carboxyl groups on both ends can

coordinate to the open-metal sites thus anchoring the molecular gate. The central pyrene allows the molecule to rotate around an axle like a rotor. Finally, the negatively charged fluorine groups and the positively charged methyl groups create a permanent dipole which enables the molecule to respond changes in an electric field. Figure – 5.1c shows a molecular gate placed in one of the channels of Mg-MOF-74 and Figure – 5.1d shows all three channels of the Mg-MOF-74 occupied by the gate molecules.

This chapter is organised as follows. First, discussions regarding to Mg-MOF-74 will be given, then the discussion will move on to current review regarding to molecular machines. Afterward, the chapter move onto review of the current research on synthesising molecular machines in MOFs. This is followed by the method that were used in simulating proposed molecular machines in Mg-MOF-74, Finally, a discussion of the main results and concluding remarks will be given.

5.2 Mg – MOF – 74

Since the first discovery and synthesis of M – MOF – 74/CPO 27 by Rosi *et al.*,(225) this one dimensional hexagonal MOFs has become a well-known material in the nano-porous material community. The fame is owned to the chemical and thermal stability through a range of conditions and high surface area (1525 $m^2\ g^{-1}$); in which the ~14 Å pore diameter channels are easily accessible to guest molecules. It is known that M-MOF-74 has strong affinity to gaseous molecules. This is due to the unsaturated open metal sites on the pore surface where a co-ordinate bond can form. These sites exhibited large guest molecules uptakes (i.e CO_2, N_2, CH_4… etc)(5, 10, 32, 86) and regenerated in relative low temperature.(6, 226) These open metal sites are found to have high selectivity in a mixture of gaseous species,

especially where the molecules have similar chemical structure (i.e. acetylene/ethylene) or relative size (i.e. CO_2/CH_4).(3, 6, 227-229)

Thus these implicit properties gave birth to the idea of industrial applications such as gas storage (i.e. H_2, CH_4),(38, 230) toxic gas filtration(24, 84-86) and chemical separations.(6, 226, 229) Although currently zeolite dominates chemical industries for their adsorption properties and catalytic usage, MOFs synthesis procedure are maturing. The development has lower over production costs and leading towards to the region where it is competitive for industrial applications.(226, 231)

M-MOF-74 has a very flexible range of design in which it can accommodated specific needs. The diversity comes from open metal site are exchangeable by various transition metals (M = Mg, Ni, Co, Zn, Mn, Fe) during synthesis process.(86, 216, 217) Each element gives diverse degree of physisoportion as the ion has different electron configuration. In general, guest species and MOFs interaction mechanisms are similar for all metal ions, the attraction comes from charge transfers between the molecules and the unoccupied orbitals in the metal.(232) However the difference between the binding affinities had led to the success in tuneable selectivity by doping different percentage of metal ion in the framework.(39, 228, 233)

Furthermore, the adaptability expand to the pores diameter as the lengthen linkers, variation from 1 phenylene ring to 2 – 9 rings in chain, can be altered into MOF-74 during synthesis while retaining one dimensional pore.(199) Extension of the pores size can permit larger compounds (i.e. biomolecules and enzyme)(82, 234) to be entrapped and release, thus potentially lead to the exploration in the direction for drug delivery.(17)

Now in this study we have selected Mg-MOF-74 for this MOF has a strong binding affinity with O atoms. Mg-MOF-74 has been considered the leading MOF for carbon storage(235-237) as its strong adsorption of CO_2 can take on the climate change arising from increasing atmospheric CO_2 level. Its high capacity uptakes of CO_2 (1 Mg ions per 1 CO_2 adsorption) and regeneration ability make it an attractive area of research for reduction of global warming. However, in the study, the attentions are not focus on CO_2 capture but the well-rehearsed mechanism between the O atoms in CO_2 and the Mg atoms in MOFs. Similar with the influenced of water molecules, the O atom is the reason for adsorption to occur as the electrons can be easily transferred to the metal ions. In experiment, the heat of adsorption of CO_2 is found to between -39 to -72 kJ mol^{-1} (5, 228, 238) and quantum mechanics simulation agrees to the experimental results.

However, this MOF is susceptible to the environment where high concentration of water presented and porosity channel will be disassemble in less than 24 hrs.(239) Tan *et al.* studied the disintegration mechanism through ab initio DFT simulation. Strong adsorption binding on the metal sites bring facile dissociation or intrusion by the O atoms in water molecules.(232) As the H_2O approached the open metal sites, charge-density between the O atoms of the linker and metal ion redistributed. Metal ions break off with the water molecules and lead to disintegration of the hexagonal structure. Although it is known water instability can be lessen by doping with different metal within the framework, the mechanism behind is yet to explore.(39)

Though there are broad ranges of experiment had been done with Mg-MOF-74, in which some experimental results can be replicated with simulations (adsorption isotherm, BET, heat of adsorption… etc).(32, 105, 240, 241) There are certain

degree of uncertainty that we ignored during computational simulation, such as structural impurities and defects. Reasoning is due to the limitation in computational power and understanding of molecular crystallisation still elusive with current knowledge. Thus, with this in mind, these factors may have contributed to the inconsistency in simulation when it is compared with experiments. However, this will not explore further and beyond the scope of this study.

It is common to use Universal force field (UFF)(176) or AMBER force field(242) for simulating MOFs structure. There are notable reliability issues on the mentioned general force field as the intramolecular interaction cannot replicate correct flexibility under experimental conditions. The complication comes from interaction between the metal sites and the linkers, where UFF and AMBER often fail to describe the connection. Addicoat *et al.* have addressed the problem with a refined UFF and developed a force field specific for MOFs (UFF4MOF), in which he added general bonding parameters for metal ions and organic linker interactions.(180) Fortunately, M-MOF-74 series is a rigid MOF and no underlying structural deformation is observed in experiment, thus flexibilities will have minimal impact in the study that is conducted in this thesis.

Intermolecular interactions placed a more important role for the study in M-MOF-74 as the interest lies with the structure abilities on gaseous species adsorption. Interactions between the guest molecules and the MOFs are dependent on the non-bonded parameter, i.e. Coulomb charges and Van der Waals (VdW) interaction. For this thesis, partial point charges are calculated through periodic Density Functional Theory (DFT) in combination with Electrostatic Potential Mapping.

To conclude, Mg-MOF-74 is well-known MOFs with high chemical and thermal stability. It is adaptable and can be tailored to specific needs as the metal ions and the linkers can interchange while retaining the hexagonal one dimensional pore. It is theoretically and experimentally proven that the material has strong binding affinity with molecules contains O atom and available force field to be used. Therefore with the mentioned reasoning, this MOF is chosen to be further study in this work.

5.3 Molecular Machines

This review will consolidate relevant literature in molecular machines to give an overview the possibilities of synthetic molecular machines, following on with the discussion on the current development in synthetic molecular machines that design to respond to various stimulants and convert energy into mechanic motions. In this section, I will first discuss the concepts and gives examples of synthetic molecular machines. Then I will explain the progressive unidirectional control mechanisms development. Finally, the discussion will end with examples of application of various synthetic molecular machines.

5.3.1 Unidirectional Rotary

Molecules rotate freely in respective to the surrounding environment, and by controlling the rotation, direction and position one could create a unidirectional molecular rotary machine. At the early stages of the development of synthetic rotary molecular machines, the machine depends on Brownian ratchets system. At the later stage of developments, for the reasons discussed later in the chapter, unidirectional rotaries uses different stimulants such as electromagnetic spectrum(53, 243, 244), thermal fluctuation(184, 245, 246) and chemical fuel(247,

248) to power molecular rotors. Further theoretical approaches such as electron tunnelling(249) and coulomb interaction driven motors(250) were mentioned as a potential fuel source for the rotary motor. Molecular machines such as nano-turbine(251) for power generation may provide future applications in industries.

'Brownian ratchets' are a well-known rotary system;(184, 245, 246) they are designed to permit thermally activated motion in one direction only. Feynman stated in an isothermal system, net motion of a ratchet and pawl system cannot be achieved if all components of the devices are treated consistently in order for 2nd thermodynamic law not to be violated, thus the clockwise rotation will be equalled to the anti-clockwise motions. Astumian(246) discussed Feynman's statement and showed the net motions can be achieved if a biased is added into Brownian motion system; by designing the system through a non-equilibrium chemical reaction(252-255) or supplied external fluctuations,(256-258) an unidirectional movement can be achieved due to the gradient difference. Physical ratchets system(191, 259, 260) is a typical choice of conserving unidirectional movement. Faucheux *et al.*(245) had suggested creating a Brownian ratchet by using optical infrared tweezer to limit the motion of molecular motor; this ratchets idea was not developed further in the direction of molecular machines but later was used on various applications such as isolation of particles in fluid(261) and electronic devices.(262)

One of the first reports on making synthetic molecular machines, Kelly *et al.* (247, 260) designed an electrochemical braking system with triptycene structures (Figure 5.2). The rotation pivot was designed with a single bond, thus allows free intra-rotation of the molecules and the triptycene wheel have free rotations at 30^{0}C. Hg^{2+} ions used as a 'brake' and halt the rotation by appending bipyridyl, similar to a "stick" stuck in the "spokes" of the wheel and restrict the movement. One should

note that this machine has no control on the rotation direction as this is concluded in the investigation by Kelly *et al.* It is revealed that clockwise rotation was equal to the anti-clockwise rotation through NMR experiments.(263)

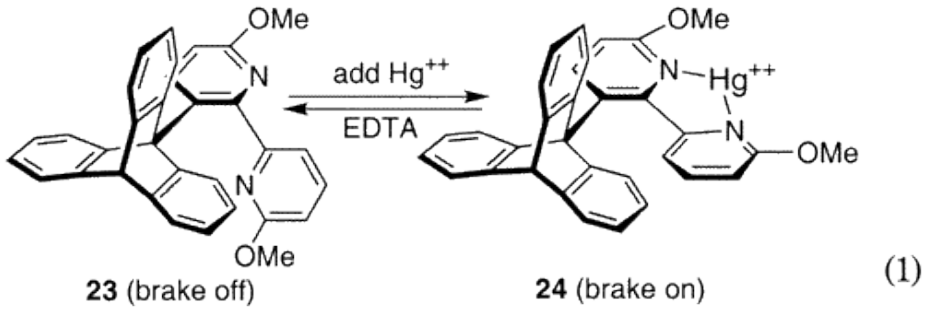

Figure 5.2 – Triptycene motor using mecuric ion and EDTA to control the rotation. Adapted with permission from Kelly *et al.*, 2001. Copyright (2001) American Chemical Society

Dahl *et al.* built a new molecular machine (Figure 5.3) with the intention of showing unidirectional rotation.(67) The machine is grounded on supramolecular disateroselectivity structure, one could identify the rotation direction through observing reaction rates; with 2aR (R axial chirality) rotation speed different to 2aS path (S axial Chirality). However, the authors pointed out the disatereomers were not uniformed and the ratio of disatereomers cannot be determined due to the conversion from step 1 to step 2aS or 2aR and reverse was too fast to observe. Fletcher *et al.* approached Feynman ratchet and pawl with a new molecular machine (Figure 5.4) which builds upon the idea of Dahl.(264) Fletcher's machine and successfully demonstrated the unidirectional molecular rotor through 4 steps chemical step. The rotation occurred around the C-C single bond, where a lock and swing mechanism minimised reverse motions. Fletcher built the molecular machine based on stereoselectivity and regioselectivity, and powered by consumption of (s)-2-methyl-oxaborolidine and borane. Although a complete 360^0 unidirectional

rotation is achieved, the whole rotation process is not instantaneous and required time and multiple chemical reactions to achieve each step.

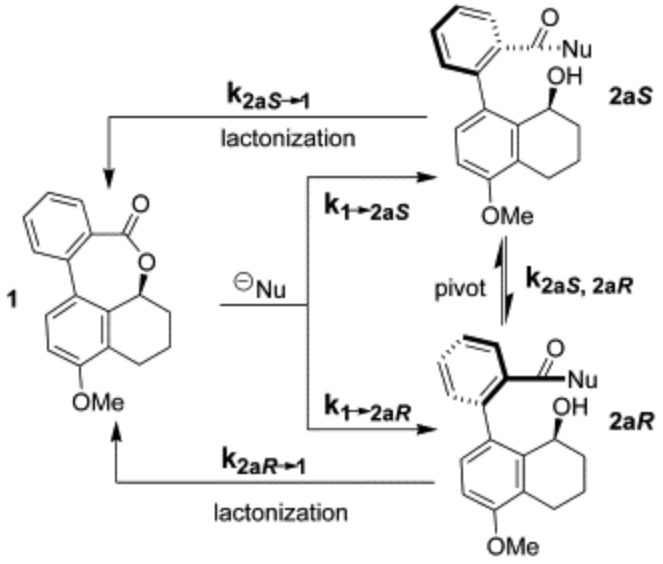

Figure 5.3 – Lactone molecular motor rotation induced by nucleophile (Nu^-) i.e N-O-dimethylhydroxylamine, LiOH. The directional rotation depends on the diasteromer once the lactone bond reacts with the nucleophile. Adapted with permission from Dahl *et al.*, 2005. Copyright (2005) Elsevier(67)

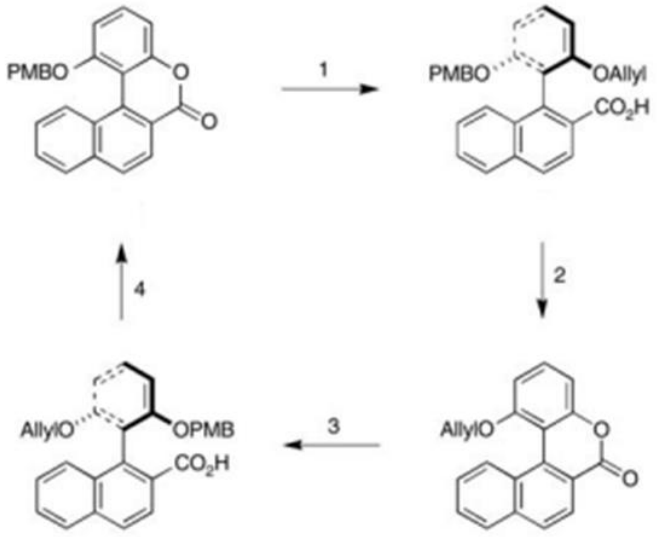

Figure 5.4 – Rotation steps of 1-(4-methoxybenzyl oxy)-6H-naphth [2,1-c]chromen-6-one motor. The rotor involves 4 intermediates steps; in step (1), the motor ring opens by reduction of the lactone group, phenolic alcohols attached onto the rotational part of the motor (the motor operate in a solution of

toluene solution with (s)-2-methyl-oxazaborolidine and borane). In step (2), the protection group para-methoxybenzyl (PMB) is oxidised and undergo lactonization with the carbocyclic acid. In step (3), the lactone is reduced by the (s)-2-methyl-oxaborolidine and borane, PMB re-attached as a protection group and swings across. In step (4), the deportation of the phenol by removing ally group with $Pd(PPh_3)_4$ and the cycle is regenerated to the original form 1. Adapted with permission from Fletcher *et al.*, 2005. Copyright (2005) The American Association for the Advancement of Science.

Koumura *et al.* reported a light driven molecular motor in 1999 and presented a new era of conformation control of synthetic molecular machines by using cis-trans isomerisation and inducing different electromagnetic wavelength under different temperature to achieve rotation.(56) Few years later, Feringa and colleagues developed multiple versions of light driven switches, which were designed to positional lock by steric hindrance and proton transfers after UV light initiate positional change (Figure 5.5).(53, 244) Klok *et al.* further developed and devised a modified version of the switch and built a rotary motor that operate under room temperature (Figure 5.6) by removing one end functional group, which reduced the steric hindrance and lower conformation energy barrier height.(243) The authors characterised the molecular machine with NMR and concluded that it has capable of achieving 3 Mhz rotation. Different function group on the stator (lower part of the machines in Figure 5.6) were tested in order to find the best conformation for rotation. Delden *et al.* attached the light driven rotor onto gold nanoparticle surface with organic alkane chains and proposed the synthesised method can enable large ensemble of functionalised molecular mechanical devices to be attached on metal surface.(68)

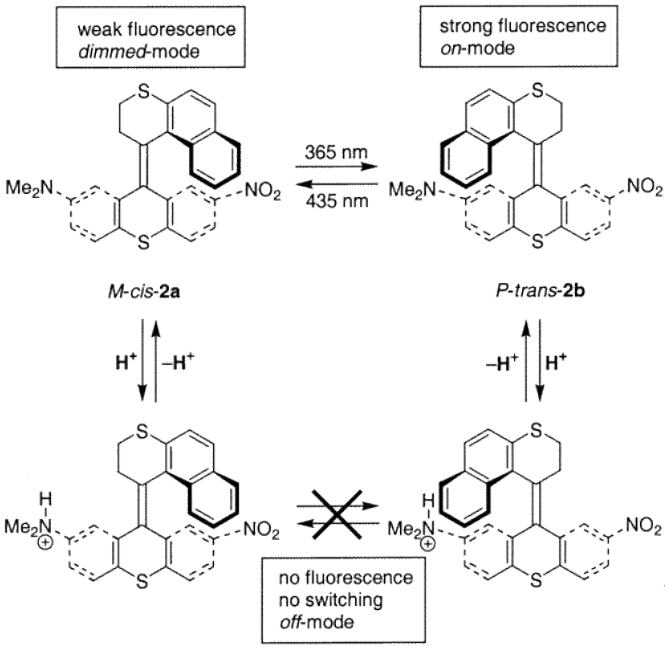

Figure 5.5 – Schematic representation of light induce molecular switch controlled by absorption of different UV light wavelength and concentration of H^+. Adapted with permission from Feringa, 2001. Copyright (2001) American Chemical Society [244].

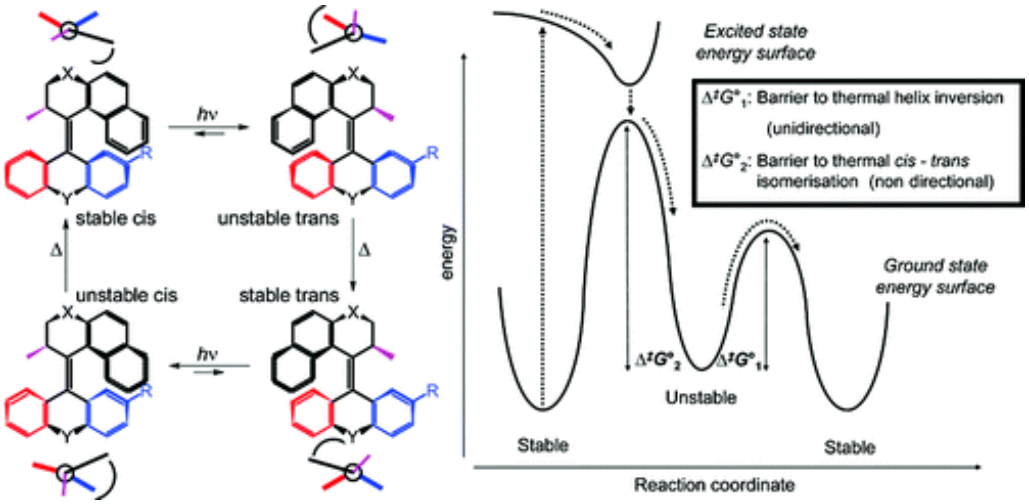

Figure 5.6 – Schematic representation of controlled light induces rotor cycle (left) and free energy diagram (right). The sequence of rotation initiate by photochemcial cis-trans isomerisation and thermal helix inversion. Adapted with permission from Ruangsupapichat *et al.*, 2008. Copyright (2008) American Chemical Society. (243)

The previous mentioned light driven molecular rotors are unidirectional, but the motion is not reversible. Ruangsupapichat *et al.* revealed by adding Lewis base

solution as a catalyst, clockwise and anticlockwise unidirectional rotation is achievable (Figure 5.7).(69) The based solution changed the motor to its opposite enantiomer conformation, thus the structural change leads to the directional changes of the rotation. Similar conformation changes that affect the rotation were found on different motor by Greb *et al*., the authors managed to reduce the steps required for a rotation while retaining unidirectional rotation.(265)

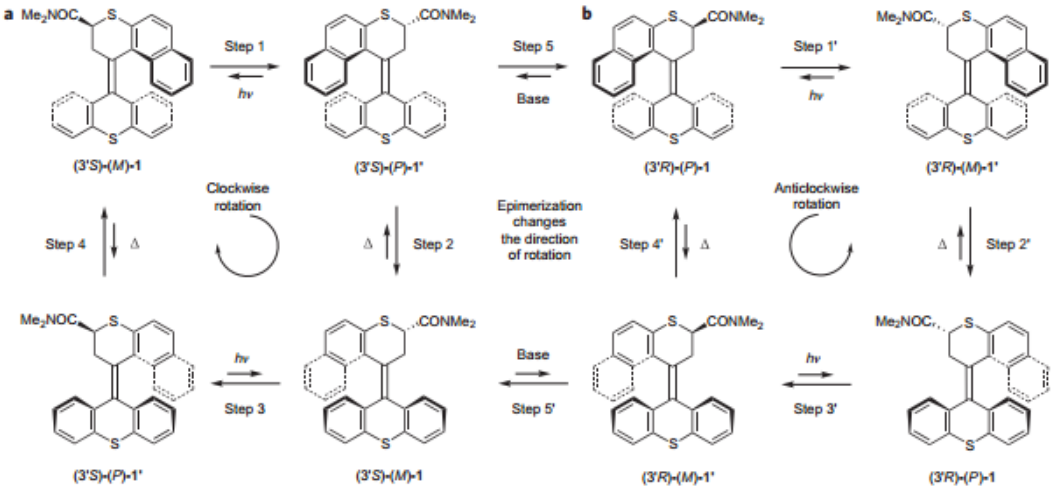

Figure 5.7 – Schematic representation of clockwise and anti-clockwise rotation of light induced molecular motor. The clockwise rotation is initiated from the stable position (3'S)-(M)-1 and through photochemical isomerisation (step 1) to give (3'S)-(M)-1 followed by thermal isomerisation (step 2). The consecutive repeats of photochemical (step 3) and thermal isomerisation (step 4) reverted the motor back to original position. The initiation of anti-clockwise rotation with the same molecules requires the opposite enantiomer at the less stable (3'S)-(P)-1' by using base-catalysed epimerization (step 5). Full anti-clockwise rotation (steps 1' – 4') proceeds analogously to the clockwise rotation steps. Reversion from anti-clockwise to clockwise position must use base-catalysed isomerisation at the less stable rotor position (3'R)-(M)-1'. Adapted with permission from Ruangsupapichat *et al.*, 2010. Copyright (2010) Springer Nature (69)

Thus one could see it is difficult to control the rotation of a molecular machine without a double bond or a ratchets system. Bedard *et al*.(192) designed and synthesised a molecular turnstile encased with organic chemical (Figure 5.8). The alkyne in the compound ensured the turnstile retained rigidity along the plane and

allowed free rotation by the benzene ring. They designed and synthesised the group R in the figure (Methyl, bromine, and so on…) to be influenced by ferroelectric liquid thus one could control the rotation speed. Following on the idea, Hsu *et al.* investigated the idea of electric revolving door (Figure 5.9) inspired by Bedard's organic structure through simulation.(194) Hsu discussed with the electric field $\geq$ 0.2 V/$\dot{A}$, molecule 4 (Figure 5.9) was able to exhibit open and close revolving door motion, and mentioned if the pore is too close to the outer ring, the steric repulsion between the hydrogen atoms of the outer ring and the hydrogen (fluorine) atoms of the inner benzene (the distance $\leq$ 1.8 $\dot{A}$) significantly raised the rotation barrier energy.

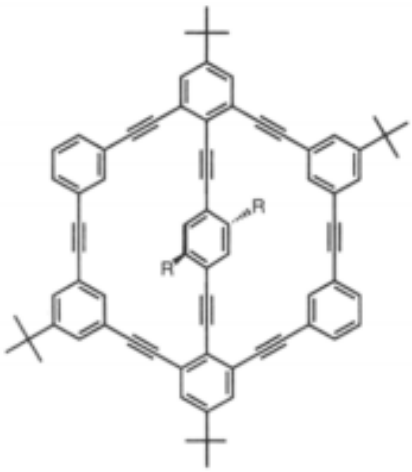

Figure 5.8 – Molecular turnstile with inner molecules rotates on the triple bond axis with R design to be replaced with functional group such as CH_3, F, etc. Adapted with permission from Bedard *et al.*, 1995. Copyright (1995) American Chemical Society(192)

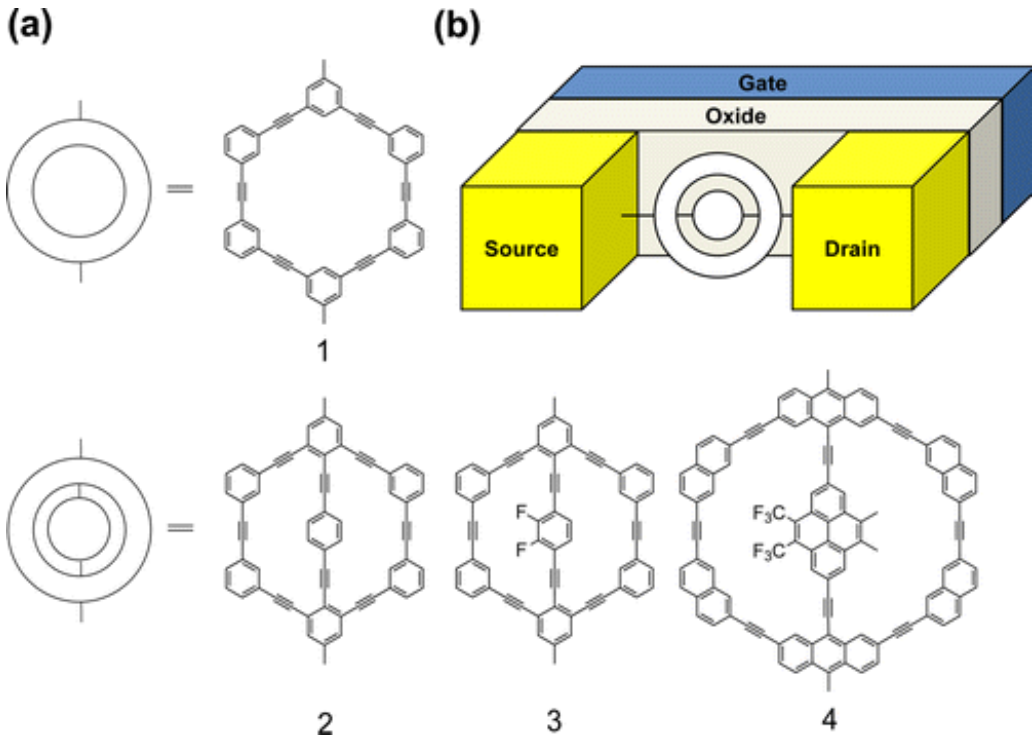

Figure 5.9 – (a) Molecular turnstile candidates for electric revolving door in (S-MERD), molecules 1 represents the frame of the revolving door and molecules 2-4 represents the door rotate on the triple bond axis (b) Illustration of S-MERD with molecules 1-4 linked to two electrodes. Adapted with permission from Hsu *et al.*, 2013. Copyright (2013) American Chemical Society.(194)

Zheng *et al.* synthesised similar inner rotors to Hsu (Figure 5.10) and reported molecular rotors responded to electric field.(193) They mounted the molecular turnstile onto a gold plate and a current 200 pA with voltage 200 mV applied send through which induced electric field. It is reported the 'blinking' effect during Scanning Tunnelling Microscope (STM) and Barrier Height Imagining (BMI) are due to the rotation of the turnstile. Horinek and Michl further investigated the effect of the molecular machines through molecular dynamic simulation and applied 1 to 5 V nm^{-1} of alternating electric field upon the turnstile.(142) Horinek concluded on the importance of conformation diastereomers as it affects the free energy rotational barriers. Thus this explains only a fraction of molecular machines

responded to the electric field in the experiment by Zheng; because the synthesised of the molecular rotors are not uniform diastereomers.

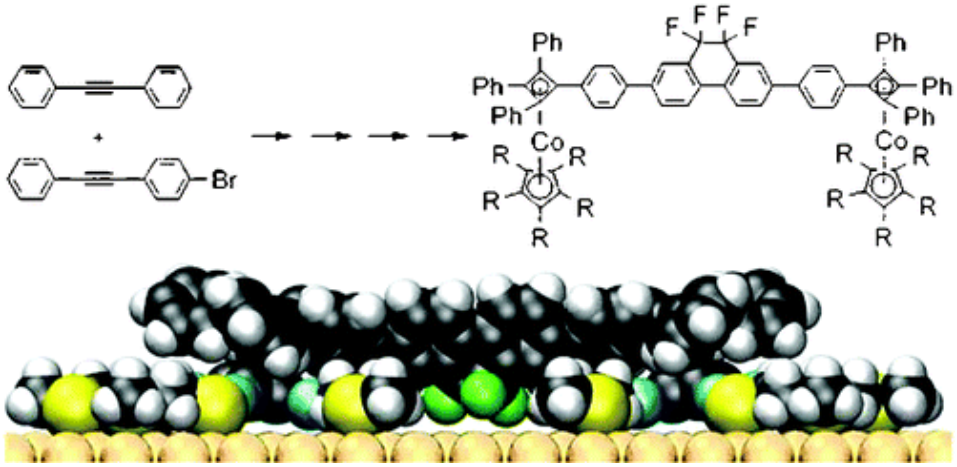

Figure 5.10 – Illustration of unidirectional rotor under the alternate electric field with frequency of 90 GHz and 6 V/nm. Adapted with permission from Zheng *et al.*, 2004. Copyright (2004) American Chemical Society. (193)

Seldenthuis *et al.* simulated a theoretical molecular turnstile (Figure 5.11) by using DFT calculation and Green's function method, Seldenthuis calculated the force required for the turnstile to rotate is around 4 V/*Å*.(58) However, the simulation environment operated at 15K and free rotation occurred at 77K in or absence of driving force. Therefore, the authors proposed to replace anthracene (Figure 5.11, left) with pyrene (Figure 5.11, right) to decrease steric hindrance between the rotor and the axles. The changes increased the rotational barrier (15.9 kcal mol^{-1}), preventing free rotation of the motor at room temperature. However, these changes consequently increased the critical electric field to 17.5 V $Å^{-1}$ at 300K.

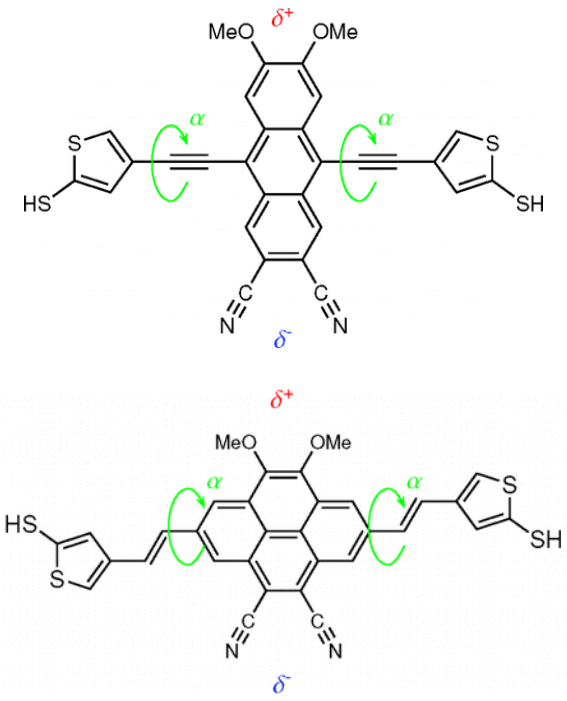

Figure 5.11 – Molecular turnstile chemical structure (left) ,10-bis((5-mercapto-3-thiophen-3-yl)ethynyl)-6,7-dimethoxyanthracene-2,3-dicarbonitrile, (right) 2,7-bis((E)-2-(5-mercaptothiophen-3-yl)vinyl)-9,10-dimethoxypyrene-4,5-dicarbonitrile) Adapted with permission from J. S. Seldenthuis *et al.*, 2010. Copyright (2010) American Chemical Society(58)

5.3.2 Application of Molecular Machines

Restriction on the thermal movements of various submolecular components or exploitation of thermal motion with additional ratcheting remains the main procedure to extract useful work at molecular scales. For any practical applications, the integrity of the molecular system must be conveyed to macroscopic world. Thus, the challenge of constructing devices with physical implications, which in turn, put further demands on the fidelity of the molecular-level mechanical processes over a range of conditions. Here, I am going to give examples of current applications of molecular machines to produce a functional property change or performed a physical task.

Stimuli-induced cessation of rotation motion can be employed as a chemical detector. Glass and Raker developed a sensor which exploits allosteric binding effects achieved in molecular brakes (Figure 5.12) with multiple binding site.(266, 267) The first dicarboxylate group binds onto the guanidinium group and freeze the rotational freedom; the restriction pre-organized and favours the receptor for a stronger second binding. When the two fluorophores in proximity hold by single dicarboxylates monomer, the fluorescence emission spectra in machines is changed. The change of emission is therefore measured and leads to identification of specific short dicarboxylates in a mix aqueous solution of monocarboxylates. Glass and Raker further proposed the sensors can be tailored through the binding sites and distance between them to match for a specific dicarboxylate.

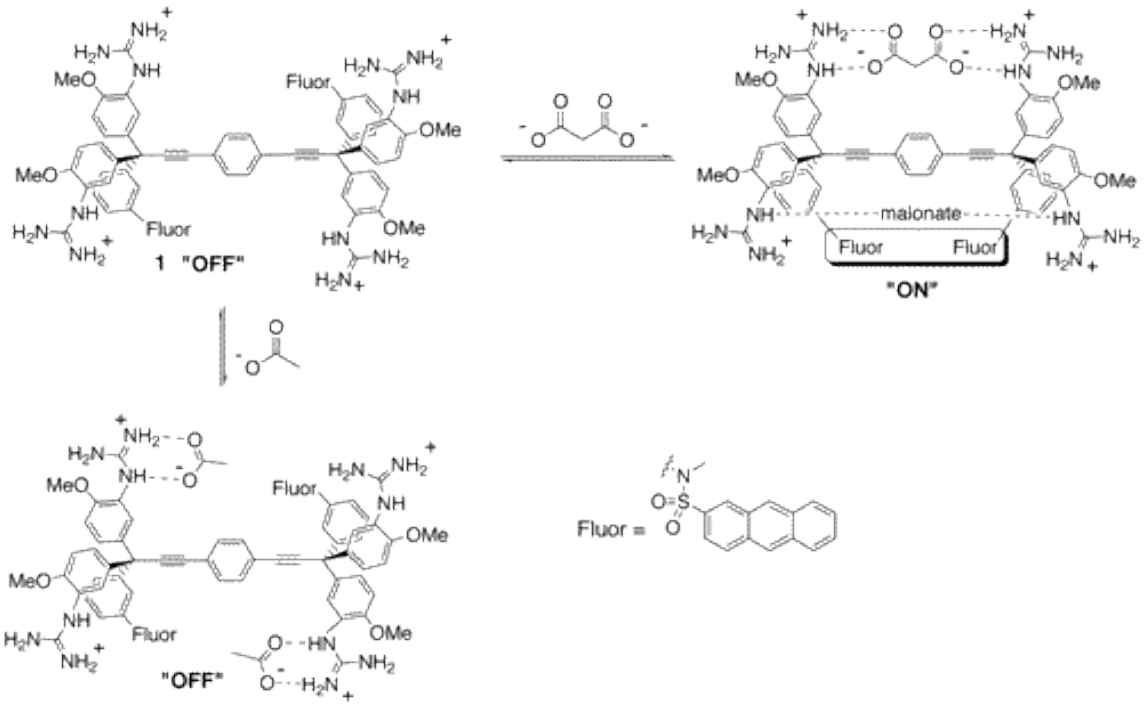

Figure 5.12 – Illustration of molecular sensor. The rotation stopped by the designate length of dicarboxylates molecules and the reduce rotation is detected through fluorescence emission spectra. Adapted with permission from J. Raker *et al*., 2002. Copyright (2002) Springer Nature (267)

With the previously discussion on light induced unidirectional motor (Figure 5.5), Eelkema *et al.* demonstrated uniformed rotation of a glass rod on a nonpolymeric liquid-crystal film doped with light driven motor (Figure 5.13).(64) Upon irradiation of the film with ultraviolet light, a photochemical isomerisation around the central double bond occurs resulting in changing the organisation of the liquid crystal. The rotation process gradually decreases until the process halts after about 10 mins, consequently this indicates photostationary state are being reached. It is demonstrated that collectively the molecular machines can move an object that is many time bigger than the machines.

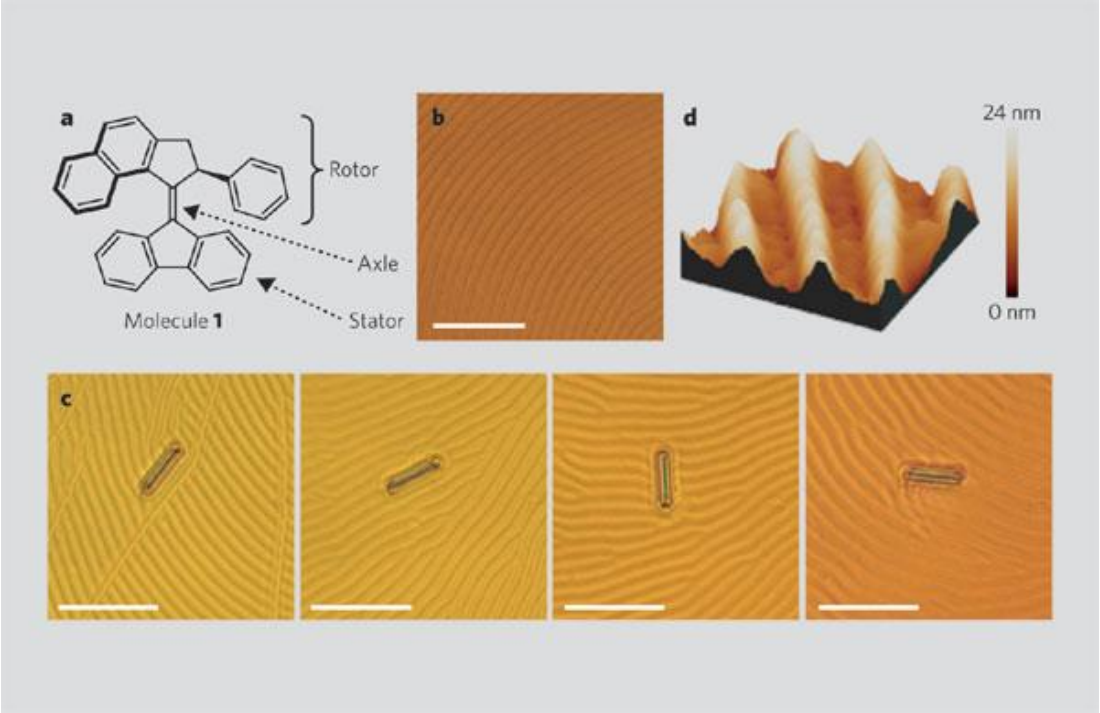

Figure 5.13 – a) Schematic representation of the light motor b) Liquid – crystal film doped with molecule (1% by weight) 1 c) Glass rod clockwise rotation from left to right under irradiation with UV light, each frame taken at 15-s intervals d) Surface structure of the liquid – crystal film. Adapted with permission from R. Eelkema *et al.*, 2000. Copyright (2000) Springer Nature (64)

A monolayer of photochromic azobenzene unit (Figure 5.14) provided a reversible photoisomerisation which controlled the motion of liquid droplets. Ichimura *et al.*

deposits a drop of olive oil on the all-cis surface and illuminated asymmetric UV light with the wavelength of 436 nm so that more isomerisation occurred at one end.(268) Cis rich state transformed back to Trans state by illuminate blue light with wavelength 436 nm. By repeating the process, one could use the asymmetric light to "chase" the droplets across the membrane surface. The potential application can be demonstrated in several ways; a liquid droplet could be used to transport millimetre-size glass bead across the surface; the approach could be used for transportation liquid in a functionalised capillary tube; thus, it could perform a chemical reaction by bringing two droplets together.

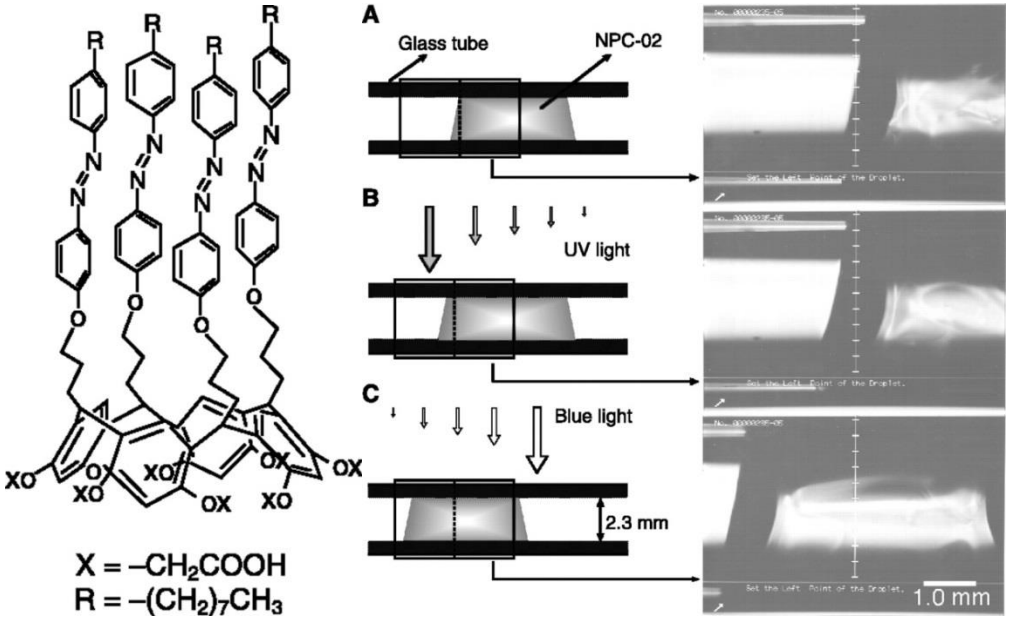

Figure 5.14 – Structure of the molecular machines on the glass tube inner surface (left) and the movement of the oil (NPC-02) droplet in the glass tube (right) due to irradiation of UV and Blue light. Asymmetric magnitude of UV and blue light move the droplet around the surface. Adapted with permission from K. Ichimura *et al.*, 2000. Copyright (2000) The American Association for the Advancement of Science. (268)

Seo *et al.* synthesised a simplistic model of a molecular gate that responses to the guest molecules inclusion.(106) The gate has a rotatable pillar made out of 2,5-Bis(2-hydroxyethoxy)-1,4-bis(4-pyridyl)benzene with ethylene glycol arm acts as

the locking/unlocking gate (Figure 5.15). The guess molecules (water) distorted the octahedral environment of the Cd^{2+}, once it is saturated the gate open and allows the guess molecules through the channel. Thus, one could control the microscopic environment condition based on saturation of the guess molecules.

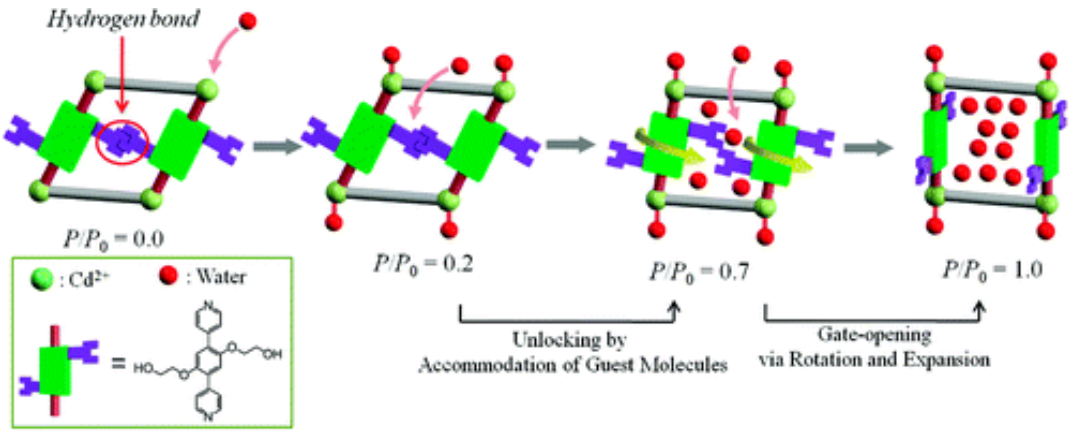

Figure 5.15 – Illustration of water molecules adsorb onto the molecular gate metal site and reconfigured the geometry position of the gate. Adapted with permission from J. Seo *et al.*, 2009. Copyright (2009) American Chemical Society.(106)

5.4 Molecular Machines in MOFs

This review will introduce the recent exploration of molecular machine built within MOF. Molecular machines are integrated into the MOFs by either pre-synthesis the machines within the linkers and self-assembly in a heated bath or post-synthesis MOF and attached the machine onto the un-coordinate metal site. Currently, this area of science is still in the early stage of development, therefore, there are limited literatures regarding this technology.

5.4.1 Metal Organic Rotaxane Frameworks (MORFs)

Mechanically Interlocked Molecules (MIMs) such as rotaxane and catenanes has received high interest since the beginning of 1990s, this is due to their intriguing structures as well as their potential applications. Here, at the beginning of 2000s,

Lee *et al.* were interested in the poly-rotaxane and experimentally demonstrated the supramolecular machines can self-assemble to a 2 dimensional structure that resembles to MOF (Figure 5.16), as the rotaxane formed coordination bonds with Cu ions. The new poly-rotaxane is named as Metal Organic Rotaxane Frameworks (MORF).(269)

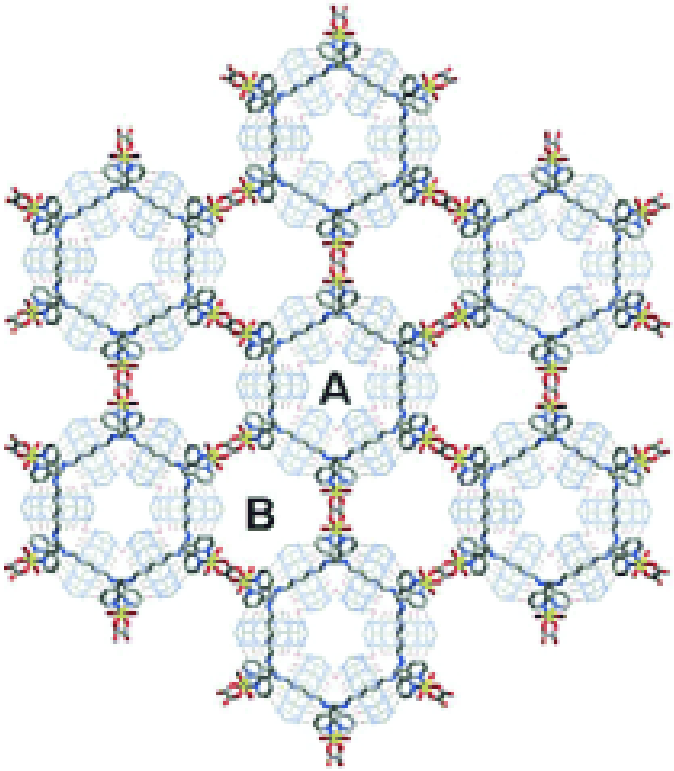

Figure 5.16 – The polyrotaxane self-assembles with Cu ions to form a 2D structure, where there are two different size channels shown as A and B. The structure has a weak Vdw interaction with each layer thus can be stacked upon each other. Adapted with permission from E. Lee *et al.*, 2001. Copyright (2001) Angew. Chem. Int. Ed.

Later on, Loeb and colleagues created a 3D polyrotaxane structure by assorting different linkers. The structure has a permanent porosity with the rotaxane ring are still able to be detect through C^{13} NMR.(71, 72) However, a major setback in the current structure is the high sensitive to the environmental changes and breakdown when the temperature is beyond ~498 – 523 K. This is due to the inherit problem

where the rotaxane ring interfered with the co-ordinate bond between the linkers and metal ions, thus weaken the overall structure stability.

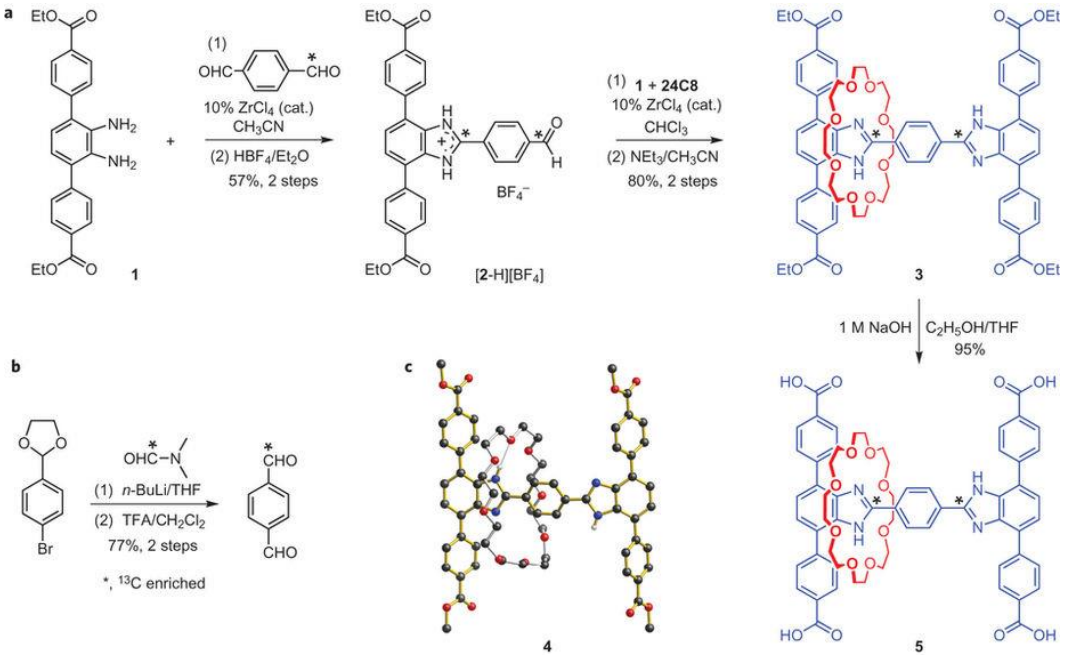

Figure 5.17 – a) Major steps in the synthesis of a molecular shuttle MOF linker comprising a rigid H-shaped axle with two benzimidazole recognition sites, four carboxylic acid groups for coordination to metal ions and a [24]crown-8 ether wheel. b) The synthetic route used to label the MOF linker with 13C enrichment to aid in characterization of the shuttling motion by 1H-13C CP/MAS SSNMR. C) A ball-and-stick representation of the single-crystal X-ray of 4, the tetra-methylester version of the tetra-carboxylic acid MIM linker 5. THF, tetrahydrofuran; TFA, trifluoroacetic acid. Adapted with permission from K. Zhu *et al.*, 2015. Copyright (2015) Nature chemistry. (270)

In the latest work, Loeb *et al.* overcame the interference of the rotaxane ring on the coordinate site by synthesising a rigid H shape linkers with 4 carboxylic acid group to form a coordinate bond with metal ions (Figure 5.17).(270) This design removed the interference by the vibration of the ring and thus allowed further stability in the crystal. This linker formed a MOF structure that resemble to IRMOF-15 and exhibited stability for a prolong exposure in solution at 358 K for 48 hours.

5.4.2 Functionalised molecular machines in MOFs

In general, most of the MOFs are classified as mono-functional. There have been several investigations on synthesising multi-functional MOFs, either adding functional group onto the bridging ligands or adding an extra ligand branch to post-synthetic MOFs.

It is common to functionalise the bridging ligands of the MOFs post-synthesises. Functionalising bridging ligands enhanced the adsorption characteristic of CO_2 in MIL-53(Al^{3+}) MOFs as this was reported by Torrisi. By simply adding a functional group OH^-, $COOH^-$, NH^{2-}, and CH_3^- to the bridging ligands, they found the enthalpies of adsorption are stronger than the original MIL-53 with bare open metal sites. The result was confirmed by DFT geometry optimisation and energy calculation. $COOH^-$ functionalisation yielded the strongest binding to CO_2 with binding energy -21.5 kJ mol^{-1} whereas original yielded -11.9 $kJmol^{-1}$. Same concept was also applied in NH_2 and CH_3 functionalisation to increase H_2 adsorption.

Panda *et al.* experimentally functionalised amino acid group onto the ligand in Zeolitic Tetrazolate Framework 1 (ZTF-1) before synthesis.(271) Resulting amino group formed a strong co-ordinate bond with the metal Zn ions, effectively increasing the CO_2 uptake to 5.6 mol kg^{-1} of framework with the binding energy of CO_2 approximately -25.4 kJ mol^{-1}. Similar procedure was used on IRMOF series and the increased adsorption of CO_2 confirmed by Zhang.(272)

Functionalisation of ligands are not limited to any particular MOFs; In IRMOF series, it is particularly common to form a MOF using the organic ligands 2,5 – dioxidoterephthalate. Chemically speaking, the hydrogen in the benzene ring is particularly easy to replace by a functional group or more electronegative elements.

Henceforth, some MOFs that considered being inert (Zr – based UiO-66 MOF) can be functionalised and became chemically active. In a computational study of UiO-66 after functionalisation, the authors mentioned that functionalisation of $–SO_3H$ and $–CO_2H$ in the MOF increased the selectivity of CO_2 within the CO_2/CH_4 mixture. Another study showed functionalisation on the organic ligand by using halogen can reduce the energy band gap to conduct electricity, thus one can use MOFs to design conductive membranes for fuel cells.

It is equally possible to functionalise the open metal site within MOFs. The open metal sites provided a good binding site for negatively charge molecules (i.e. amines and alkoxysilane functional group). However, the bond is relatively weak because it is not a full covalent bond hence in comparison not as stable to functionalisation onto the bridging ligands. The additional functional group on the open metal site can help obtain stronger binding with adsorbates i.e. water to encourage a stronger bond with CO_2 adsorption. In the paper by Yazaydin and colleagues, they explained when water molecules attached to the metal open site, the coulombic force increased due to polarity of the water molecules which leads to stronger binding strength with CO_2 molecules.(210)

Li and Zhang *et al.* reported to successfully mount ethylenediamine onto the open-metal sites of MIL-101-Cr.(208) Ethylenediamine attached onto the metal open site enhanced the stronger binding with the CO_2 in comparison to the bare ion. The addition of the amine resulted in increased CO_2 storage by 150 wt%.

J. Fraser Stoddart, a chemistry Nobel Prize laureate regarding his work in molecular machines, collaborated with Farha group who synthesised a MOF which hosted a semi-rotaxane molecular switches.(70) In their work, they selected NU-1000 as a

host for semi-rotaxane molecular machines. NU-1000 is formed by a tetratopic 4,4′,4″,4‴-(pyrene-1,3,6,8-tetrayl)tetrabenzoate linkers (PyTBA) self-assemble with hexa-Zr-joints. The structure has a one-dimension hexagonal shape channel with the BET surface area of 2315 m^2 g^{-1}.(273) This MOF is versatile as it can be functionalised easily with different carboxylate group, as the carboxylate can form a coordinate bond with the Zr atoms in the metal corner cluster.(274) Thus, with those inherited function in the MOF, it is a promising candidate for hosting a semi-rotaxane group which contains a carboxylate functional group. (Figure 5.18)

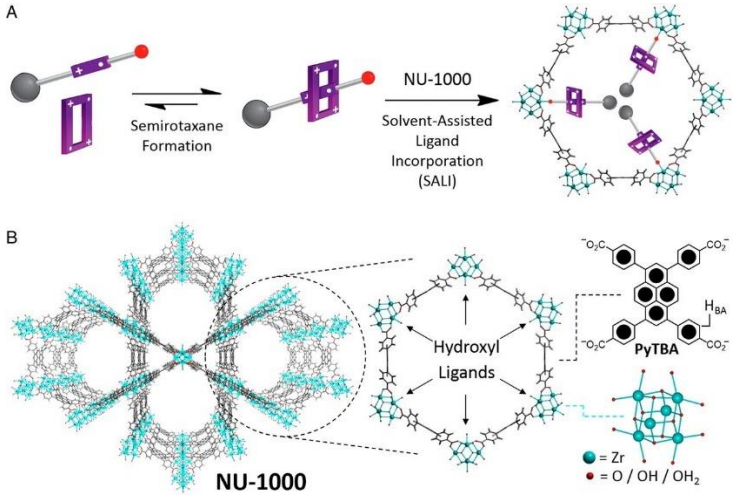

Figure 5.18 – The semi rotaxane formation a) and it is attached to NU-1000 through Solvent Assisted Ligand Incorporation (SALI). b) NU-1000 contains 6 sites where it can form a coordinate bond with the semi-rotaxane. Adapted with permission from P. R. McGonigal, *et al,* 2015. Copyright (2015) National Academy of Science.

5.5 Simulation Method

5.5.1 DFT Calculations

In order to assess the stability of a molecular gate mounted on Mg-MOF-74, we carried out DFT calculations. The crystal structure of Mg-MOF-74 was obtained from Cambridge Crystallographic Data Centre (CCDC).(275) There are 162 atoms

in a unit cell of Mg-MOF-74, and the unit cell dimensions and the angles are a=25.873, b=25.873, and c=6.930 and α=90.00, β=90.00 and γ=120.00, respectively. For the DFT calculations, Mg-MOF-74 unit cell was replicated 2 times in the z-direction to give a 1 x 1 x 2 structure. The gate was placed in one of the three channels of Mg-MOF-74 with the carboxyl groups positioned approximately 2.5 Å away from the magnesium atoms (Fig. 1c). The MOF-molecular gate complex was then geometry optimised (flexible cell) with periodic planewave DFT calculations using ultrasoft pseudopotentials with the CASTEP 16.1 software(276) with the gate molecule at different rotational angles with respect to the x-y plane. Details of convergence criteria are given in Appendix 9.1.1. The PBE functional(183) with semi empirical dispersion corrections derived by Tkatchenko and Scheffler (DFT-D2)(277) was used with the cut off energy and the k-point mesh set at 500 eV and 1x1x1, respectively. Binding energies of the gate molecule in the optimized configurations were calculated by subtracting the energies of the MOF and the gate from the energy of the MOF-molecular gate complex.

5.5.2 Molecular Dynamic Simulations

MD simulations were carried out with the GROMACS(278) software in order to investigate the effect of an external electric field on the molecular gates mounted on Mg-MOF-74. Because of the external electric field an additional force is exerted on the atoms due to partial charges. This force is calculated according to the following formula,

$$F_{ez} = qE_z$$

where F_{ez} is the force provided by the electric field, q is the partial atomic charges and E_z is external electric field. The total force acting upon an atom becomes:

$$\Delta F_z = -\frac{\partial U(r)}{\partial z} + qE_z$$

ΔF_z is the change of force at z direction upon an atom. $\frac{\partial U(r)}{\partial z}$ is the change of potential energy in respect to the change of z distance with the interacting atoms. Thus, this is applied to the Verlet algorithm during the integration of motion for the z direction component and it is changed according to the strength of the electric field.

Here, the molecules in the system is assumed not be ionised or polarised by the electric field, as this is not possible to calculate without the usage of ab initio molecular dynamics and system is too large for such calculation. Also, there is no polarised force field developed for MOFs thus polarised effect cannot be estimated. Furthermore, the screen effect in the system is ignored due to no mobile charge carriers and the gate molecules are relatively rigid within the framework. Thus, the Coulombic equation is sufficient to estimate the molecular interactions. The long range charge potentials were calculated by Ewald summations and it is rely upon to calculate the screening effect at long distance.

The electric field was applied in the z-direction which Mg-MOF-74 channels run through. Mg-MOF-74 unit cell was replicated 5 times in the z-direction to obtain a 1 x 1 x 5 structure. We considered two different gated structures; in the first one a single gate molecule was placed in one of the channels (Fig. 1c); and in the second one, a gate molecule was placed in each channel, resulting in a structure with all three channels occupied by the gate molecules (Fig. 1d). Furthermore, for the fully

gated complex we simulated a system with methane molecules present in order to investigate the possibility of controlling fluid transport in the channels of Mg-MOF-74. For this purpose a graphene wall was placed 2.5 nm away from the gate molecules, and the pore volume between the graphene wall and the molecular gates was saturated with methane such that the distance between the centre of methane molecules and the centre of atoms of MOF, graphene wall and the gate molecules was slightly larger than the sum of their van der Waals radii. Here, there are no partial charge are given to the graphene wall and is set to have no interaction with the MOF frameworks. Furthermore, the graphene is not considered as a conductor. Thus, the graphene is only used as an artificial wall to keep the methane molecules between the gate molecules and ensure no diffusion through the periodic box at z direction. In total 103 methane molecules were inserted. UFF(176) force field was used to model the MOF and the gate molecules and the graphene wall. MOF and the gate molecules were treated as flexible bodies. Methane was modelled as an united atom and it is described by the TraPPE force field.[279] The REPEAT[280] method was used to derive partial atomic charges by fitting them against the periodic electrostatic potential of the optimized MOF-molecular gate complex at the closed configuration obtained from DFT calculations. Duration of the MD simulations ranged from 1 to 30 ns. Verlet velocity algorithm[281] was employed to integrate Newton's equation of motion with a time step of 1fs. The cut-off distance was set at 12 Å. MD simulations were run at 298 K and 0 bars in the NPT ensemble using a Nose-Hoover thermostat and barostat for the MOF-molecular gate systems with no methane molecules; whereas, the system with the graphene wall and the methane molecules were simulated in the NVT ensemble.

5.6 Results and Discussion

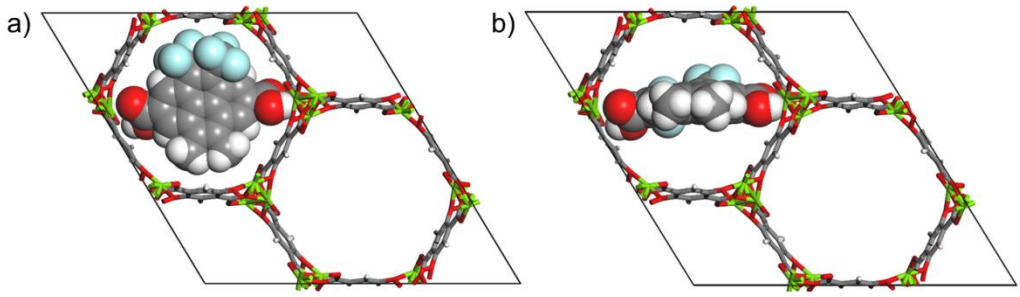

Figure 5.19 – a) DFT optimized closed gate configuration and b) open gate configuration. Atom colours are same with those in Figure – 5.1.

Closed (Figure 5.19a) and open (Figure 5.19b) configurations of the MOF-molecular gate complex with one gate molecule were optimized with periodic dispersion corrected DFT calculations. Binding energies of the gate molecule in the closed and open configurations were calculated as -357 kJ mol^{-1} and -278 kJ mol^{-1}, respectively. These indicated that both the closed and open gate configurations were stable and the gate molecule binds to the MOF strongly. Furthermore, the MOF-molecular gate complex preserved the original hexagonal shape of the Mg-MOF-74 channels. For instance, for the closed gate configuration the cell dimensions and the angles showed small deviations with respect to the experimental values and changed from a=25.873, b=25.873, and c=13.860 to a=26.526, b=26.345 and c=13.861 Å, and from α=90.00, β=90.00 and γ=120.00 to α =90.30, β=89.68 and γ=121.16, respectively.

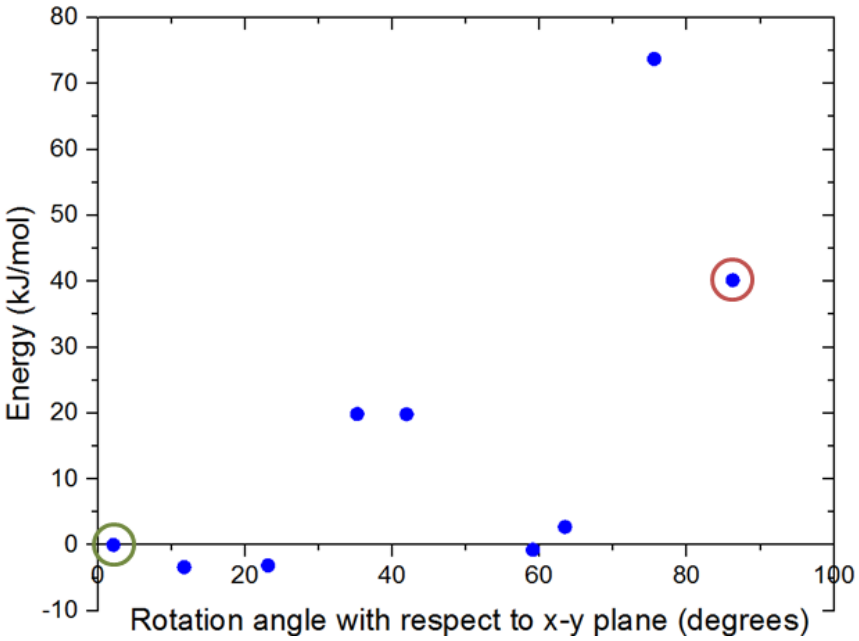

Figure 5.20 – Energy variation of the MOF-molecular gate complex with the rotation of the gate molecule with respect to the x-y plane predicted by DFT calculations. The closed gate configuration, which was taken as the reference point, is circled with green and the open gate configuration with red.

Figure 5.20 shows the changes in the total energy of the complex obtained by DFT calculations with respect to the closed configuration as the molecular gate rotates until it reaches to the open configuration. Two rotational barriers were identified, one is 20 kJ mol^{-1} and located around 40 degrees, and the other one is 73 kJ mol^{-1} and located at 75 degrees. Closed and open configurations of the MOF-molecular gate complex with one-gate molecules were also optimized with classical MD simulations in the NPT ensemble. Binding energies of the molecular were -203 kJ mol^{-1} and -126 kJ mol^{-1} for the closed and open configurations, respectively. These values are lower than those obtained by the dispersion corrected DFT calculations; but still indicate the molecular gate is predicted to bind strongly to the MOF in classical MD simulations. The stability of the MOF-molecular gate complex with one gate molecule was further tested under increasing electric field strengths. It was found that the complex retained its structural integrity up to 8 V nm^{-1}. On the other

hand, the minimum electric field to overcome the intrinsic rotational barrier of a single molecular gate and bring it from the closed to open configuration was found to be 0.5 V nm^{-1}. A system with all three channels occupied by molecular gates was also considered (Figure – 5.1d). Figure 5.21 shows the total energy of this system with the electric field (3 V nm^{-1}) turned on and off with consecutive periods of 1 ns. The simulation started with molecular gates at their closed configurations and run for 1 ns. Then the electric field was turned on in the z-direction for 1ns during which the molecular gates switched to their open configurations. When the electric field was turned off for the next 1 ns, the molecular gates reverted back to their closed configurations. The energy difference between the closed and the open configurations was about 350 kJ mol^{-1}.

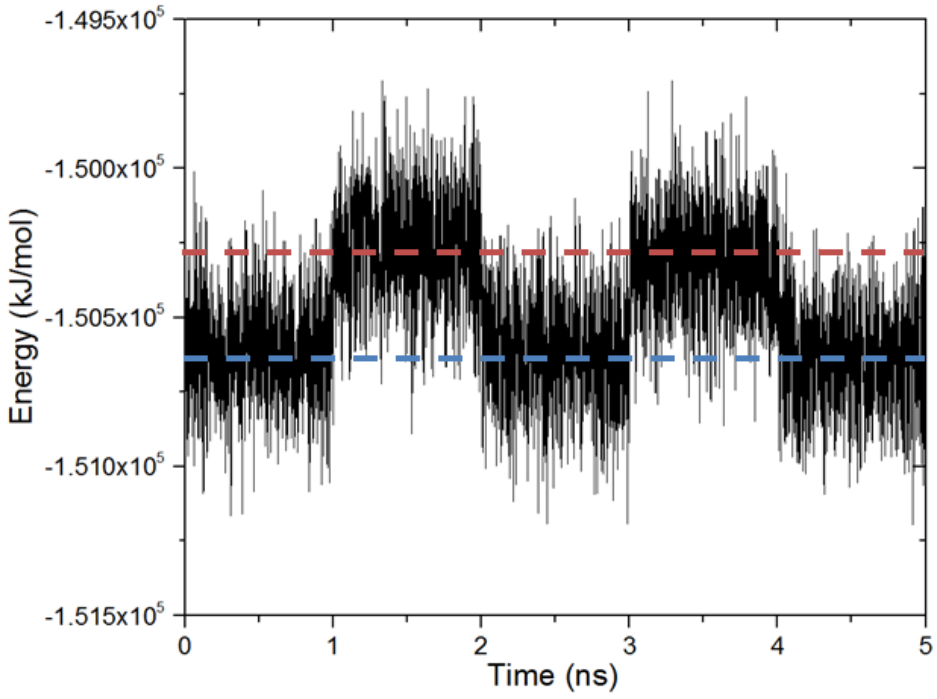

Figure 5.21 – The energy of the MOF-molecular gate complex with all three channels occupied by the molecular gates form the MD simulation. An electric field with a 3 V nm^{-1} strength turned on and off with consecutive periods of 1 ns. The gate is at the closed configuration when the electric field is turned off (blue line) and at the open configuration when the electric field is turned on (red line).

5.6.1 Channel porosity control through electric field and methane simulation

The complex with all three channels occupied by the molecular gates was further tested with methane molecules placed between the gates and the graphene wall in an NVT ensemble MD simulation (Figure 5.22a). First, the system was simulated with the gate molecules in the closed configuration for 30 ns and no electric field was applied. The molecular gates resisted to rotation despite the pressure due to the presence of methane molecules and remained in closed configuration as shown in Figure 5.22a. During this period no methane molecules diffused to the empty pore volume behind the gates. This was visually confirmed and quantified with the number density of methane along the z- direction (Figure 5.23a). Then the electric field in the z-direction was turned on (3 V nm^{-1}) and the system was simulated for another 30ns. With the electric field turned on, the molecular gates switched to open configuration (Figure 5.22b) and the methane molecules diffused to the empty pore volume (Figure 5.23b).

It should be noted that gate effects reported in the MOF literature are substantially different than the molecular gate concept we present in this study. Rather than involving a door type mechanism which opens and closes, previously reported gate effects were all based on either the reorientation of ligands or a shift in the topology of the structure, such that the pore volume decreased or increased up on exposure to external stimuli, e.g., gas adsorption or light.[105, 107, 138] To the best of our knowledge, this is the first specific molecular gate design in MOFs dedicated to open and close the MOF pores for diffusion of molecules without the MOF undergoing any structural change. Overall, the MOF-molecular gate complex we designed resembles a butterfly valve mounted inside a pipe in order to regulate or

prevent flow. By employing different functional groups it would be possible to adjust the electric field required to open or close this nanovalve. One could also imagine controlling the degree of opening of the valve by applying an electric field with different angles with respect to the x-y plane and thus regulating the flow rate.

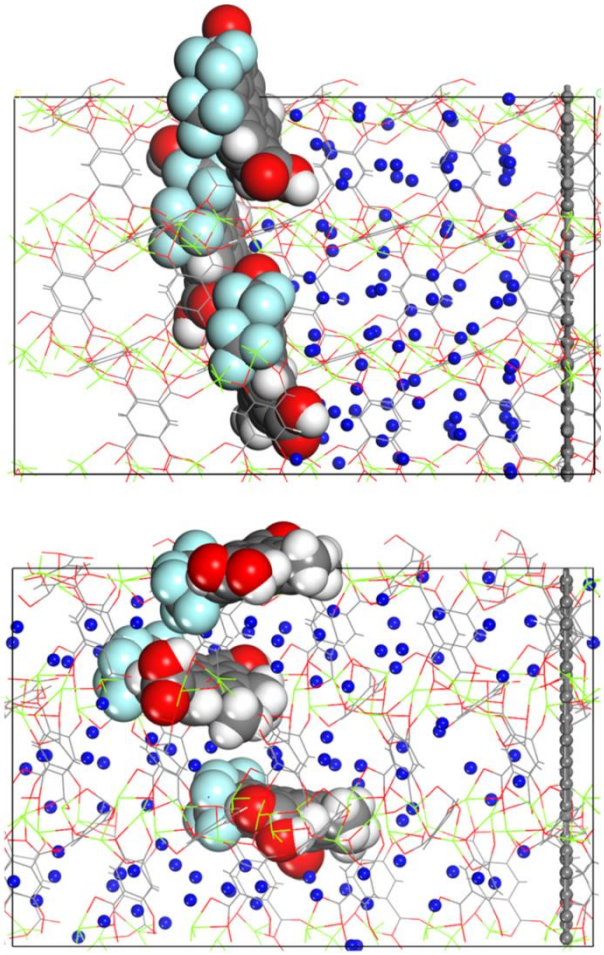

Figure 5.22 – a) Methane molecules placed between the molecular gates and the graphene wall, and b) molecular gates switched to their open configurations and the methane molecules diffused towards the empty pore volume after the electric field was turned on. Methane molecules (blue), all other atom colours are same with those in Figure – 5.1

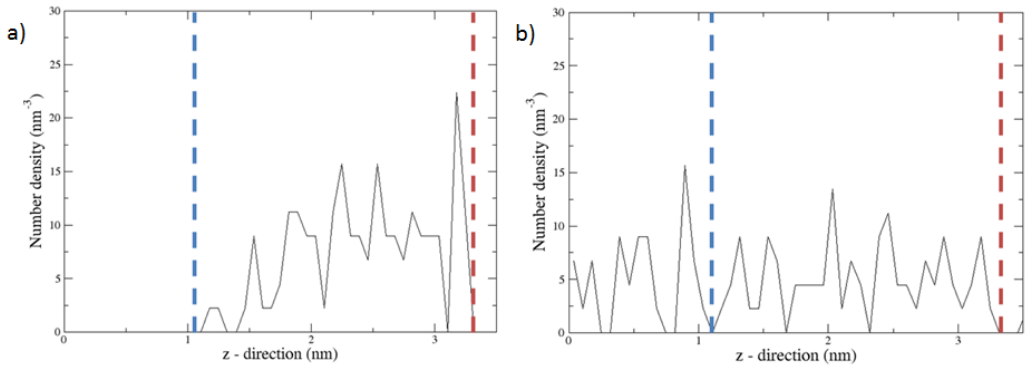

Figure 5.23 – Number densities of methane along the z-direction averaged over 30 ns with the molecular gates are in a) closed configuration and b) open configuration. The blue and red dashed lines represent the positions of the gate molecules and the graphene wall, respectively

We recognise that the synthesis of a device which integrates a MOF and a molecular gate responding to an external electric field is a daunting task. However, there have been recent reports of experimental work which demonstrated the incorporation of molecular machines in MOFs. Stoddard and colleagues(51, 70) mounted rotaxane and catenane based molecular switches on the open-metal coordination sites of NU-1000 MOF.(273) Zhu *et al.* synthesized a molecular shuttle in the form of a crown-8 wheel which moved back and forth on the ligands of UWDM-4 MOF.(270) The use of an electric field as an external stimulus has also been demonstrated. Zheng *et al.*(193) used the tip of a scanning tunnelling microscope (STM) to create an electric field in order to switch the configuration of a fluorine functionalised phenanthrene molecular turnstile between two different stable positions. Remarkably, the strength of the electric field used in the study of Zheng *et al.*, which was 1 V nm^{-1}, compares very well with the range of electric field we used in our computational study. In another ground breaking study, again an STM tip was used to drag a molecular car over a distance of several nanometres.(59) At the very least these experimental studies suggest that the incorporation of more complex molecular machines controlled by an external electric field in MOFs, or in other

porous materials, such as the molecular gate we propose, can one day go beyond the level of conceptual design based on molecular simulations and become reality.

5.7 Conclusion

By taking advantage of open-metal coordination sites in MOFs we computationally designed a molecular gate mounted on MOFs. Mg-MOF-74, a MOF with hexagonal channels with open-metal coordination sites at each corner, was used as the host material. For the gate molecule 4,5-dimethyl-9,10-bis(trifloromethyl)pyrene-2,7-dicarboxylic acid was considered. This gate molecule has carboxyl groups to coordinate to the open-metal sites, a permanent dipole to respond to an electric field and a pyrene backbone to act as an axle. By carrying out dispersion corrected DFT calculations we showed that the gate molecule binds to the MOF strongly. MD simulations demonstrated that the gate molecules switch between two stable configurations, closed and open, by turning on and off an electric field. We then showed that this can be used to control the flow of methane molecules in the channels of Mg-MOF-74. The concept of electric field controlled molecular gates mounted on MOFs presented in this study can inspire the rational design of new molecular machines and nanodevices which can store, deliver and select molecules on demand and with atomic precision.

6 Grand Canonical Monte Carlo Simulations of Various Water Models in Zeolitic Imidazole Framework-8

Adsorption of different water model in hydrophobic ZIF-8 was studied by the means of Grand Canonical Monte Carlo (GCMC) simulation and continuous fractional component Monte Carlo (CFC MC). This study reveals the impact of different water models (SPC/E, TIP3P, TIP4P, TIP4P-EW and TIP4P-2005) and the framework force field evidently played a lesser role in finding the adsorption isotherm at experimental conditions. Through GCMC simulation, we found SPC/E and TIP4P-2005 shown good agreement with experimental adsorption data while the common water model TIP3P and TIP4P performed poorly in this hydrophobic framework. We confirmed our finding with CFC MC method and noted the strong adsorbate – adsorbate interaction was the driver to the formation of a stable water cluster in the hydrophobic pore.

6.1 Introduction

With the global demands for energy growing with population, there are exponential progress in the development for finding a clean and renewable alternative energy solutions. Economic and environmental conscience drives the search for efficient energy usage with the possibility to store and restore unused energy.(282, 283)

MOFs are one of the most exciting recent advance in nano porous materials science,(153, 196, 284) MOFs are crystalline materials formed by self-assembly of metal clusters and organic linkers via coordination bond. The topologies and energy landscapes are similar to those found in zeolites,(97, 285, 286) but it is

comparatively more flexible as the material have tailorable pore size, large surface area (up to 10,000 m^2 g^{-1}) and different pore geometries as well as thermal and chemical stability of the zeolites.(29)

Among the MOFs materials, ZIF-8 is a one of the most investigated MOFs because of its thermal and chemical stability, permanent porosity and uniform pore size.(97-99) It is assembled from a tetrahedral zinc metal centers and bridged by imidazolate linkers. The crystallized structure has a sodalite topology where the smaller cages are inaccessible to molecule intrusion. Whereas the larger cages (diameter of ~11.6 Å) are interconnected and accessible by the six-membrane ring opening (diameter of ~3.40 Å). Albeit ZIF-8 is considered as rigid, it has been known that the ring aperture linkers can rotate and open further; movement that reassemble to the opening of "saloon door" and molecules larger than the aperture can diffuse into the pore. Petroleum industry has undertaken great interest in the material as the restricted pore potential has the potential of separation by shape and size, thus can be used as an alternative to energy intensive separation.(7, 100, 108)

Another well-known property of ZIF-8 is the hydrophobicity and remains stable under submergence in water.(97, 287) Though the structure contains no hydrophilic functional group and have weak polarity, water can condensed in the pores of ZIF-8 under high pressure (>26.6MPa) and exhibit type V isotherm with hysteresis loop.(26, 27) Ortiz *et al.,* explored the idea of using hydrophobic with hysteresis cycle to store and recover mechanical energy.(26, 27) As mechanical energy supply to compress water into the hydrophobic material (intrusion) are stored, energy dissipate when the pressure release (extrusion). Thus, the act of sorption can be exploited as a spring, shock absorber or bumper.(26, 28) ZIF-8 can recover mechanical energy without notable irreversible structure deformation. This robust

material has shown to endure water intrusion-extrusion over several cycles with a repeatable energy storage yield close to 85% of the first cycle. (27)

In general, TIP4P is a widespread water model choice for water adsorption in the MOF community as this water model describes the structural properties of bulk liquid water in the best manner.(288) We noticed that there has been inconsistency during the selection of water model for computational simulation in ZIF-8. Ortiz *et al.* demonstrated that ZIF-8 and TIP4P water model in simulation and found the water model did not reflect experimental intrusion pressure.(4, 122) Zhang *et al.* further explored modulated water model such as TIP4P-EW(289) and TIP4P-2005(290) in ZIF-8, however their study did not reproduced adsorption isotherm at experimental pressure.(37) TIP3P water model is another popular choice of water model to use within MOFs community.(291, 292) Hu *et al.* utilized the water model in desalination simulations with ZIF-8 membrane.(22) Yet, in most of the studies, the reasoning to use such a model is unclear and diverse. Thus, we are to do an extensive study on the selected water models.

Here, the first goal of this chapter is to further probe TIP4P water model responses towards different proposed force field in the literature. To the best of knowledge, current available force fields for ZIF-8 are developed in the system for non-polar organic molecules;(4, 293-296) thus, the polar adsorbates response toward the force field are unknown. We are to assess the performance of individual force field and provide a clear sense of the adsorption isotherm in relation to framework force field. Krokidas *et al.,* Zheng *et al.,* Hertag *et al.* Amrouche *et al.,* Wu *et al.* and Zhang *et al.* ZIF-8 force fields were chosen to be studied in this work.(4, 37, 135, 293-296) An in depth literature review of the force field is discussed in the later chapter 6.2.

Then, the second goal of this work is to determine the adsorbate – adsorbent interactions between different water model and ZIF-8. We intended to investigate the well-known TIP3P, TIP4P, TIP4P-2005, TIP4P-EW and SPC/E(297) and explore the adsorption performance in the hydrophobic MOFs. TIP3P and SPC/E are 3 sites rigid model, where the point charge is situated at the center of the associate atoms. While TIP4P, TIP4P-2005 and TIP4P-EW are 4 sites rigid model, the negative charge is distributed on the pseudo-atom in order for the molecule to remain neutral. ZIF-8 force field created by Krokidas *et al.* were used to probe the water interaction with the framework.(294)

This chapter will establish in this order. First, a comprehensive review regarding the six flexible force fields that were found in literature will be given. Then the chapter will move onto an introduction to the methods that were used in this study. Finally, a discussion and concluding remarks regarded to the result which was generated from the simulation will sum up in the final section of this chapter.

6.2 ZIF-8 Force Field

ZIF-8 has a sodalite topology and formed by self-assemble of zinc ions and Imidazolate linkers. The sodalite cages are interconnected by double four-membrane rings and molecules can enter the cage through a six-membrane ring opening. It has a surface area of 1630 $m^2 g^{-1}$ and the pore diameter of ~3.40 Å and the cavities around ~11.6 Å.

There are wide range of force field developed for ZIF-8. The force field are obtained from a well-known database (AMBER, UFF, DREIDING, .etc) with empirical modifications added to describe the ZnN_4 tetrahedral torsion parameter.(4, 34, 295, 298, 299) Individually, each force field gives comparable

result for a specific experimental set up and no common force field that can describe and reflect all experiments.

In the work of Hertäg *et al.,* the group developed the ZIF-8 force field specifically for H_2 and CH_4 diffusion.(293) Hertäg used AMBER and DREIDING to describe the interaction parameters of the lattice atoms. They found DREIDING force field over emphasised the stiffness of the framework. Thus inspired by the work of Hertäg, Krokidas *et al.*(120) and Zheng *et al.*(295) developed their ZIF-8 force field based on AMBER database. Both group looked into the force field provided by Hertäg and individually concluded the force field provided cannot replicated accurately for many adsorbates diffusivity and crystal structure flexibility. Thus, Krokidas created a force field to study the propylene and propane separation while Zheng created a force field for CO_2 adsorption.

Zheng *et al.* have approached on flexible force field through modification in AMBER force field and neglected selective dihedral angle for ZnN_4 to give flexibility that mimic experiment.(295) They validated the force field through focusing on the structural properties of ZIF-8 crystal, however this model was investigated through canonical (NVT) and mircocanonical (NVE) ensemble and did not validate through different pressure. Wu *et al.* found that Zheng force field predicts CO_2 system accurately, but lack transferability to other gaseous molecules (N_2, CH_4, H_2).(296) Hence, Wu also developed a force field by combining UFF (for the description of Zinc) and AMBER (for the description of the organic linkers) force field.

In some cases, rigid force field are enough to describe adsorption process, such as force field developed by Fairen-Kimenez *et al.* who successfully replicated

experimental CO_2/CH_4 adsorption results; the group modified the force field by reduction in UFF Lennard-Jones energy well depth ε parameter.(33, 105) Interestingly, with a different parameter but also originated from UFF, Amrouche *et al.* able to replicate CO_2 adsorption isotherm at low pressure, where the UFF force field are used without modifications of Lennard Jones parameter.(12)

However, it is important to note that force fields mentioned before are tested with non-polar molecules. Ortiz *et al.*(122) used Amrouche force field and found the water isotherm simulations were greatly exaggerated, intrusion point was found to be at 140 MPa whereas the experimental value is around 26.6 MPa.(27) Zhang *et al.,* derived the force field from DREIDING and found water condensed at low pressure.(37) Thus, to the best of knowledge, currently there are no ZIF-8 force field is developed for water related investigation.

To sum up, ZIF-8 has generated strong interests in scientific community due to its molecular selectivity, hydrophobicity and the 'gate' effect due to rotation of the linker. Although there are many force fields to describe ZIF-8, not one common force field which can effectively describe all gaseous adsorption system. Furthermore, there is a lack of comparative data on force field regarding the study of ZIF-8 – water system. Thus, one could see a knowledge gap in this well-known material.

6.3 Simulation Method

By employing Grand Canonical Monte Carlo (GCMC) and continuous fractional component Monte Carlo (CFC MC) simulations, in the range of 1 MPa to 180 MPa

and at 298K, we are to demonstrate drastic difference in adsorption pressure with different water model as well as the response towards different force field models.

6.3.1 Grand Canonical Monte Carlo Simulation

Grand canonical Monte Carlo (GCMC) method was used to simulate the adsorption of TIP4P, TIP4P-2005, TIP4P-EW, TIP3P and SPC/E in ZIF-8. The system is simulated in the range from 10MPa to 180 MPa with 10 MPa increment. Simulations for adsorption in ZIF-8 simulations were conducted at the temperature of 298 K. All simulations were carried out with RASPA molecular simulation software.(300) The ZIF-8 atoms were kept fixed at their experimentally determined crystallographic positions and the ZIF-8 unit cell was replicated by 2 x 2 x 2 to achieve the dimension of a=b=c=33.982 Å.(97) For ZIF-8 atoms force field parameters were taken from the work of Krokidas *et al.,*(294) Hertag *et al.,*(293) Zheng *et al.,*(295) Wu *et al.,*(296) Amrouche *et al.*(4) and Zhang *et al*.(37) Periodic boundary conditions were applied in all three dimensions and the cut-off distance was set to 14 Å. Ewald summation was used to compute coulombic interactions and short range interactions were handled with the Lennard Jones potential. The Lorentz-Berthelot mixing rule was used to determine interaction parameters between alike atoms. Each simulation was equilibrated for 500,000 cycles followed by a 500,000 cycle production run. One cycle is equal to N steps where N is the number of molecules present in the system. For all GCMC simulations, translation, rotation, insertion, deletion and reinsertion moves were sampled with equal probability for water molecules.

6.3.2 Continuous Fractional Component Monte Carlo (CFC MC)

Grand Canonical Monte Carlo (GCMC) simulations can accurately predict equilibrium adsorption in materials. The volume, temperature, chemical potentials are kept at constant while the number of molecules in the simulation box fluctuated. New system configurations are dependent on the imposed free energy (chemical potential) and the compositions change in respond to the chemical potential relative to the old system configurations. The compositions or evaluation the chemical potential in the system are changed by *insertion* or *deletion* of molecules. The precision and accuracy of the simulation are critically dependent on the abilities to perform insert and delete moves. However, in a dense/high pressure system, infrequent acceptance of the new system configuration due to unavailable suitable size cavity for accommodate new molecule leading to poor sampling. Thus, long simulations time is required to compensate the low acceptance probability of new molecules.

Continuous Fractional Component Monte Carlo (CFC MC) targets this type of system.(36) The method drawn on many features on various biasing methods and accelerate the acceptance for insertion and deletion of molecules in Grand Canonical ensemble (μ, V, T).(301) It offers various attractive features for simulating in phase transition system, in particular where the method offers a self-adapting biasing capability without the needs of foreknowledge for any biasing function.

In GCMC simulation, often Lennard Jones equation was used to calculate electrostatic interactions. The energy potential is cut and shifted as the following:

$$U_{LJ}(r) = \begin{cases} 4\varepsilon\left[\left(\frac{\sigma_{ij}}{r_{ij}}\right)^{12} - \left(\frac{\sigma_{ij}}{r_{ij}}\right)^{6}\right], & r < r_c \\ 0 \quad , & r \geq r_c \end{cases}$$

Here, the method introduced a pseudo-continuous parameter λ and it is imposed on the coupling molecules. λ are utilised to scale down the repulsion force potential, which effectively changed the inserted molecule to a "fractional" component. The insertion of an "integer" molecule is replaced with the insertion of a "fractional" molecule, the reduce molecule has a higher probability of accepting into a system. Once the fractional molecule inserts into the system, a set of Metropolis-like acceptance rules can be derived for making changes in the value of λ and if the parameter is > 1, then the existing fractional molecule is converted to an integer molecule. Then a new fractional molecule is randomly position into the system with a λ – 1 coupling parameter. Vice versa, if the λ parameter is < 0, the fractional molecules are removed from the system and next fractional molecule is randomly inserted into system with the λ + 1 parameter.

$$U_{LJ-CFC\,MC} = 4\lambda\varepsilon\left[\frac{1}{\left(\xi(1-\lambda)^2 + \left(\frac{r_{ij}}{\sigma}\right)^6\right)^2} - \frac{1}{\xi(1-\lambda)^2 + \left(\frac{r_{ij}}{\sigma}\right)^6}\right]$$

ξ is an adjustable parameter that was set as 0.5, r_{ij} is the distance between integer species, λ is the scaled parameter between 0 to 1 and when normal Lennard Jones is recovered when λ reaches 1. This type of scaling significantly reduced the repulsive force when atoms come close to each other. Subsequently, the coulombic interactions will only turn on when $\lambda > 0.8$. Thus, the system is well behaved where there is overlapped during insertion stage. The general set up of the simulation are to be exactly the same as the mentioned in GCMC, where the insertion and deletion

are replaced with continuous fractional lambda swap probability. Here, we sampled the pressure range from 1 to 70 MPa with 10 MPa increment. The continuous fractional lambda swap has equal probability as translation, reinsertion and rotation move.

6.4 Results and Discussion

6.4.1 Multiple Force Field Adsorption Simulation

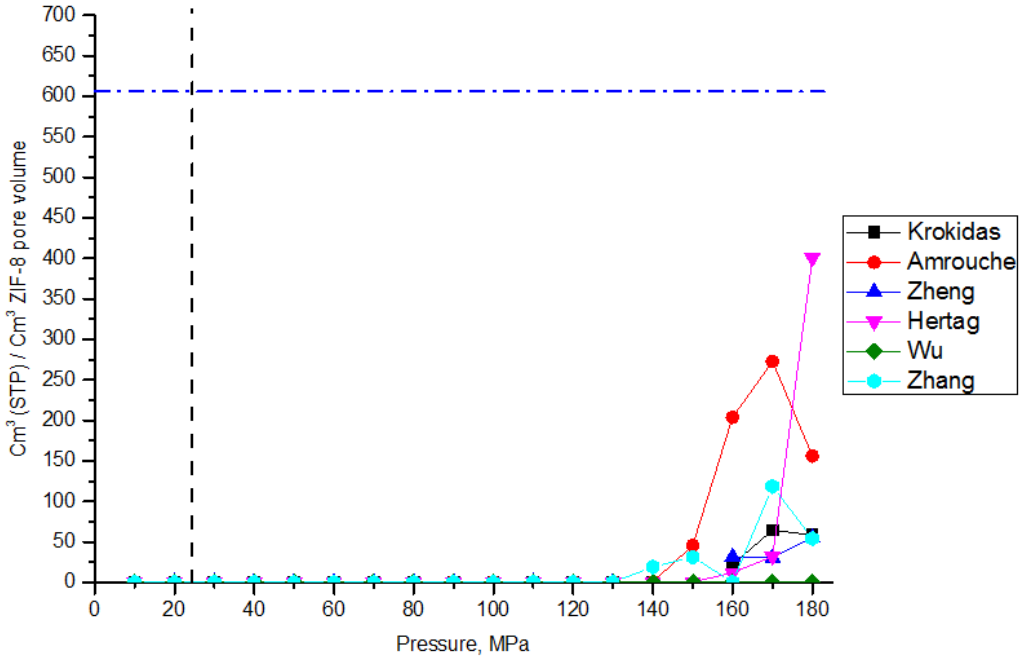

Figure 6.1 – Water adsorption Isotherm with TIP4P water model and force field from Krokidas (black) , Amrouche (red), Zheng (blue), Hertäg (pink), Wu (green) and Zhang (cyan). The black and blue dash line represents the experimental adsorption pressure and experimental loading, respectively.

First, we are going to present the TIP4P water adsorption isotherms in ZIF-8 at 298 K. Figure 6.1 is the result of the adsorption isotherm of water between 10 MPa up to 140 MPa. The figure point to minimal water adsorption and no indication of adsorption occurred at experimental intrusion pressure (26.6MPa, expressed by the dotted line).(122) We observed no vapour phase of water in ZIF-8 during the

simulation; a clear indication of the established hydrophobic nature of the solid. At the range beyond 140MPa, adsorption occurred for Krokidas, Amrouche, Hertäg and Zhang force field. However, the pore condensation did not reach experimental loading value. Zheng's force field shows the start of pore condensation adsorption at 160 MPa, while no condensation was observed in Wu's force field. Further higher pressures are not explored as the range is beyond experimental condition.

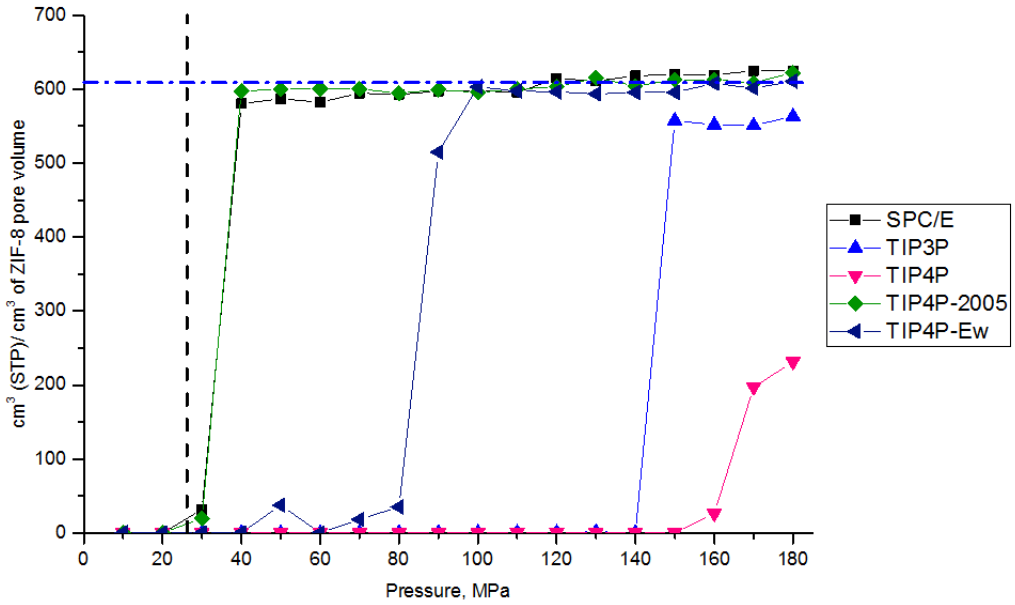

Figure 6.2 – SPC/E (black), TIP3P (blue), TIP4P (pink), TIP4P-2005 (green), TIP4P-EW (purple) water model are tested with Krokidas force field. The black and blue dash line represents the experimental adsorption pressure and experimental loading, respectively.

Then we move on to the investigation regarding to water model. Figure 6.2 shows the effect on different water model and the condensation behaviour. It is clearly shown that different water models have a substantial difference and adsorption pressure on ZIF-8 framework. SPC/E and TIP4P-2005 clearly shows pore condensation at 40 MPa and this is in relative proximity to experimental intrusion

pressure. The water model reached experimental water loading (~ 615 cm^3/ cm^3 pore volume of ZIF-8 or 80 molecules/unit cells).(122)

TIP4P-EW indicated adsorption to occur at 80 MPa and it will reach full saturation at 100 MPa. Whereas TIP3P reached pore saturation level at 150 MP and it does not reach experiment water loading. TIP4P only begin to display adsorption at 160 MPa and above, yet it does not exhibit full loading within the 500,000 production run.

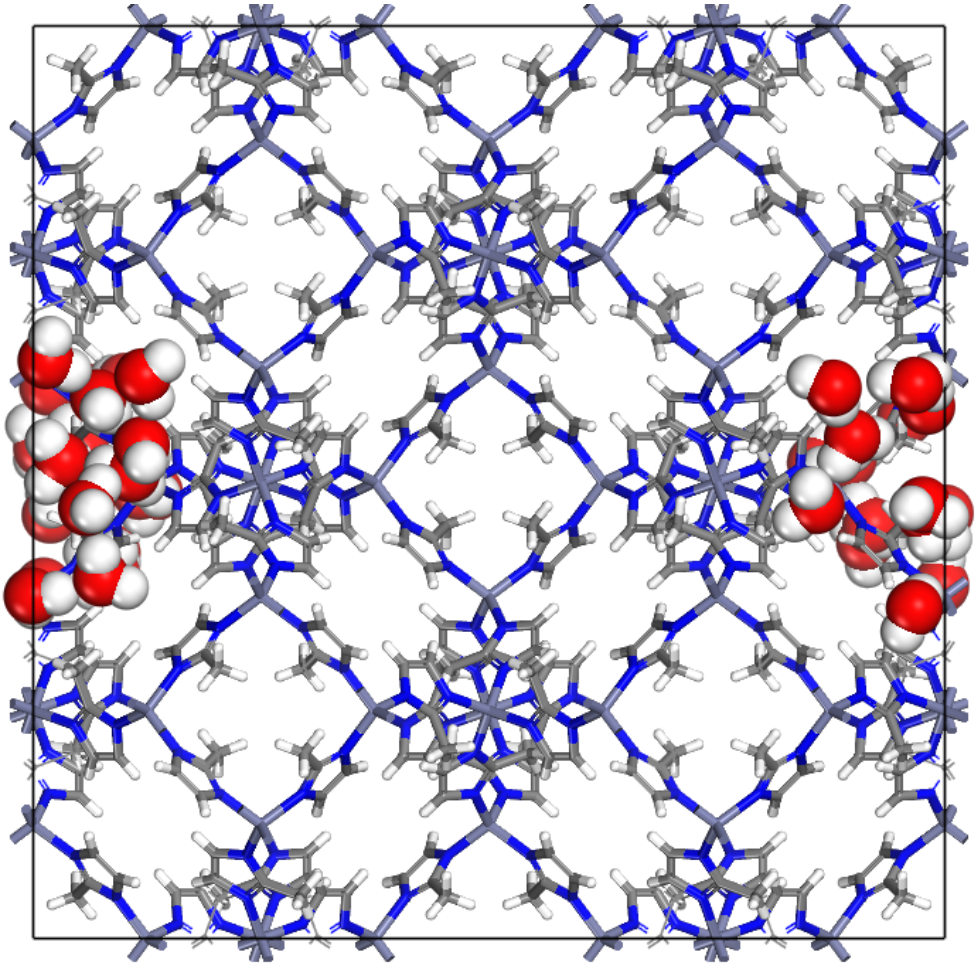

Figure 6.3 – Partial pore condensation of TIP4P-2005 in ZIF-8.

In the analysis of the production cycle, the results reveal that the process of adsorption and condensation is dependent on adsorbate – adsorbate interaction. It

is more energetically favourable for two water molecules to occupy inside a single cage in comparison to individual water molecule occupation per cage. Thus, the formation of metastable clusters is first to occur (Figure 6.3) before the adjacent cage is filled with water. However, the hydrophobic nature of ZIF-8 implicitly causes high rejection rate of insertion which needs prolong simulation time to sufficiently sample all of phase space.

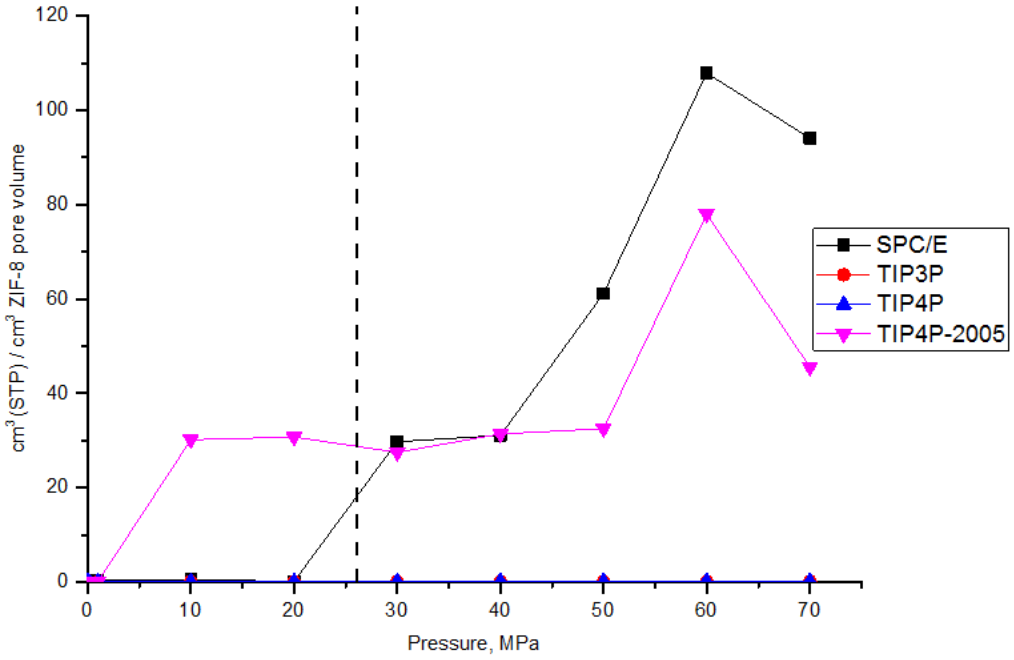

Figure 6.4 – CFC MC simulations for SPC/E (black), TIP3P (red), TIP4P (blue) and TIP4P-2005 (pink) with Krokidas force field to describe the atoms in the framework. The black dash line represents the experimental intrusion pressure.

Thus, CFC MC are utilised to bias the acceptance move for these prolong simulation. From Figure 6.2, it is apparent to choose SPC/E and TIP4P-2005 model as the adsorption isotherm are in proximity with experimental intrusion pressure. TIP3P and TIP4P are simulated with this method in order to test the current model that is broadly used in the MOF community.

Here, we used Zhang and Krokidas force fields for the description of ZIF-8 framework atoms. The simulation results of the adsorption isotherms for the mentioned water models are presented in Figure 6.4 and Figure 6.5. In both force field models, there are no adsorptions occurred for TIP3P and TIP4P water model; this is in agreement with the GCMC simulations.

In Figure 6.4, Krokidas' description of ZIF-8 atoms illustrated TIP4P-2005 was to form water aggregation at 10 MPa (appendix 9.2.3) and implied full system saturation will occur with longer simulations. Remarkably, SPC/E water cluster formed at 30 MPa and above in the simulation; only gaseous phase was observed and no sign of pores condensation at 20 MPa or below.

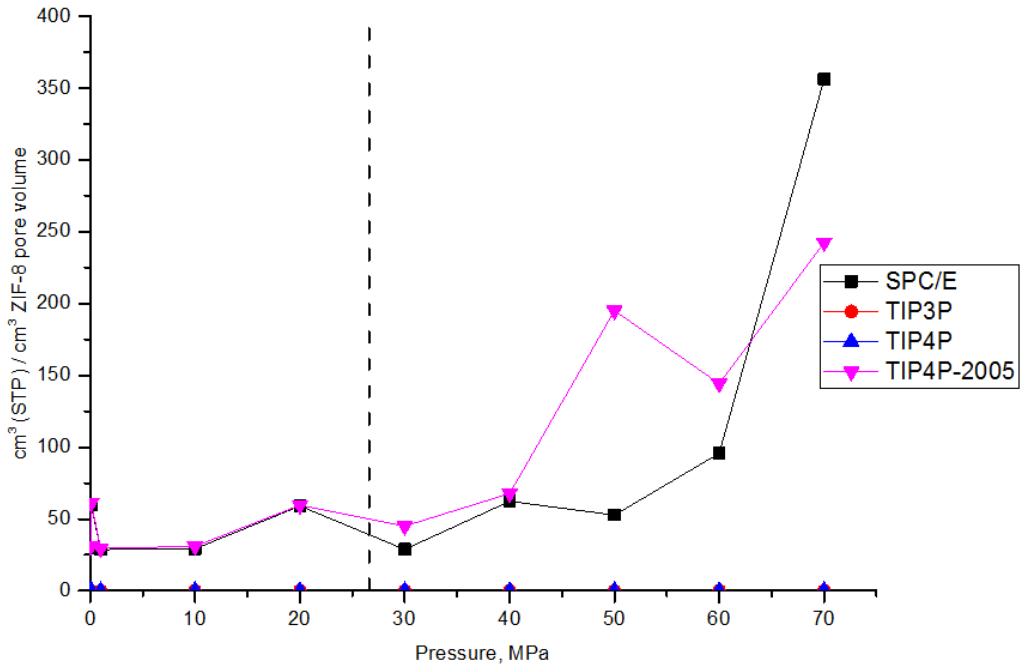

Figure 6.5 – CFC MC simulations for SPC/E (black), TIP3P (red), TIP4P (blue) and TIP4P-2005 (pink) with Zhang force field to describe the atoms in the framework. The black dash line represents the experimental intrusion pressure.

Figure 6.5 shows the Zhang's description of ZIF-8 atoms that SPC/E and TIP4P-2005 is presented within the framework at pressure below experimental. It is

notable water cluster presented in the pore for SPC/E and TIP4P-2005 at low pressure. Thus, the simulations suggests both water model will reach full framework saturation level with longer simulation cycle.(37)

6.4.2 Heat of Adsorption

We derived isosteric heats of adsorption by using the derivative of the total potential energy:

$$q = \frac{1}{\beta} - \left(\frac{\partial \langle U \rangle}{\partial \langle N \rangle}\right)_T$$

We broke down the potential energy to host – adsorbate (Figure 6.6) and adsorbate – adsorbate (Figure 6.7) interactions and finally the sum of the interactions (Figure 6.8). We further probed the method GCMC and CFC MC by the comparison of heat of adsorption energy.

As you can see from Figure 6.6 (Top), by using CFC MC method, TIP3P and TIP4P have a relative strong host – adsorbate interactions with decreasing pressure (~ 50 – 35 kJ mol^{-1}). The adsorbate – adsorbate interaction remains relatively weak (~ 5 kJ mol^{-1}) and it remains steady with increasing pressure (Figure 6.7, Top). A constant host – adsorbate interaction is observed for SPC/E and TIP4P-2005 and the interaction energy is found at ~10 kJ mol^{-1}, however the interaction between adsorbate – adsorbate are relative high and reach ~40 kJ mol^{-1}. However, one must notice the relatively large error bar for Figure 6.6 and Figure 6.7. This is due to the infrequent molecule acceptance into the hydrophobic framework and the error will reduce with longer simulation cycle.

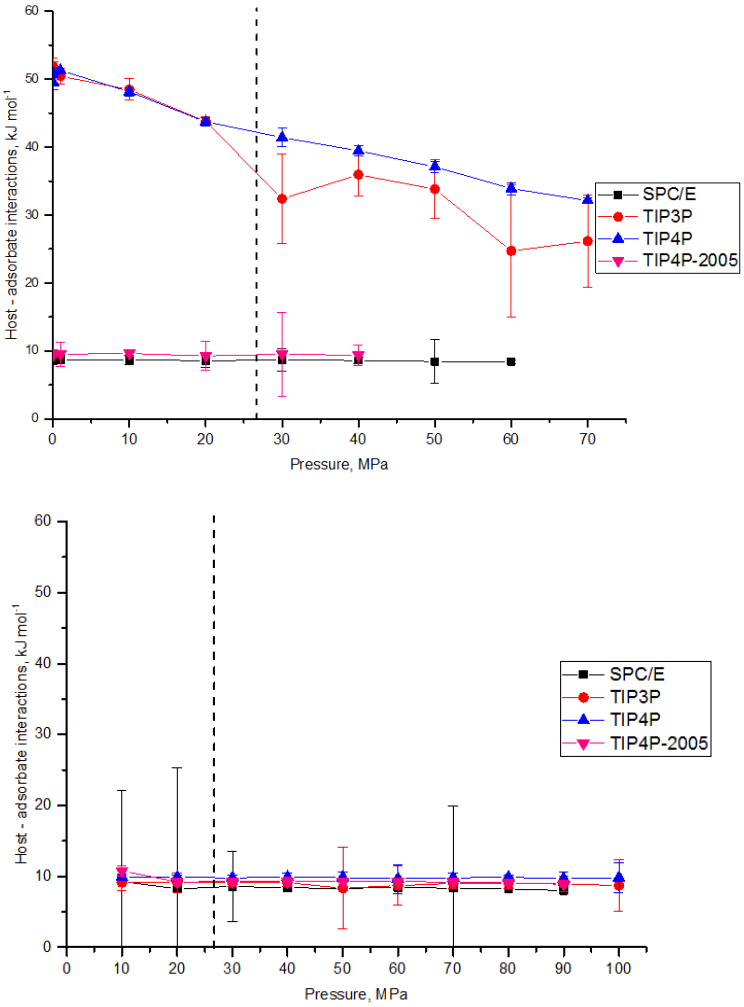

Figure 6.6 – Host (ZIF-8) - adsorbate (water) interactions calculated through CFC MC (Top) and GCMC (bottom) methods. The black dash line represents the experimental intrusion pressure. SPCE (black), TIP3P (red), TIP4P (Blue) and TIP4P-2005 (pink), respectively. The black dash line represents the experimental intrusion pressure.

This is a stark contrast to GCMC adsorption calculation (Figure 6.6, bottom) where all water models exhibited similar host – host interaction energy, at the region of ~10 kJ mol^{-1}. The GCMC adsorbate – adsorbate interactions (Figure 6.7, bottom) clearly demonstrated relatively weak adsorbate – adsorbate interactions at 10 MPa. At > 20 MPa, SPC/E and TIP4P-2005 reveal an increase of adsorbate – adsorbate energy to ~36 kJ mol^{-1} and water clusters were found in the pore. However, TIP3P and TIP4P have a relatively weak interaction (< 10 kJ mol^{-1}) between adsorbates

and resulting low loading of water as shown in Figure 6.2. This is in agreement with the work done by Vega *et al.* on bulk water simulation where the strength of adsorbate interaction is in the order TIP4P/2005 > SPC/E > TIP4P > TIP3P. (302)

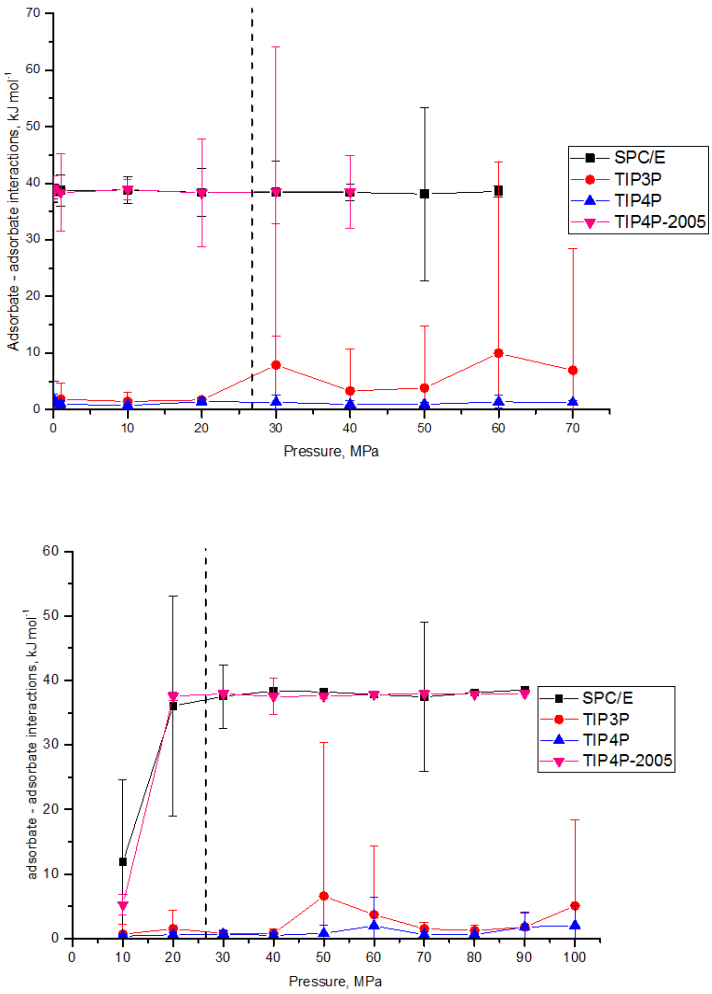

Figure 6.7 – Adsorbate (water) - Adsorbate (water) interactions calculated through CFC MC (top) and GCMC (bottom) methods. The black dash line represents the experimental intrusion pressure. SPCE (black), TIP3P (red), TIP4P (Blue) and TIP4P-2005 (pink), respectively.

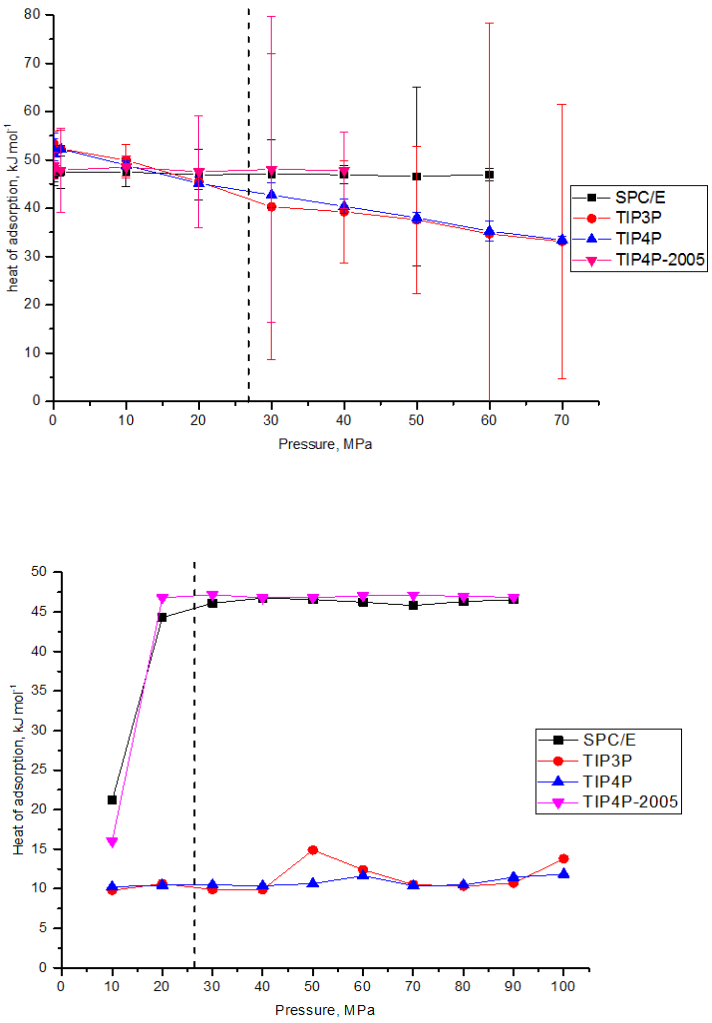

Figure 6.8 – Average isoteric heat of adsorption through derivation of total potential energy at pressure between 10 kPA to 70 MPa in CFC MC simulation (Top) and GCMC (bottom). SPCE (black), TIP3P (red), TIP4P (Blue) and TIP4P-2005 (pink), respectively. The black dash line represents the experimental intrusion pressure.

In Figure 6.8, the total average isosteric heats of adsorptions are shown for CFC MC and GCMC. In CFC MC simulations, we can see consistent heat of adsorption level for SPC/E and TIP4P-2005 where it remains around ~48 kJ mol^{-1}, whereas TIP3P and TIP4P display a decrease of heat of adsorption with increasing pressure due to the decreasing host – adsorbate interaction. In contrast, GCMC have shown that TIP3P and TIP4P have low heat of adsorption energy (~10 kJ mol^{-1}) in the sampled pressure range, whereas SPC/E and TIP4P-2005 at 10MPa. The low value

of heat of adsorption energy related to unfavourable insertion of water molecule and leads to low loading of water molecules.

6.5 Conclusion

We simulated the isotherms for water in six different ZIF-8 force fields and found that all showed pore condensation occurred at pressure 140 MPa and above. Thus, from that we put forward the assumption that water models have similar responses to the current available intermolecular force field. Then, the study turned toward the investigation towards water model responses to force field proposed by Krokidas. We found a great degree of variance in the response between water models. It is notable the common water model (TIP3P, TIP4P) did not show pore condensation at lower pressure, while SPC/E, TIP4P-2005 and TIP4P-EW showed condensation at lower pressure <100 MPa. TIP4P-EW condensed at 100 MPa thus it is discarded and not investigated further. Afterward, we assessed the method, GCMC and CFC MC, and found CFC MC overestimated the host-adsorbate interaction for TIP3P and TIP4P. This might be due to unrealistic equal weight probability that was given to continuous fractional lambda factors, however, the weighting probability will not further explore here. SPC/E and TIP4P-2005 demonstrated consistent host-adsorbate interactions for GCMC and CFC MC, however in CFC MC the interaction between adsorbate – adsorbate was overestimated at low pressure for Zhang force field. This was not observed in Krokidas force field. Evidently TIP3P and TIP4P have shown no pore condensation within ZIF-8 in CFC MC and GCMC simulation, while SPC/E and TIP4P-2005 displayed adsorption in close proximity of experimental adsorption pressure. Thus, the preliminary results shown SPC/E and TIP4P-2005 are good candidates for water simulation in this hydrophobic MOF.

However, we acknowledged there are number of limitations in this simulation study. 1) A rigid model was used in the simulation of ZIF-8 structure. The flexibility may change the adsorption/intrusion pressure of water. 2) As the ZIF-8 cage is greater than the pore entrances, the direct insertion moves in MC will bypass the resistance provided by the small pore aperture. 3) Inherit sampling issue in MC may play a major role for TIP4P and TIP3P, as no condensation was reported in this study as mentioned by Zhang *et al.*, where the group shows pore condensations for TIP4P water model after 110 days simulations.(37) Despite these limitations, this simulation study demonstrated alternative water models such as SPC/E and TIP4P-2005 provided better descriptions for molecular simulation in ZIF-8. Because the mention inherited problems, we instigate further on the investigation regarding water and ZIF-8 with MD simulations.

7 Molecular Dynamic Simulations of Water Intrusions in Flexible ZIF-8

Instigated with the previous chapter, we investigated and performed molecular dynamics simulations for flexible ZIF-8 model and water systems in order to mimic experimental water adsorption set up. A graphene piston was employed in the NVT ensemble simulation to provide a pressure gradient. We simulated TIP4P, TIP3P and SPC/E water models with the atomistic ZIF-8 flexible force fields descriptions provided by Krokidas, Zheng and Wu. Here, we found the current available force field fail to replicate experimental phenomenon and further studies are required to address the problem.

7.1 Introduction

In recent years, researches related to nano porous materials were broadly examined. MOFs are the latest class of crystallised porous materials. The choices of pore size and structure topology are controllable by varying organic linkers and metal nodes. Thus the volume, porosity and functionality can be tailored to specific needs. In particular, many MOFs exhibit chemical/thermal stability in various conditions and can have an internal surface area up to 6000 $m^2 g^{-1}$. Diverse potential applications such as gas storage,(3, 9, 230, 303) separation,(3, 85, 120, 229, 304) sensor,(15, 16, 203, 204) catalysis(81, 203) and drug delivery(17, 82, 305, 306) can be implemented. However, the progression in potential applications involving water has been less successful, due to many MOFs are known to destabilise in liquid water or even under humid conditions. Early periods MOFs such as IRMOF-1, HKUST-1, M-MOF-74 are example of thermal and chemical stable, yet it loses crystallinity with the present of polar solvents.(239, 307) Given that, there are

MOFs have shown stability in water which soaked for days (UIO-66, ZIF-8).(97, 239, 308) In particular, our interested lies with a branch family of MOFs called Zeolitic imidazolate frameworks (ZIFs), where the topology mimics those aluminosilcate zeolites and transition metals (zinc, cobalt, copper etc.) are used as a connective node to link with imidazolate or benzimidazolate linkers.(97, 102, 119, 309)

ZIFs have interesting properties and vast amount of effects have been invested for the understanding of the underlying molecular mechanisms. Many investigations have shown the dynamics and thermodynamics of the guest molecules are dependent on the selective choice of metal atoms, organic linkers and structure topology.(1, 129, 229, 296) In contrast to rigid framework of zeolites, ZIFs have inherited flexibility feature within the structure. For example, the 2-methylimidazole organic linkers in ZIF-8 can re-orientate and goes through phase transition.(35, 37) At the ground state, ZIF-8 has a pore aperture diameter of 3.4 Å and cage diameter of 14 Å,(12) however the pore aperture linkers can rotate and allowed molecules (methane, ethane and propane) to intrude into the cage albeit the molecule sizes are larger than the aperture. This physical mechanic movement in the structure while retaining the crystallography position and symmetry is known the ‘gate’ effect.(33, 35, 105)

This ‘gate’ effect in ZIF-8 has been broadly investigated and multiple studies have given the energy required to cross the aperture barrier. Zheng *et al.* approached the investigation of ZIF-8 ‘gate effect’ by the application of an artificial harmonic bond, which derived through DFT calculation, between the pore carbons atoms and compute molecular dynamic simulation.(135) This idea gave a novel insight to simulate gate opening mechanisms. The energy profile to cross the gate is found to

be ~ 20.92 kJ mol^{-1} for selective light hydrocarbons. This result is in agreement with Tanaka *et al.* where the maximum rotational energy is found at ~18 kJ mol^{-1}.(299) Many approached the gate opening mechanism with molecular dynamics simulation. Krokidas *et al.* created a force field and observed the pore opening as various light petroleum and small gaseous molecules (He to n-butane).(120) In their work, the authors found the gate opening energy around ~27 kJ mol^{-1} for various molecules and the force field retained the crystallographic atoms distance of ZIF-8.

Our interested of this study aligned with the proposition from Ortiz *et al.* The author utilised the 'gate' effect in ZIFs and proposed the usage of hydrophobic materials for the shock absorber applications.(25, 26) ZIF-8 is known for its hydrophobicity and under high pressure it is possible for water to condense in the hydrophobic cages.(26, 27, 122) The material has shown to exhibit type V isotherm and endured water intrusion-extrusion over several cycles without irreversible structure deformation.(27) By utilising the properties of ZIF-8, one can used the porous material for shock absorber or as storage units for mechanical energy.

However, to the best of knowledge, there is no force field designated for water – flexible ZIF-8 molecular simulations. The current available force fields are generated for system that polar molecules are not presented. Thus, various water studies have found the intrusion pressures to be either over or under exaggerated the adsorption pressure.(37, 122, 310) In this work, we demonstrated current force field cannot mimic water intrusion at correct pressure range. We replicated the water intrusion experiments by utilising a graphene piston in molecular dynamics simulations. The piston provided a pressure gradient toward the water-ZIF-8 system which imitated water pushed through the ZIF-8 crystals in experiment.

The structure of this chapter is the following: Firstly, we are to give a description of the methodology that was employed in this chapter. Afterward, the ZIF-8 structure is tested with TIP4P, SPC/E and TIP3P water model in order to distinguish the responses upon the crystal. Here, we used Krokidas *et al.,* Zheng *et al.* and Wu *et al.* work to describe the atomic interaction of ZIF-8.(294-296) Following on, we compared the water intrusion pressure with available experimental data. Finally, a conclusion is specified for the work that has been done in this chapter.

7.2 Simulation Method

7.2.1 Piston Molecular Dynamic Simulation

Here, in the molecular dynamic (MD) simulation were carried out with GROMACS software in order to investigate water intrusion into ZIF-8 membrane.(278) A total 945 atoms single layer carbon graphene piston covered the x-y plane of the simulation box and accelerated toward z direction in order to provide a pressure. The graphene is not considered as a conductor.

Considering the potential energy of an atom, $U(r)$ as it is mentioned in chapter 4.3, the force acting upon an atom at z direction is calculated through the equation:

$$\Delta F_z = -\frac{\partial U(r)}{\partial z}$$

$\frac{\partial U(r)}{\partial z}$ is the change of potential energy in respect to the change of distance with the interacting atoms. Here, we applied an extra force through the acceleration of an individual graphene carbon atoms and it is calculated according to Newton's second law of motion,

$$F_g = m_g a_z$$

where F_g is the force that applied on the individual graphene's carbon atom, m_g is the mass of the carbon atoms of the graphene piston and a_z is the acceleration provided at the z direction. The acceleration is provided to the GROMACS software. Therefore, the total force acting upon individual carbon atoms on the piston becomes:

$$\Delta F_z = -\frac{\partial U(r)}{\partial z} + m_g a_z$$

Here, the GROMACS software will use the equation above to integrate in Verlet algorithm at z direction. However, to calculate the desire pressure, we know that $\frac{\partial U(r)}{\partial z} \ll m_g a_z$ in order for the piston to move. Therefore it is assumed $\frac{\partial U(r)}{\partial z}$ is negligible and the equation becomes:

$$\Delta F_z \approx m_g a_z$$

The force is related to the pressure at z direction by following equation,

$$\Delta P_z = \frac{\sum_N \Delta F_z}{A}$$

where ΔP_z is the pressure provided by the piston and A is the x-y dimension surface area of the piston with N carbon atoms.

The force exerted by the piston pushes the water towards the MOF. Furthermore, it is understood that water density change is negligible when the pressure is <100MPa, thus it is assumed incompressible.(311) Frictional forces and gravitation has negligible effect on the system. Thus, by moving the graphene piston, the water feels the acceleration from the piston which corresponded as the pressure. This pressure-driven operation condition has been widely used in non-equilibrium MD

such as pervaporation, desalination and reverse osmosis.(22, 312-318) The piston is to provide 10 MPa and 30 MPa of pressure towards the system at Z direction as represented in Figure 7.1.

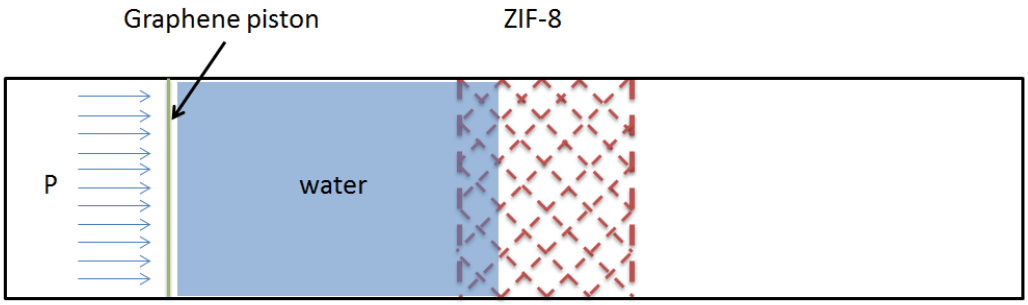

Figure 7.1 – Visual representation of the simulation system. The graphene piston provided a pressure which push water molecules toward ZIF-8 structure and this mimic water intrusion experiment. The right hand side of the simulation box remained vacuum.

ZIF-8 was taken from the work by Semino *et al*. and have a dimension of 50.98 x 48.06 x 118 Å in the x, y and z direction respectively.(319) The simulation box is expanded at z direction to 500 Å in order to avoid artificial electrostatic interactions and the periodic image have been turned off at Z direction to avoid overlap interactions.(320) 8573 of the water molecules were incorporated at left side of the box, while the ZIF-8 membrane separated the right vacuum chamber. TIP4P, TIP3P and SPC/E were utilised for the description of water molecules.

The flexible frameworks atoms were described by the work of Krokidas *et al.,*(294) Wu *et al.*(296) and Zheng *et al.*(295) The coulomb charges are modified in order to achieve neutrality for the Semino's ZIF-8 structure. Ewald summation with the correction term (EW3DC) were used to compute coulombic interactions and short range interactions were handled with the Lennard Jones (LJ) potential and the cut-off distance was set to 14 Å.(320) Lorentz-Berthelot mixing rule were used to determine interaction parameters between alike atoms, while the graphene piston

only interact with oxygen of water atoms. Verlet velocity algorithm was employed to integrate Newton's equation of motion with a time step of 1fs.[281] MD simulations were run at 298 K in the NVT ensemble and controlled by Nose-Hoover thermostat. 1-4 interaction for LJ and coulomb is scaled according to the respective force field. The system initially is subjected to energy minimisation using steep descent method with the maximum step size of 0.01 nm and a force tolerance of 0.1 kJ mol^{-1} nm^{-1}. Then the system is subjected to 1 ns of equilibration run and followed by up to 300 ns production run.

7.3 Results and Discussion

7.3.1 Piston Molecular Dynamic Simulations

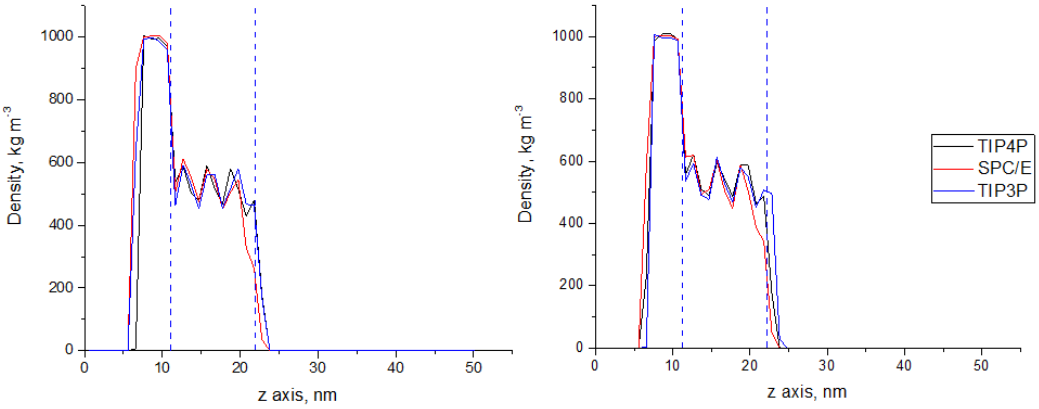

Figure 7.2 – Z direction density plot of TIP4P, SPC/E and TIP3P water model in the ZIF-8 membrane where the atoms are described by Krokidas force field. The pressure difference is 10 (Left) and 30 (right) MPa, respectively. The ZIF-8 membrane is between the two blue dotted lines.

While there are many comparison studies regarding water models, there are only few comparison studies of water model in nano porous crystal.(290, 302, 321) Thus, we first sampled TIP4P, SPC/E and TIP3P responses towards the ZIF-8 membrane at room temperature and high pressure. Krokidas' description of ZIF-8 framework atoms was used in Figure 7.2. Here, TIP3P saturated the ZIF-8 structure

and reached the end of the surface within 70 ns (Appendix 9.3.6). Whereas, TIP4P required 220 ns and 180 ns to reach the other side of the surface for 10 and 30 MPa, respectively (Appendix 9.3.4). Similarly, SPC/E required 240 ns and 220 ns for water to diffuse across the membrane at 10 and 30MPa, respectively (Appendix 9.3.7).

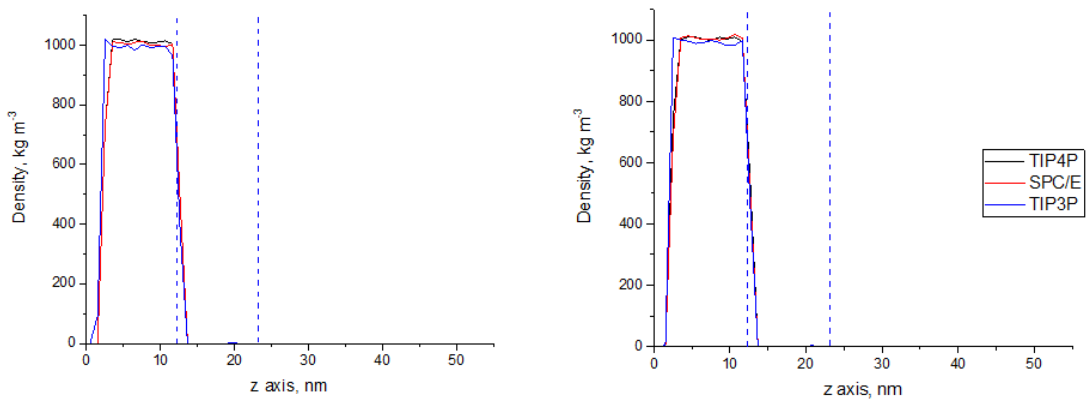

Figure 7.3 – Z direction density plot of TIP4P, SPC/E and TIP3P water model in the ZIF-8 membrane where the atoms are described by Wu force field. The pressure difference is 10 (Left) and 30 (right) MPa, respectively. The ZIF-8 structure is between the two blue dotted lines.

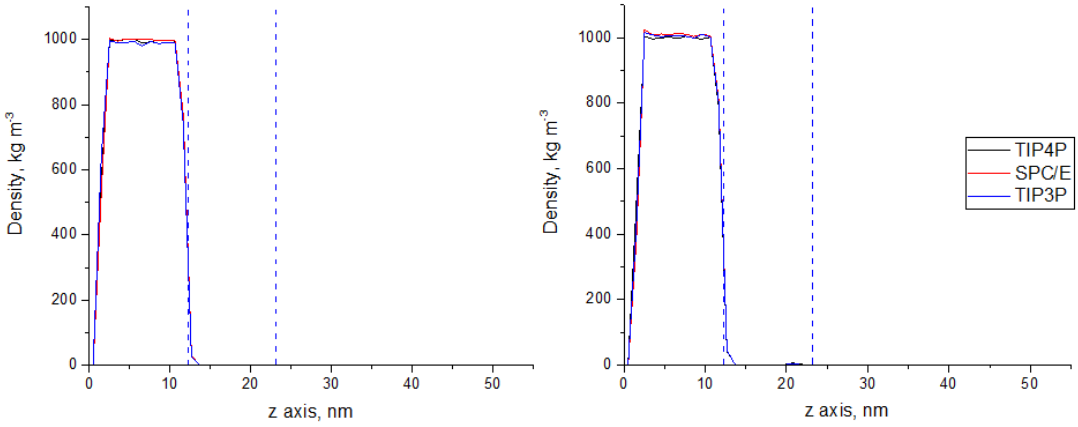

Figure 7.4 – Z direction density plot of TIP4P, SPC/E and TIP3P water model in the ZIF-8 membrane where the atoms are described by Zheng force field. The pressure difference is 10 (Left) and 30 (right) MPa, respectively. The ZIF-8 structure is between the two blue dotted lines.

Interestingly, with the force field produced by Wu and Zheng, pore condensation was not observed for any water models. Figure 7.3 and Figure 7.4 clearly displayed that TIP3P, SPC/E and TIP4P will not diffuse across the ZIF-8 structure after 100 ns simulation. The frameworks have relative strong rigidity and no pore apertures opening were observed when water approached the pore gate.

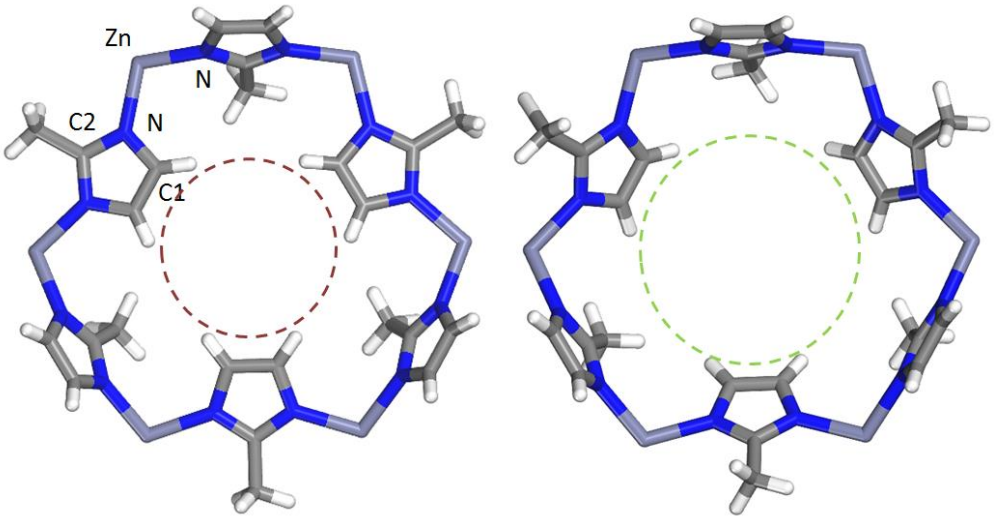

Figure 7.5 – An illustration of the closed and opened 6-ring window of ZIF-8 framework, the dihedral angle is calculated with the atoms N – Zn – N – C1 and N – Zn – N – C2. The red and green ring represents the pore opening before and after water intrusion, respectively.

Hence, we focused and probed further into the force field created by Krokidas. The transition of the dihedral angle of Zn – N – Zn – C1 and Zn – N – Zn – C2 was isolated as these angle responds to the linker rotations (Figure 7.5). In the work mentioned by Krokidas, it is expected the gate can swing open from 3.44 Å to ~ 4.0 Å and allowed water diffused through the gate.(294) From visual inspection of the trajectory of water molecules, only one water molecule can go through the pore aperture at a time (kinetic diameter ~ 2.56 Å). The present of the first water molecule prompt as a platform for further water molecules to cluster in the pore. Thus, after the intrusion of first water molecule, the pore condensation will

followed. Zhang *et al.* reported once the cluster of water are found within ZIF-8, adjacent cavities are facilitated by the water condense pore and will saturate first.(37) This phenomenon was also observed in the simulation as first pore first saturated before the remained adjacent pore are filled with water molecules. (Appendix 9.3.4)

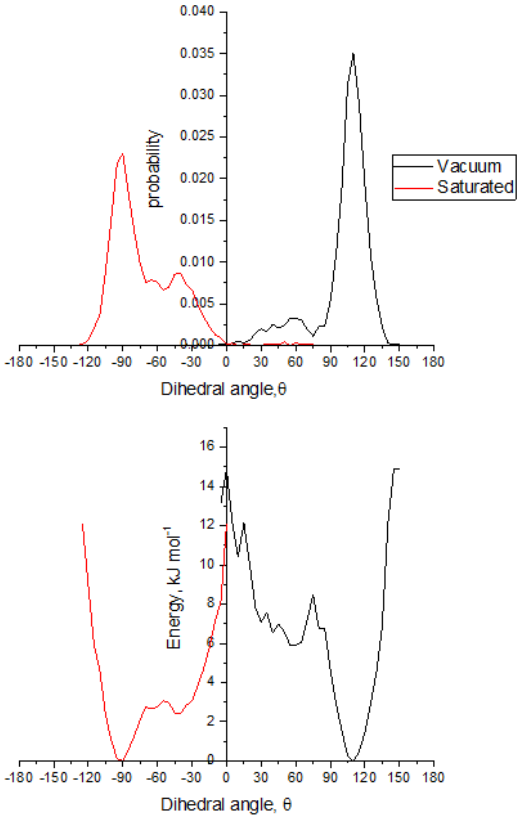

Figure 7.6 – Probability profile of the imidazolate swing angle (Top) and the corresponded potential mean force (bottom) as a function of the dihedral angle. The black and red line represented when the pore is empty and saturated with water, respectively.

The top graph in Figure 7.6 shows histogram distribution of the dihedral angle of Zn – N – Zn – C1 and revealed the responses when the pore is saturated with and without water. The figure clear displayed the shift of the dihedral angle from the central point ~ 120^0 to ~ -90^0. The potential mean force (PMF) as a function of the angle was shown at the bottom graph of Figure 7.6. This is generated based on the

equation, $F(\theta) = -kTln(P)$, where the probability,(P) is obtained from the histogram above. The swing motion for the linker peaked at ≈ 15 kJ mol^{-1} and ≈ 12 kJ mol^{-1} for the vacuum and water saturated pore, respectively. The results are in agreement with the calculation done by Coudert on ZIF-8 swing motion.(322) It is notable the water in the pore has lower the energy required for the gate to swing open.

7.4 Conclusion

We demonstrated the current available ZIF-8 flexible force fields were unable to reproduce water intrusion at experimental pressure. Firstly, we focused on TIP3P, TIP4P and SPC/E water model and their respective response towards the force field of Krokidas, Zheng and Wu. We revealed that water model choice have no impact on intrusion pressure. In the force field described by Zheng and Wu, water pore condensation was not observed in the 100 ns simulation. Whereas in Krokidas' force field displayed water intrusions at pressure 10 MPa. It is notable that TIP3P diffused through ZIF-8 at shorter amount of time in comparison to TIP4P and SPC/E. Then we probed the gate opening motion with Krokidas' force field and found the central distributions of the swing motion changed from ~120^0 to ~ - 90^0 thus permit water to diffuse through the crystal. Furthermore, the torsion barriers were reduced from 15 kJ mol^{-1} to 12 kJ mol^{-1} by the present of water. This observation affirmed water stimulated and changed the free energy landscape of the pore aperture in ZIF-8.

8 Conclusion and Future studies

The main aim of this thesis was to investigate the stimuli responsive effect in flexible. These materials have attracted widespread attention and used in a wide range of applications due to their intriguing properties, including, but not to limited to, tuneable structure (volume, pore size, aperture size etc) and their chemical properties (hydrophobic, hydrophilic etc).

The key findings of the research are listed as following:

In chapter 5, we concentrated on the development of a theoretical material that will respond to the imposed electric field; the material is based on the host, Mg-MOFs-74 and a gate molecule that contains a permanent dipole moment. The gates are mounted on the open metal sites within the host and the permanent dipole response to the direction of the electric field, thus the gate can rotate on its axis which intrinsically allows to control over the direction of flow. 3 V nm^{-1} of electric field were applied onto the system in parallel to the channel and the channel open. Once the electric field was turned off, the gates return to close position. We demonstrated potential applications with methane molecule where the gate managed to withhold 30 MPa of pressure and diffused once electric field is applied. Therefore, we successfully demonstrated using electric field to stimuli the system to control the direction of the flow.

In chapter 6, we identified 5 water models (SPC/E, TIP3P, TIP4P, TIP4P-2005 and TIP4P-EW) and six force fields for ZIF-8. We simulated and produced water isotherm in order to understand the responses for different ZIF-8 force field. It is concluded and identified force field played a lesser role in comparison to the water model in generating water isotherm that resemble to experiment. Afterward, the

system with TIP4P and all ZIF-8 force field adsorbed at 140 MPa and above. Thus, this leads to investigation on simulating with 5 different water models by using Krokidas ZIF-8 force field. We observed a vastly different water adsorption isotherm, where the performance by SPC/E and TIP4P-2005 intruded into the framework nearby experimental intrusion pressure. To further examined the water model, we used the state of the art method, continuous fractional component Monte Carlo to further simulate with different water model and found TIP3P and TIP4P water model were not adsorbed onto the ZIF-8. This is different from the work proposed by Zhang *et al*.(37) as they mentioned adsorption for the mentioned models occurs at 1000 kPa. Furthermore, we noticed that the force field produced by Zhang showed pore condensation for TIP4P-2005 and SPC/E at lower pressure whereas at the same pressure, Krokidas force field showed gaseous phase of TIP4P-2005 and SPC/E in the crystal.

In chapter 7, we used MD simulations to reproduce experimental set up at atomistic scale. By using a graphene sheet, we provided a pressure towards water press through ZIF-8. 3 difference force fields atomic description for ZIF-8 (Krokidas, Zheng and Wu) and 3 water models (TIP3P, TIP4P, SPC/E) were tested. Here, with flexibility of the framework taken into account, we found that the flexibility play a role in the intrusion of water, which is in contrast to the conclusion that generated from chapter 6. Zheng and Wu force field was unable to reproduce water intrusion for all water model while Krokidas force field showed water intrusion at pressure lower than experimental value. Furthermore, we probed the dihedral angle rotation in ZIF-8 linkers are stimulated by the intrusion of water molecules. Also, it has shown that the present of water condensation changed the free energy landscape of the pore aperture.

Overall, we demonstrated the effect of the stimuli (electric field and adsorbates intrusion) and their responses upon the structure that we studied. A narrow but deep insight toward stimuli responsive MOFs were given and established in this thesis. In conclusion, by using computational tools to simulate the crystalline systems, we efficiently and effectively revealed microscopic properties in consequence to the effect of stimuli. Thus, by comprehending and control physical motions at nano-scale, this will give further insights during the process of creating smart materials.

8.1 Future Scope

From the research conducted in the thesis, insights regarding the MOFs and their potentials applications are given by understanding their responses at nano-scale. It is anticipated that the studies can lead to further scope and progress in the field. The following is derived from the progress and recommendations for the future work are given:

1) Design different electric field responsive gateway that anchored onto MOFs that contain metal-open sites. Here, the molecular gate designed should have lower rotational barriers, thus leading to smaller electric fields that are required to rotate the gate. Furthermore, these studies should expand to other MOFs that consist of open metal sites.
2) Proposed and use different stimuli, such as magnetic field or temperature, for the study of stimuli responsive gate effects in various MOFs.
3) Investigate and demonstrate e suitable molecular machine in order to reproduce rotator motions, here we proposed to use asymmetric permanent dipolar molecular machines as it may be able to produce uni-directional rotation on its axis when one directional electric field applied.

4) Optimised Lambda weighting factor in CFC MC method for ZIF-8 – water simulation and diagnosed the reasons for water condensation at low pressure for Zhang force field.
5) Extend simulations for the CFC MC simulation for water adsorption until reaching saturation level; this will also lead to reduction in sampling and numerical error.
6) Expanded the investigation of water model in different flexible MOFs and observation of the structure different deformation effects, including, but not limited to, breathing effects and replicated observations in experiments.
7) Modify the ZIF-8 force field that was described by Krokidas and added the dihedral term N – Zn – N – C1 and N – Zn – N – C2 in order to replicate experimental intrusion pressure.
8) Examine and modify the ZIF-8 force field that was described by Wu and Zheng, propose changes in the electrostatic charges in order to replicate experimental intrusion pressure.
9) Investigate SPC/E, TIP3P, TIP4P and TIP4P-2005 on different hydrophobic MOFs and analysis the water adsorption curve in order to discover a common water model that can be used for all hydrophobic MOFs.

9 Appendix

9.1 Supporting information for Chapter 5

9.1.1 Details of convergence criteria for DFT geometry optimisation simulations

Energy tolerance	2.0 e-6 eV/atom
Max. force tolerance	0.05 eV/Angstrom
Max. stress tolerance	0.1 GPa
Max. displacement tolerance	0.002 Angstrom

9.1.2 Force field for Mg-MOF-74

Lennard Jones potentials

Atoms	Sigma, nm	Epsilon, kJ mol^{-1}
Mg	0.2691	0.4647
C	0.3431	0.4396
O	0.3118	0.2512
H	0.2571	0.1842
F	0.2997	0.2093
Methane (CH_4)	0.3730	1.2300

Intramolecular force field for Mg-MOF-74

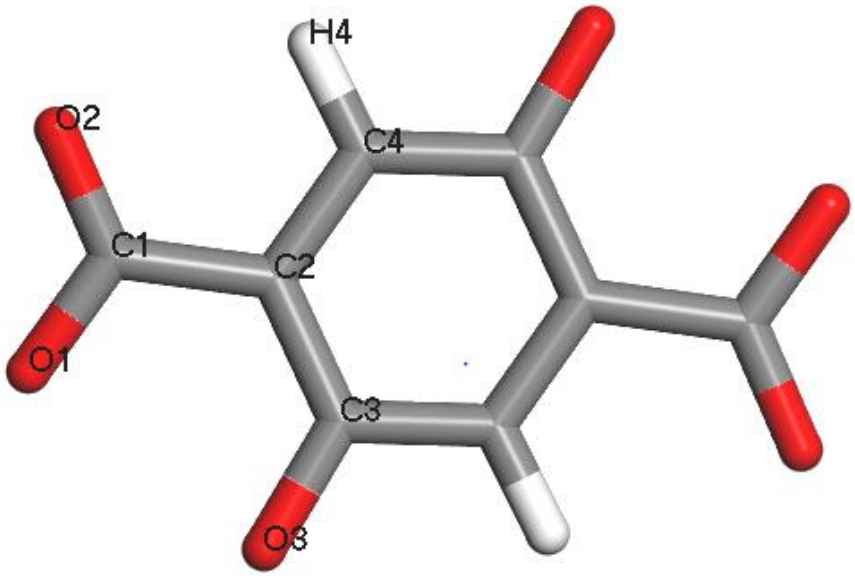

Charges

Atoms	Charges
Mg	1.566
C1	0.936
C2	-0.325
C3	0.457
C4	-0.235
O1	-0.915
O2	-0.768
O3	-0.907
H4	0.191

Bond

$k_{ij}(l_{ij} - l_{ij_0})^2$			
i	j	K_{bond}, kJ mol^{-1} nm^{-2}	θ_{bond}, nm
C1	O1	501905.602	0.1346
C1	O2	451545.168	0.1394
C3	O3	674291.146	0.1219
C1	C2	325952.190	0.1461
C2	C3	387408.861	0.1379
C2	C4	387408.836	0.1379
C3	C4	387408.861	0.1379
C4	H4	299306.278	0.1081

Angle

$k_\theta(\theta - \theta_0)^2$				
i	j	k	K_{angle}, kJ mol^{-1} rad^{-2}	θ_{angle}, degree
O1	C1	O2	2162.321	120.000
O1	C1	C2	1373.527	120.000
O2	C1	C2	1563.552	120.000
C1	C2	C3	1102.913	120.000
C1	C2	C4	1102.913	120.000
C2	C3	O3	1508.734	120.000

C2	C4	H4	620.3582	120.000
C2	C4	C3	1205.193	120.000
C2	C3	C4	1205.193	120.000
C4	C2	C3	1205.193	120.000
O3	C3	C4	1508.734	120.000

Torsion

$k(1+\cos(n\varphi-\varphi_0))$						
i	j	k	l	n	$K_{torsion}$, kJ mol^{-1}	$\theta_{torsion}$, degree
O1	C1	C2	C3	2	5.234	180.000
O1	C1	C2	C4	2	5.234	180.000
O2	C1	C2	C3	2	5.234	180.000
O2	C1	C2	C4	2	5.234	180.000
O5	C5	C6	C7	2	5.234	180.000
C1	C2	C3	O3	2	5.234	180.000
C1	C2	C3	C4	2	14.104	180.000
C1	C2	C4	H4	2	14.104	180.000
C2	C3	C4	C2	2	14.104	180.000
C2	C4	C3	O3	2	14.104	180.000
C3	C2	C4	H4	2	14.104	180.000
C3	C4	C2	C1	2	14.104	180.000
C4	C2	C3	O3	2	14.104	180.000
C4	C3	C2	C4	2	14.104	180.000

9.1.3 Force field for 4,5-dimethyl -9,10- bis(trifloromethyl)pyrene-2,7-dicarboxylic acid

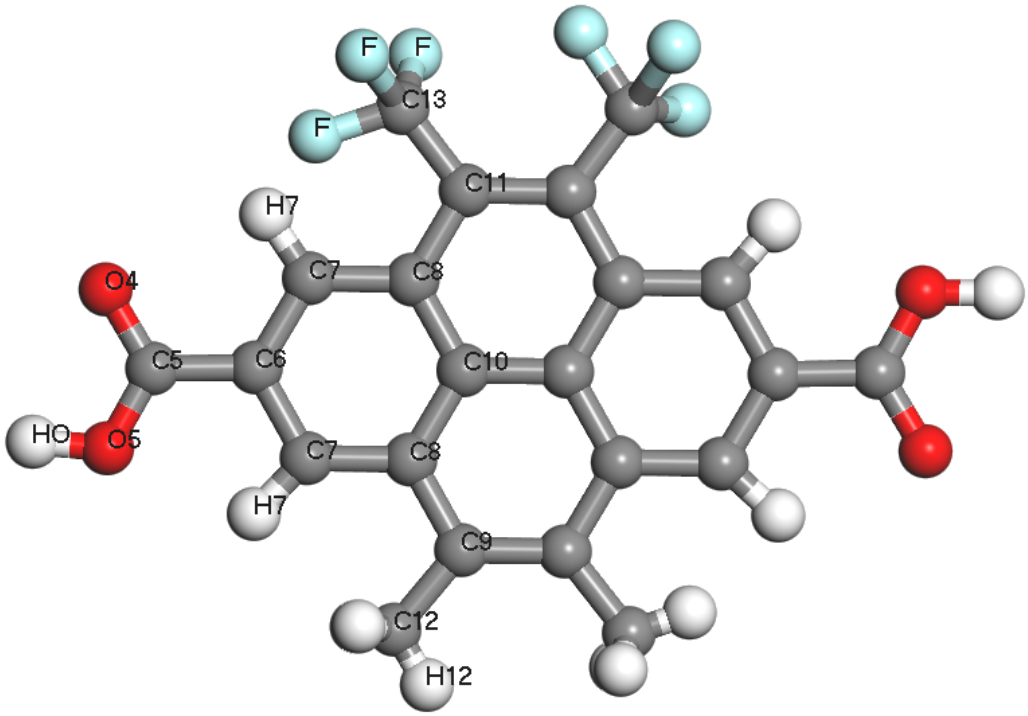

Charges

Atoms	Charges
C5	0.794
C6	-0.089
C7	-0.162
C8	0.120
C9	0.007
C10	-0.030
C11	-0.172

C12	-0.267
C13	0.634
O4	-0.605
O5	-0.515
HO	0.342
H7	0.132
H12	0.108
F	-0.201

Bond

$k_{ij}(l_{ij} - l_{ij_0})^2$			
i	j	K_{bond}, kJ mol^{-1} nm^{-2}	θ_{bond}, nm
O4	C5	479397.137	0.1366
O5	C5	479397.137	0.1366
O5	HO	504455.078	0.0966
C5	C6	327968.383	0.1458
C6	C7	387408.836	0.1379
C7	H7	299306.278	0.1081
C7	C8	387408.836	0.1379
C8	C10	387408.836	0.1379
C8	C11	387408.836	0.1379
C8	C9	387408.836	0.1379
C9	C9	387408.836	0.1379
C9	C12	309776.253	0.1486

C10	C10	387408.836	0.1379
C11	C11	387408.836	0.1379
C11	C13	309776.253	0.1486
C12	H12	277224.263	0.1109
C13	F	349820.315	0.1382

Angle

$k_\theta(\theta - \theta_0)^2$				
i	j	k	K_{angle}, kJ mol^{-1} rad^{-2}	θ_{angle}, degree
O4	C5	O5	1794.000	120.000
O4	C5	C6	1348.928	120.000
O5	C5	C6	1348.928	120.000
C5	C6	C7	1106.499	120.000
C6	C7	H7	620.3582	120.000
C6	C7	C8	1205.193	120.000
C7	C8	C10	1205.193	120.000
C7	C8	C11	1205.193	120.000
C7	C6	C7	1205.193	120.000
C8	C10	C8	1205.193	120.000
C8	C10	C10	1205.193	120.000
C8	C11	C11	1205.193	120.000
C8	C11	C13	1073.514	120.000
C8	C9	C9	1205.193	120.000
C8	C9	C12	1073.514	120.000

C9	C9	C12	1073.514	120.000
C9	C8	C7	1205.193	120.000
C9	C8	C10	1205.193	120.000
C9	C12	H12	494.503	109.470
C10	C8	C11	1205.193	120.000
C11	C11	C13	1073.514	120.000
C11	C13	F	927.0964	109.470
HO	O5	C5	737.4562	104.510
H4	C4	C3	620.358	120.000
H7	C7	C8	620.358	120.000
H12	C12	H12	306.579	109.47
F	C13	F	942.705	109.47

Torsion

$k(1+\cos(n\varphi-\varphi_0))$						
i	j	k	l	n	$K_{torsion}$, kJ mol^{-1}	$\theta_{torsion}$, degree
O4	C5	C6	C7	2	5.234	180.000
C5	C6	C7	H7	2	14.104	180.000
C5	C6	C7	C8	2	14.104	180.000
C6	C7	C8	C9	2	14.104	180.000
C6	C7	C8	C10	2	14.104	180.000
C6	C7	C8	C11	2	14.104	180.000
C7	C6	C7	C8	2	14.104	180.000
C7	C6	C7	H7	2	14.104	180.000

C7	C8	C9	C9	2	14.104	180.000
C7	C8	C9	C12	2	14.104	180.000
C7	C8	C10	C8	2	14.104	180.000
C7	C8	C10	C10	2	14.104	180.000
C7	C8	C11	C11	2	14.104	180.000
C7	C8	C11	C13	2	14.104	180.000
C8	C9	C9	C8	2	14.104	180.000
C8	C9	C9	C12	2	14.104	180.000
C8	C9	C12	H12	6	0.349	-180.000
C8	C10	C8	C7	2	14.104	180.000
C8	C10	C8	C9	2	14.104	180.000
C8	C10	C8	C11	2	14.104	180.000
C8	C10	C10	C8	2	14.104	180.000
C8	C11	C11	C8	2	14.104	180.000
C8	C11	C11	C13	2	14.104	180.000
C8	C11	C13	F	6	0.349	-180.000
C9	C9	C12	H12	2	14.104	180.000
C9	C9	C8	C10	2	14.104	180.000
C9	C8	C10	C10	2	14.104	180.000
C10	C8	C11	C11	2	14.104	180.000
C10	C10	C8	C11	2	14.104	180.000
C11	C11	C13	F	6	0.349	-180.000
HO	O5	C5	C6	2	10.467	180.000
HO	O5	C5	O4	2	1.047	0.000

H7	C7	C8	C9	2	14.104	180.000
H7	C7	C8	C10	2	14.104	180.000
H7	C7	C8	C11	2	14.104	180.000

9.2 Supporting Information for Chapter 6

9.2.1 Force field for ZIF-8

$$\Upsilon(r^N) = \sum_{i=1}^{N} \sum_{j=i+1}^{N} \left(4\varepsilon_{ij} \left(\left(\frac{\sigma_{ij}}{r_{ij}} \right)^{12} - \left(\frac{\sigma_{ij}}{r_{ij}} \right)^{6} \right) + \frac{q_i q_j}{4\pi\varepsilon_0 r_{ij}} \right)$$

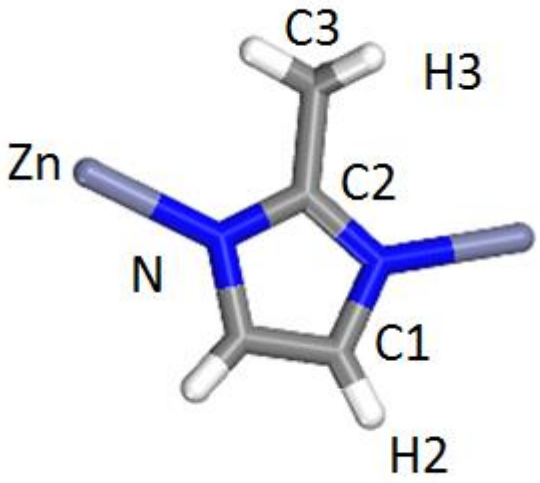

9.2.1.1 **Amrouche *et al.***

Atoms	**Sigma, Å**	**Epsilon, K**	**Charges**
C1	3.259	36.483	-0.08
C2	3.259	36.483	0.64
C3	3.259	36.483	-0.67
H2	2.440	15.288	0.144
H3	2.440	15.288	0.144
N	3.997	23.974	-0.54
Zn	2.338	43.084	1.1

9.2.1.2 **Hertag *et al.***

Atoms	**Sigma, Å**	**Epsilon, K**	**Charges**
C1	3.4	43.28	-0.1
C2	3.4	43.28	0.81901
C3	3.4	55.06	-0.4780
H2	2.511	7.55	0.1270
H3	2.65	7.89	0.1140
N	3.25	85.56	-0.685
Zn	1.96	6.29	1.2660

9.2.1.3 **Krokidas *et al.***

Atoms	**Sigma, Å**	**Epsilon, K**	**Charges**
C1	3.4	43.28	-0.0622
C2	3.4	43.28	0.7551
C3	3.4	55.06	-0.2697
H2	2.511	7.55	0.0912
H3	2.650	7.90	0.0499
N	3.25	85.56	-0.6822
Zn	1.96	6.29	1.3429

9.2.1.4 **Zheng *et al.***

Atoms	**Sigma, Å**	**Epsilon, K**	**Charges**
C1	3.4	43.28	-0.1924
C2	3.4	43.28	0.4339
C3	3.4	55.06	-0.6024

H2	2.511	7.55	0.1585
H3	2.650	7.90	0.1572
N	3.25	85.56	-0.3008
Zn	1.96	6.29	0.7362

9.2.1.5 **Zhang *et al.***

Atoms	**Sigma, Å**	**Epsilon, K**	**Charges**
C1	3.473	47.856	-0.196
C2	3.473	47.856	0.4190
C3	3.473	47.856	-0.6010
H2	2.846	7.649	0.1680
H3	2.846	7.649	0.1680
N	3.263	38.949	-0.3130
Zn	4.045	27.677	0.7200

9.2.1.6 **Wu *et al.***

Atoms	**Sigma, Å**	**Epsilon, K**	**Charges**
C1	3.431	33.55	-0.0839
C2	3.431	33.55	0.4291
C3	3.431	33.55	-0.4526
H2	2.571	14.03	0.1128
H3	2.571	14.03	0.1306
N	3.261	22.03	-0.3879
Zn	2.462	39.59	0.6918

9.2.2 Water Model Force Field

Type	Atoms	Sigma, Å	Epsilon, K	Charges
SPC/E	H	-	-	0.4238
	O	3.166	78.18	-0.8476
SPC-P	H	-	-	0.3650
	O	3.196	80.48	-0.7300
TIP3P	H	-	-	0.417
	O	3.15061	76.55	-0.834
TIP4P	H	-	-	0.52
	O	3.15365	77.94	-
	M	-	-	-1.04
TIP4P_2005	H	-	-	0.5564
	O	3.1589	93.204	-
	M	-	-	-1.1128
TIP4P_EW	H	-	-	0.5242
	O	3.1644	81.90	-
	M	-	-	-1.0484

9.2.3 Water cluster formation at 10 kPa

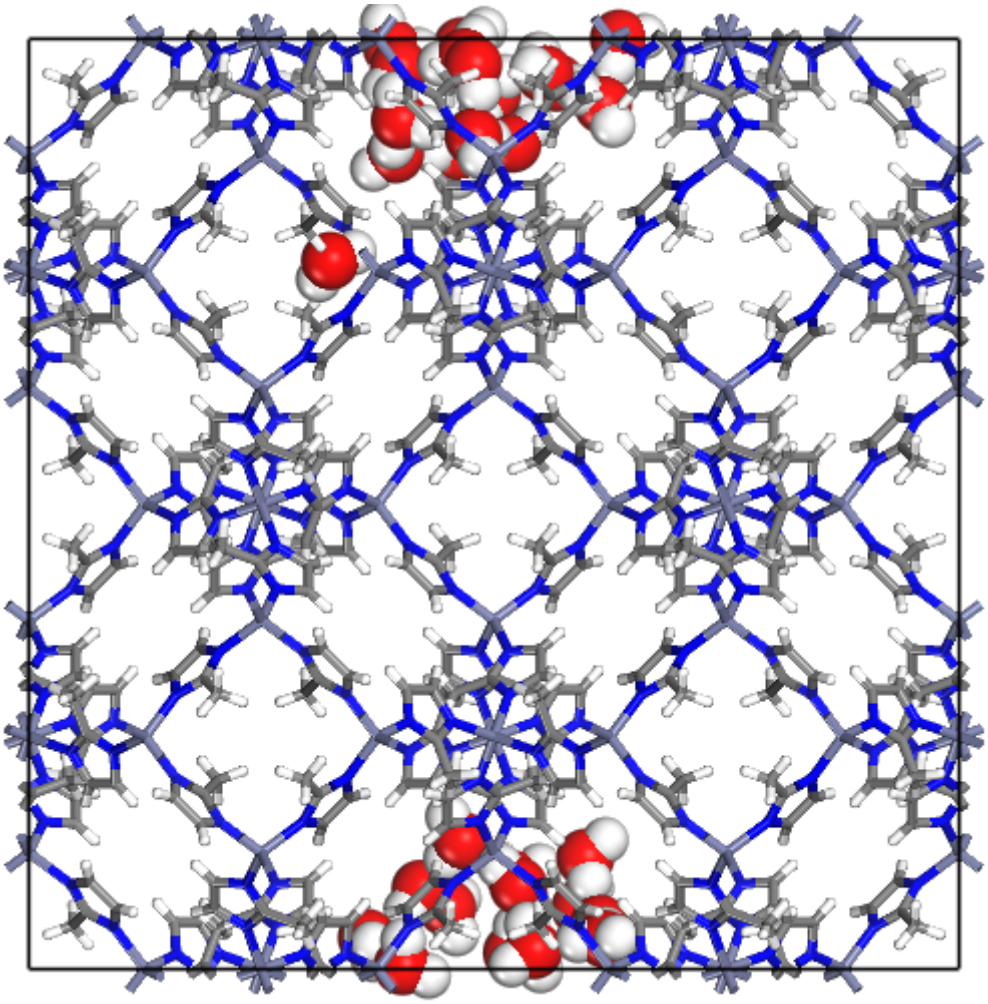

9.3 Supporting information for Chapter 7

9.3.1 Krokidas intramolecular Force Field

Bonds

$k_{ij}(l_{ij} - l_{ij_0})^2$			
i	**j**	**K_{bond}, kJ mol^{-1} nm^{-2}**	**θ_{bond}, nm**
Zn	N	52802.1	0.20111
N	C1	253048.3	0.13350
N	C2	253048.3	0.13700
C1	C3	203760.8	0.14900
C2	C2	339991.8	0.13500
C2	H2	327690.9	0.10800
C3	H3	286855.0	0.10900

Angle

$k_\theta(\theta - \theta_0)^2$				
i	**j**	**k**	**K_{angle}, kJ mol^{-1} rad^{-2}**	**θ_{angle}, degree**
N	C1	N	955.630	112.161
N	C1	C3	958.970	123.921
N	C2	C2	909.610	108.650
C2	C2	H2	552.290	125.681
C1	C3	H3	565.680	109.320

C1	N	Zn	462.740	128.330
C2	N	Zn	462.740	128.333
C1	N	C2	1077.80	105.270
N	C2	H2	549.780	125.682
N	Zn	N	296.230	109.480

Torsion

$k(1+\cos(n\varphi-\varphi_0))$						
i	**j**	**k**	**l**	**n**	**$K_{torsion}$, kJ mol^{-1}**	**$\theta_{torsion}$, degree**
Zn	N	C2	H2	2	25.1	180
Zn	N	C2	C2	2	25.1	180
C1	N	C2	C2	2	25.1	180
C1	N	C2	H2	2	25.1	180
N	C2	C2	H2	2	90	180
N	C1	N	C2	2	41.8	180
N	C1	N	Zn	2	41.8	180
C3	C1	N	Zn	2	41.8	180
C3	C1	N	C2	2	41.8	180

9.3.2 Zheng Intramolecular Force Field

$k_{ij}(l_{ij} - l_{ij_0})^2$			
i	**j**	**K_{bond}, kJ mol^{-1} nm^{-2}**	**θ_{bond}, nm**
Zn	N	32813.0	0.20111
N	C1	203984.0	0.13350
N	C2	184007.8	0.13700
C1	C3	144855.0	0.14900
C2	C2	225824.1	0.13500
C2	H2	153406.0	0.10800
C3	H3	142120.0	0.10900

Angle

$k_\theta(\theta - \theta_0)^2$				
i	**j**	**k**	**K_{angle}, kJ mol^{-1} rad^{-2}**	**θ_{angle}, degree**
N	C1	N	315.825	112.161
N	C1	C3	275.943	123.921
N	C2	C2	308.275	108.650
C2	C2	H2	206.705	125.681
C1	C3	H3	201.008	109.320
C1	N	Zn	203.482	128.330
C2	N	Zn	135.754	128.333

C1	N	C2	297.842	105.270
N	C2	H2	206.705	125.682
N	Zn	N	147.303	109.480

Torsion

$k(1+\cos(n\varphi-\varphi_0))$						
i	**j**	**k**	**l**	**n**	**$K_{torsion}$, kJ mol^{-1}**	**$\theta_{torsion}$, degree**
Zn	N	C2	H2	2	9.7185	180
Zn	N	C2	C2	2	9.7185	180
C1	N	C2	C2	2	9.7185	180
C1	N	C2	H2	2	9.7185	180
H2	C2	C2	H2	2	21.527	180
N	C2	C2	H2	2	21.527	180
N	C1	N	C2	2	20.9	180
N	C1	N	Zn	2	20.9	180
C3	C1	N	Zn	2	20.9	180
C3	C1	N	C2	2	20.9	180

Improper Dihedral

$k_\varphi(l_\varphi-l_{\varphi_0})^2$					
i	**j**	**k**	**l**	**$K_{torsion}$, kJ mol^{-1}**	**$\theta_{torsion}$, degree**

N	C3	C2	N	8.36	180
C1	H2	C1	N	8.36	180
C2	Zn	N	C1	8.36	180

9.3.3 Wu Intramolecular Force Field

$k_{ij}(l_{ij} - l_{ij_0})^2$			
i	**j**	**K_{bond}, kJ mol^{-1} nm^{-2}**	**θ_{bond}, nm**
Zn	N	35965.2	0.1987
N	C1	204179.2	0.1339
N	C2	171462.0	0.1339
C1	C3	132569.4	0.1492
C2	C2	339991.8	0.1375
C2	H2	153479.4	0.0929
C3	H3	142188.0	0.0959

Angle

$k_\theta(\theta - \theta_0)^2$				
i	j	k	K_{angle}, kJ mol^{-1} rad^{-2}	θ_{angle}, degree
N	C1	N	292.74	112.17
N	C1	C3	292.74	123.89
N	C2	C2	292.74	108.67
C2	C2	H2	209.1	125.67
C1	C3	H3	209.1	109.5
C1	N	Zn	209.1	127.5
C2	N	Zn	146.37	128.0
C1	N	C2	292.74	104.5

N	C2	H2	209.1	125.67
N	Zn	N	43.911	109.47

Torsion

$k(1+\cos(n\varphi-\varphi_0))$						
i	**j**	**k**	**l**	**n**	**$K_{torsion}$, kJ mol^{-1}**	**$\theta_{torsion}$, degree**
Zn	N	C2	H2	2	20.074	180
Zn	N	C2	C2	2	0.4182	180
C1	N	C2	C2	2	0.4182	180
C1	N	C2	H2	2	20.074	180
H2	C2	C2	H2	2	16.728	180
N	C2	C2	H2	2	16.728	180
N	C1	N	C2	2	20.074	180
N	C1	N	Zn	2	0.4182	180
C3	C1	N	Zn	2	0.4182	180
C3	C1	N	C2	2	17.355	180
N	Zn	N	C1	3	0.7277	0.0
N	Zn	N	C2	3	0.7277	0.0

Improper Dihedral

$k(1+\cos(n\varphi-\varphi_0))$						
i	**j**	**k**	**l**	**n**	**$K_{torsion}$, kJ mol^{-1}**	**$\theta_{torsion}$, degree**
N	C3	C2	N	2	4.598	180
C1	H1	C1	N	2	4.598	180

9.3.4 Snap shot of pore saturation for every 10 ns

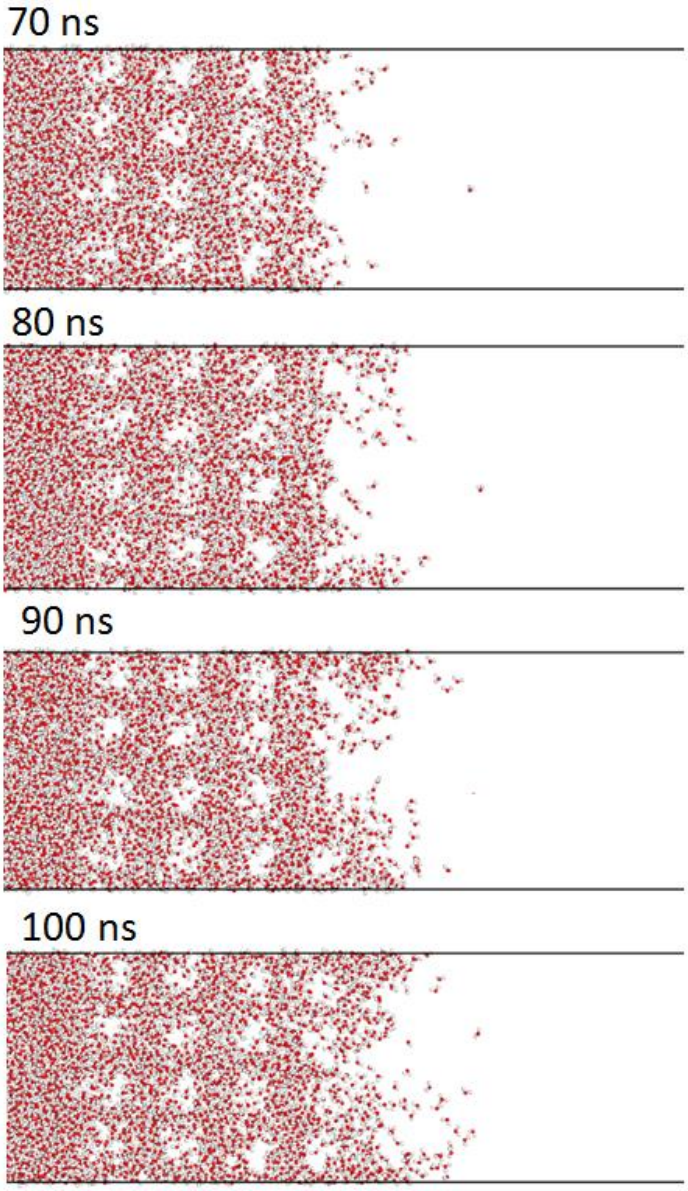

9.3.5 Z-Density plot for TIP4P for ZIF-8 structure described by Krokidas at 10 MPa (Top) and 30 MPa (Bottom)

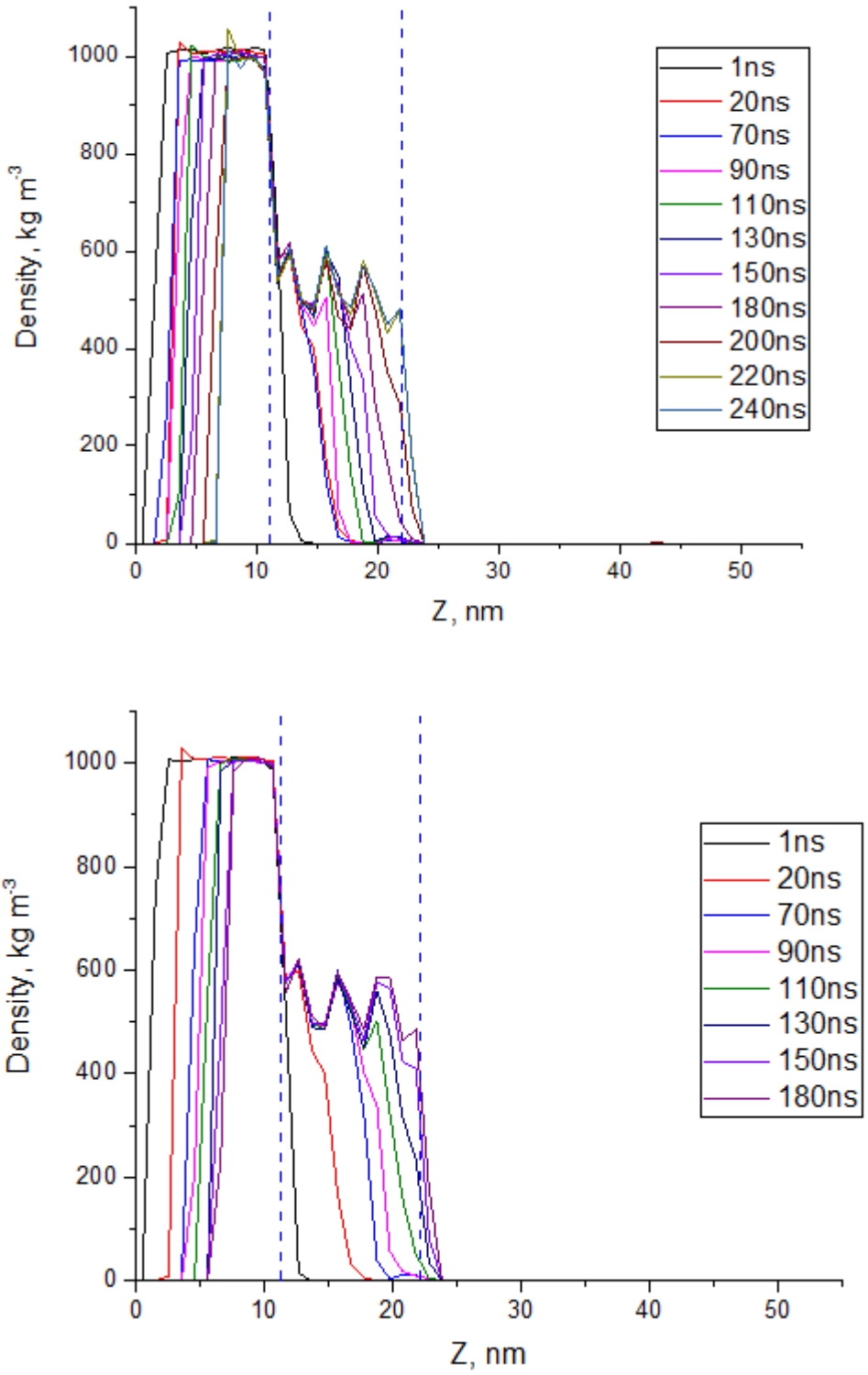

9.3.6 Z-Density plot for TIP3P for ZIF-8 structure described by Krokidas at 10 MPa (Top) and 30 MPa (Bottom)

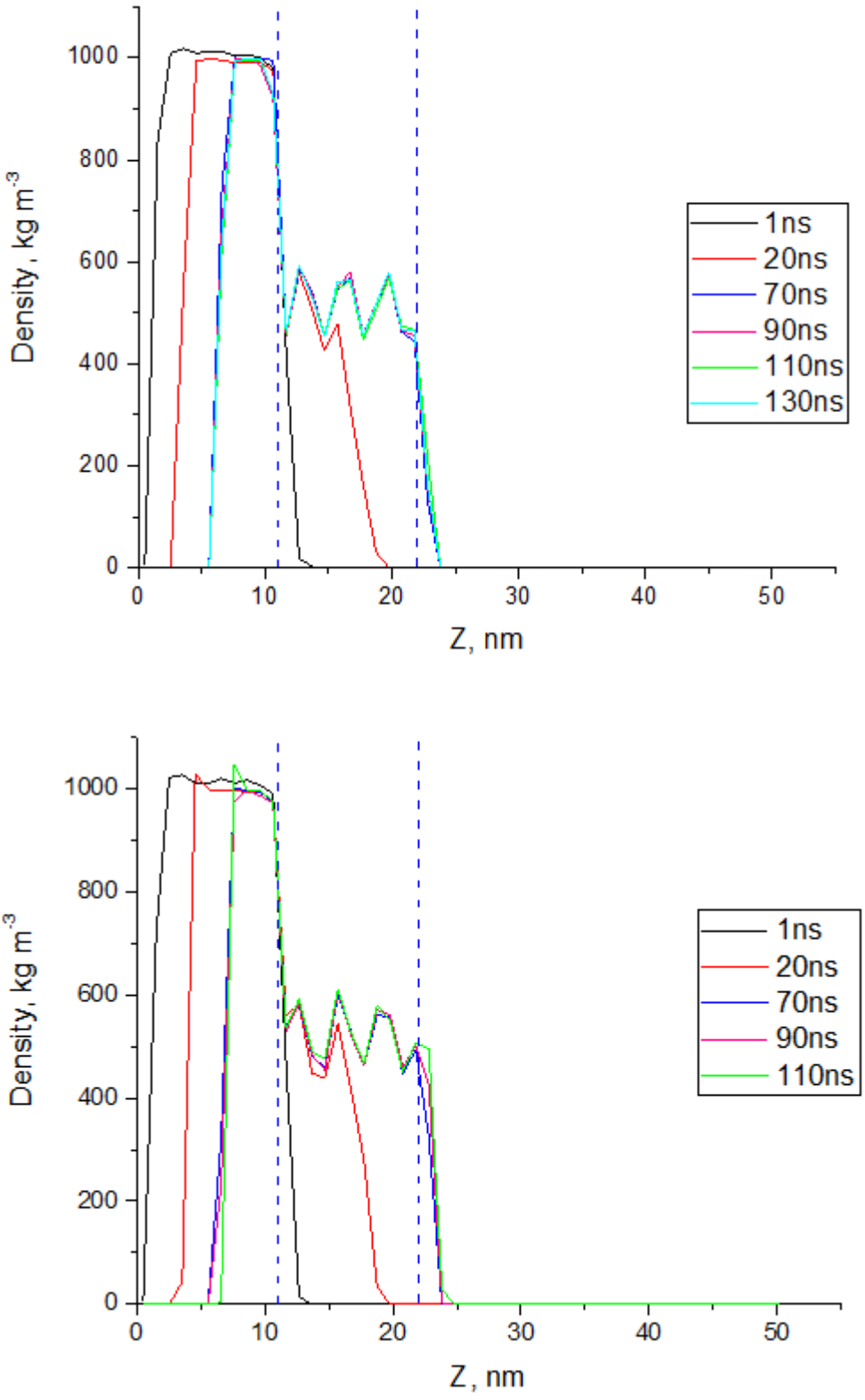

9.3.7 Z-Density plot for SPC/E for ZIF-8 structure described by Krokidas at 10 MPa (Top) and 30 MPa (Bottom)

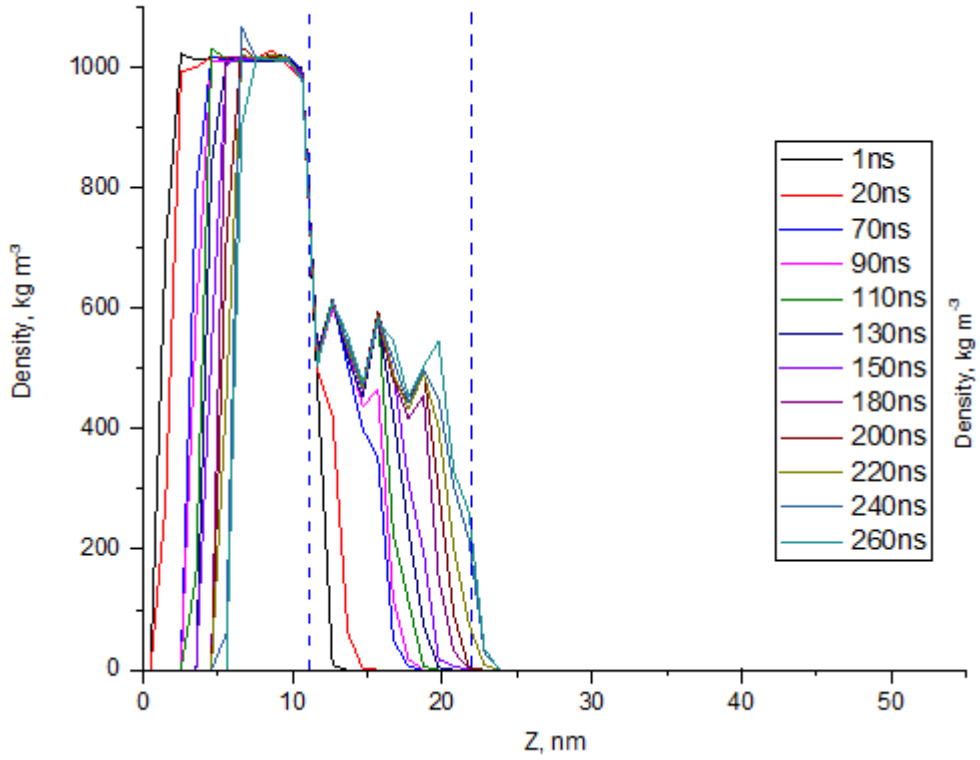

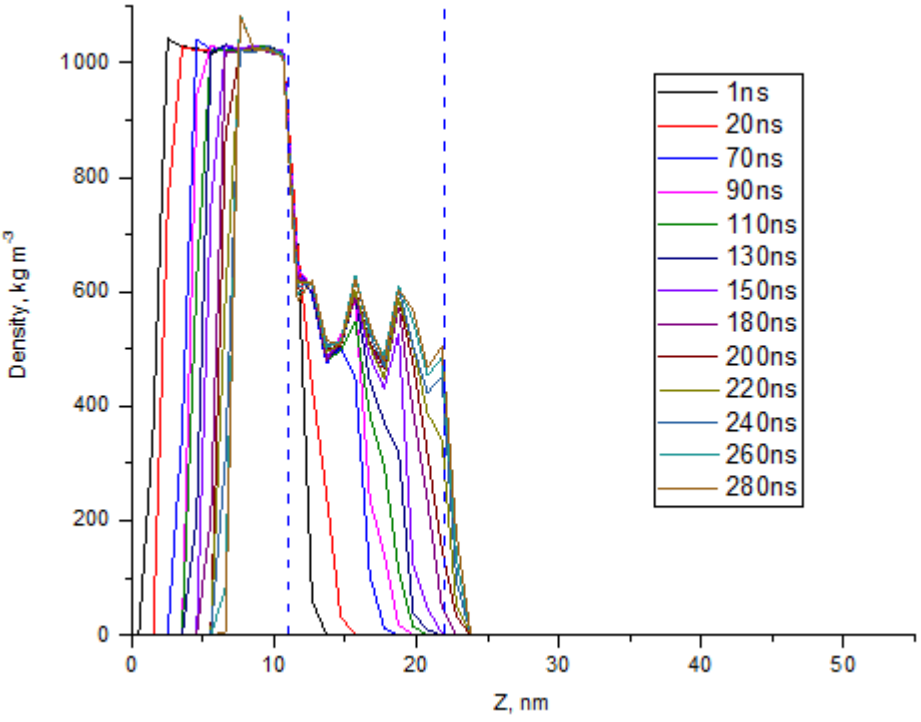

9.3.8 Z-Density plot for TIP4P for ZIF-8 structure described by Zheng at 10 MPa (Top) and 30 MPa (Bottom)

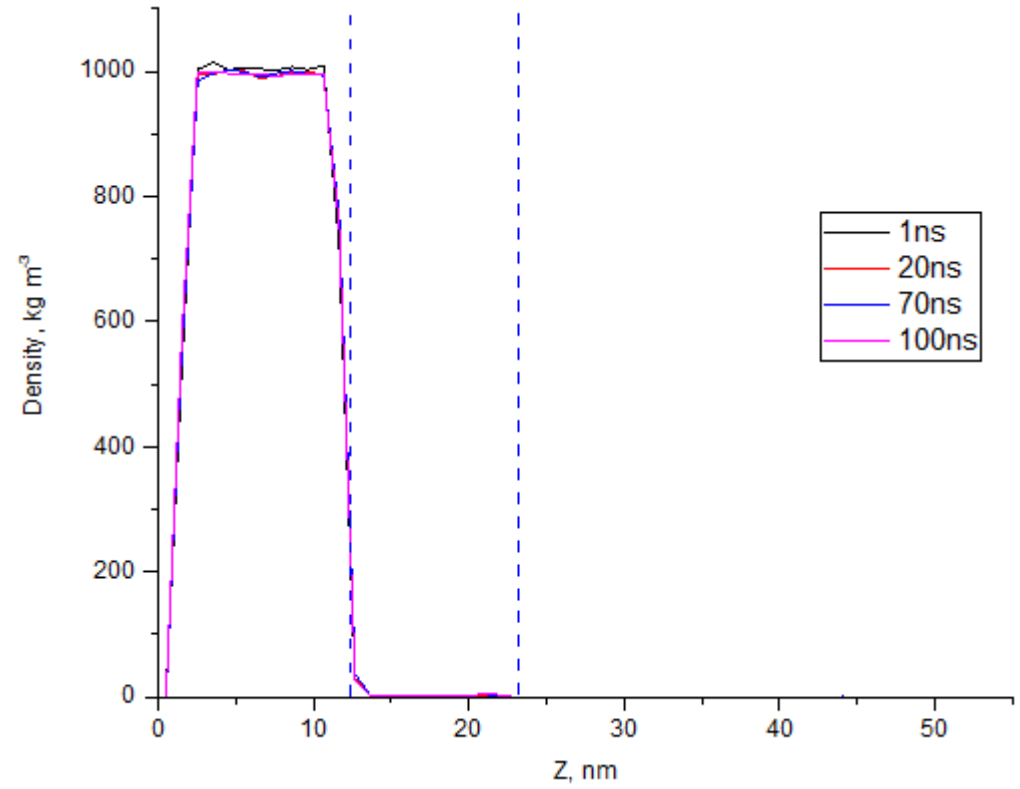

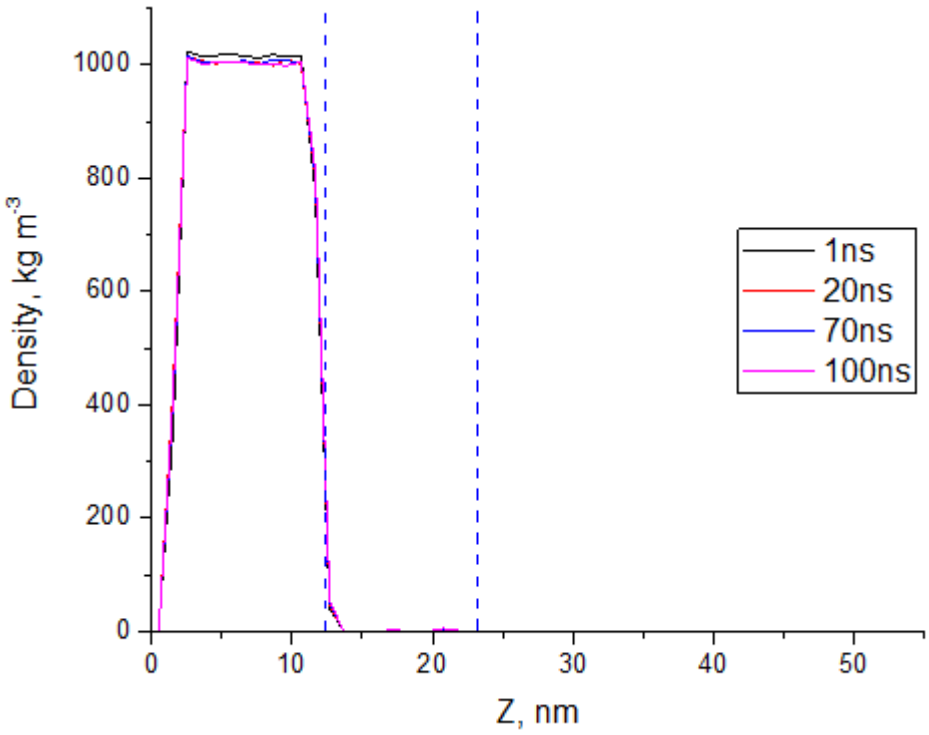

9.3.9 Z-Density plot for TIP3P for ZIF-8 structure described by Zheng at 10 MPa (Top) and 30 MPa (Bottom)

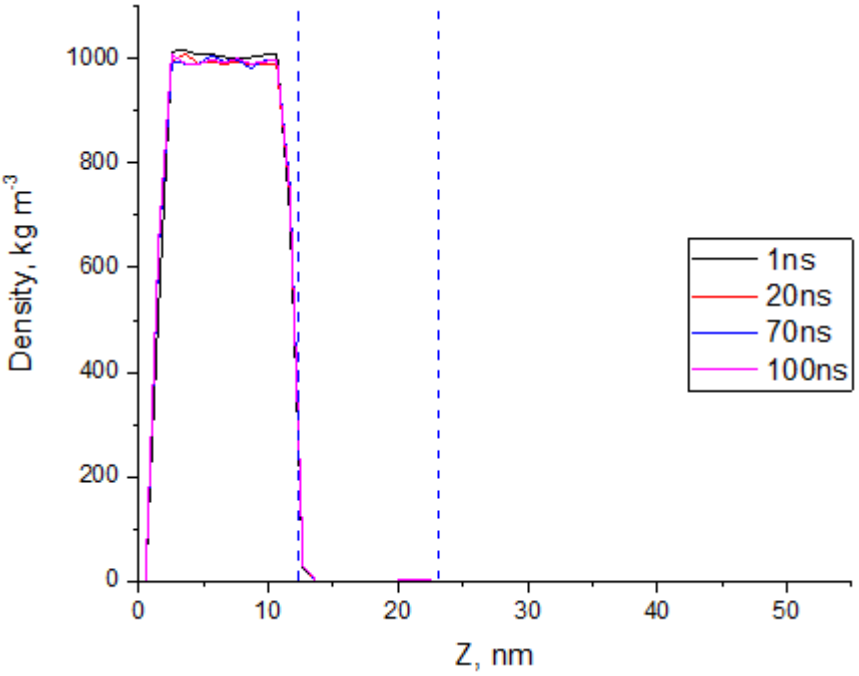

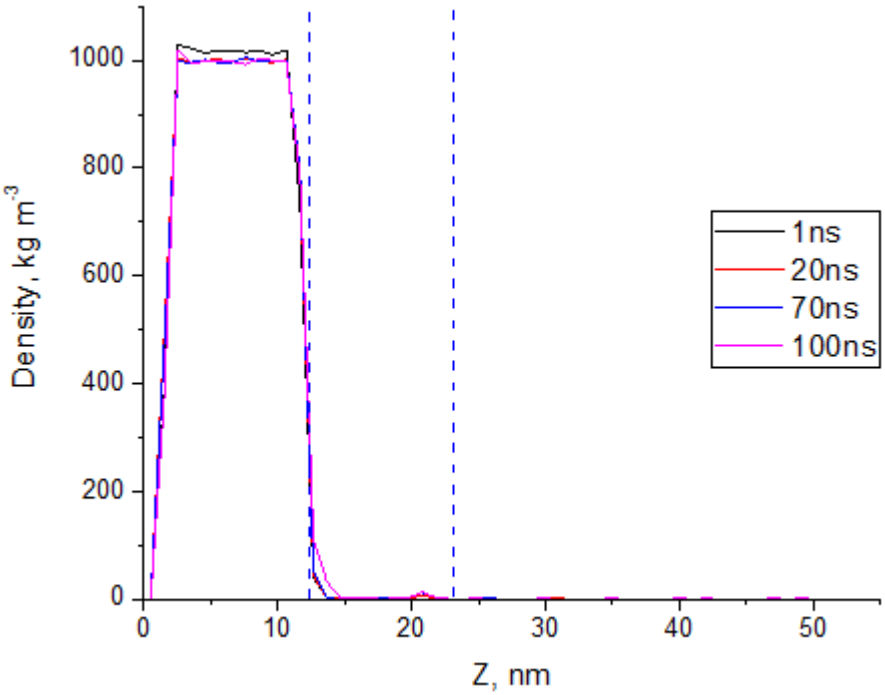

9.3.10 Z-Density plot for SPC/E for ZIF-8 structure described by Zheng at 10 MPa (Top) and 30 MPa (Bottom)

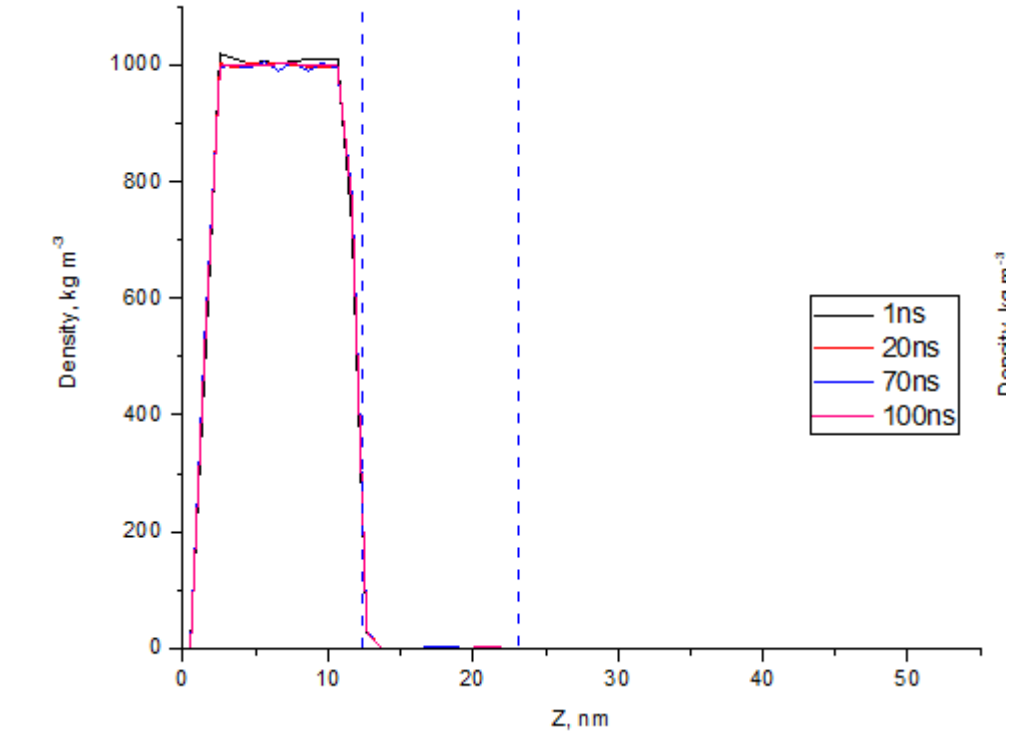

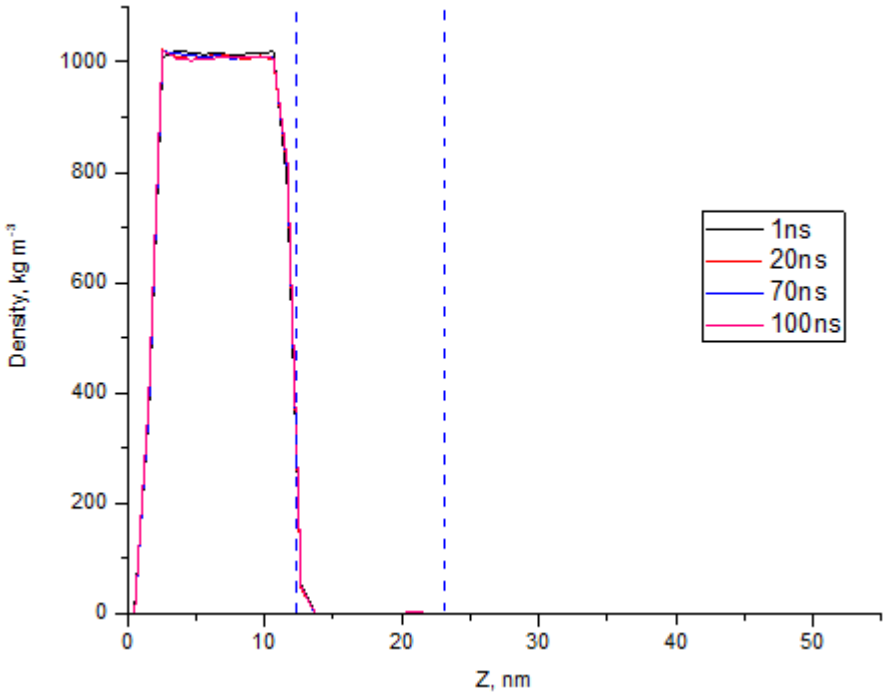

9.3.11 Z-Density plot for TIP4P for ZIF-8 structure described by Wu at 10 MPa (Top) and 30 MPa (Bottom)

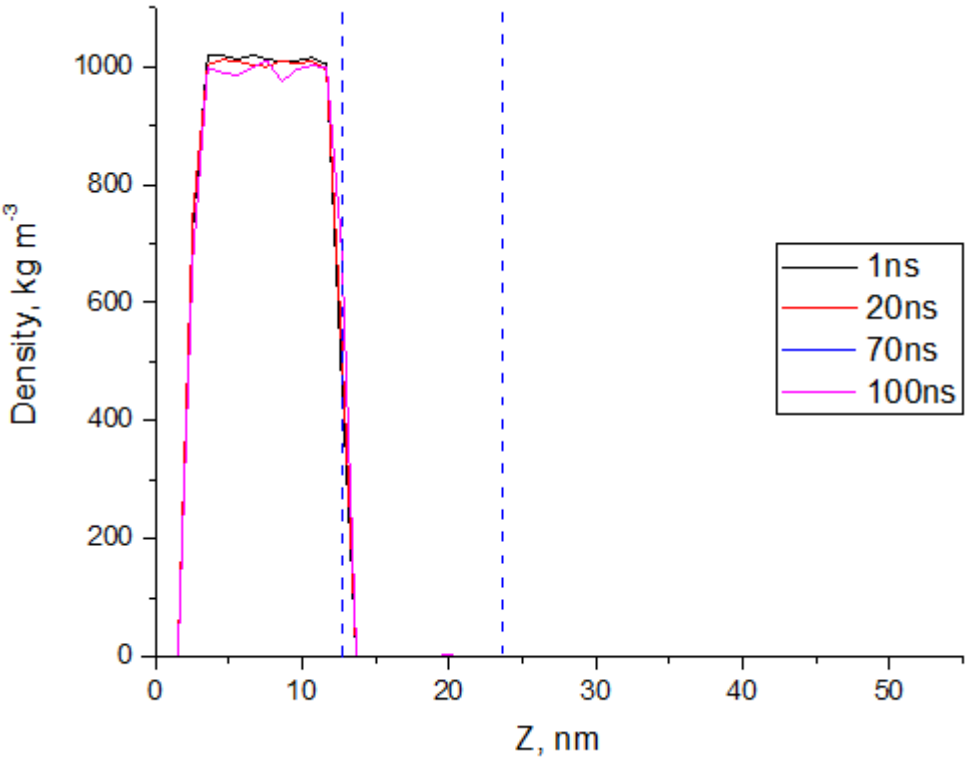

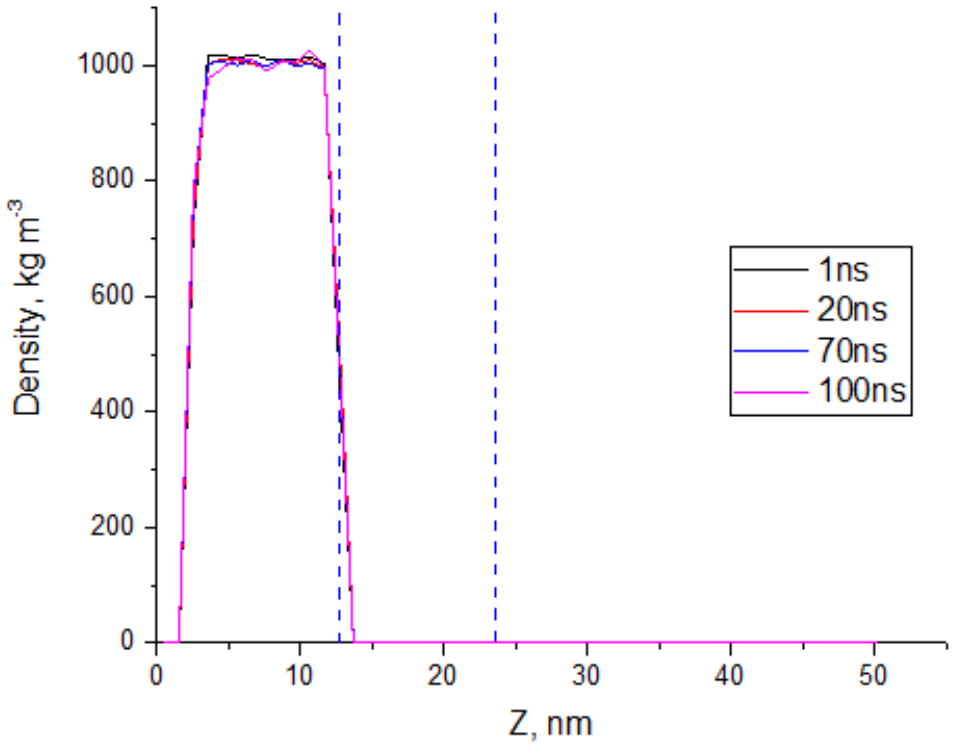

Reference

1. Schneemann A, Bon V, Schwedler I, Senkovska I, Kaskel S, Fischer RA. Flexible metal-organic frameworks. Chem Soc Rev. 2014;43(16):6062-96.
2. Furukawa H, Cordova KE, O'Keeffe M, Yaghi OM. The Chemistry and Applications of Metal-Organic Frameworks. Science. 2013;341(6149).
3. Adhikari AK, Lin K-S. Improving CO2 adsorption capacities and CO2/N2 separation efficiencies of MOF-74(Ni, Co) by doping palladium-containing activated carbon. Chem Eng J. 2016;284:1348-60.
4. Amrouche H, Aguado S, Pérez-Pellitero J, Chizallet C, Siperstein F, Farrusseng D, et al. Experimental and Computational Study of Functionality Impact on Sodalite–Zeolitic Imidazolate Frameworks for CO2 Separation. J Phys Chem C. 2011;115(33):16425-32.
5. Bao Z, Yu L, Ren Q, Lu X, Deng S. Adsorption of CO2 and CH4 on a magnesium-based metal organic framework. J Colloid Interface Sci. 2011;353(2):549-56.
6. Britt D, Furukawa H, Wang B, Glover TG, Yaghi OM. Highly efficient separation of carbon dioxide by a metal-organic framework replete with open metal sites. Proc Natl Acad Sci USA. 2009;106(49):20637-40.
7. Bux H, Chmelik C, Krishna R, Caro J. Ethene/ethane separation by the MOF membrane ZIF-8: Molecular correlation of permeation, adsorption, diffusion. Journal of Membrane Science. 2011;369(1):284-9.
8. Caro J. Are MOF membranes better in gas separation than those made of zeolites? Current Opinion in Chemical Engineering. 2011;1(1):77-83.
9. Mu L, Liu B, Liu H, Yang Y, Sun C, Chen G. A novel method to improve the gas storage capacity of ZIF-8. J Mater Chem. 2012;22(24):12246-52.
10. Millward AR, Yaghi OM. Metal−Organic Frameworks with Exceptionally High Capacity for Storage of Carbon Dioxide at Room Temperature. J Am Chem Soc. 2005;127(51):17998-9.
11. Alezi D, Belmabkhout Y, Suyetin M, Bhatt PM, Weseliński ŁJ, Solovyeva V, et al. MOF Crystal Chemistry Paving the Way to Gas Storage Needs: Aluminum-Based soc-MOF for CH4, O2, and CO2 Storage. J Am Chem Soc. 2015;137(41):13308-18.
12. Pérez-Pellitero J, Amrouche H, Siperstein FR, Pirngruber G, Nieto-Draghi C, Chaplais G, et al. Adsorption of CO2, CH4, and N2 on Zeolitic Imidazolate Frameworks: Experiments and Simulations. Chem Eur J. 2010;16(5):1560-71.
13. Poloni R, Lee K, Berger RF, Smit B, Neaton JB. Understanding Trends in CO2 Adsorption in Metal–Organic Frameworks with Open-Metal Sites. J Phys Chem Lett. 2014;5(5):861-5.
14. Chen B, Wang L, Zapata F, Qian G, Lobkovsky EB. A Luminescent Microporous Metal−Organic Framework for the Recognition and Sensing of Anions. J Am Chem Soc. 2008;130(21):6718-9.
15. Liu C-S, Zhang Z-H, Chen M, Zhao H, Duan F-H, Chen D-M, et al. Pore modulation of zirconium-organic frameworks for high-efficiency detection of trace proteins. Chem Commun. 2017;53(28):3941-4.
16. Wang J-H, Li M, Li D. A dynamic, luminescent and entangled MOF as a qualitative sensor for volatile organic solvents and a quantitative monitor for acetonitrile vapour. Chem Sci. 2013;4(4):1793-801.
17. Wu M-X, Yang Y-W. Metal–Organic Framework (MOF)-Based Drug/Cargo Delivery and Cancer Therapy. Adv Mater. 2017;29(23):1606134.
18. Suyetin MV, Vakhrushev AV. Temperature-sensitive nanocapsule for drug delivery. IET Micro & Nano Letters. 2011;6(1):39-42.

19. Filippousi M, Turner S, Leus K, Siafaka PI, Tseligka ED, Vandichel M, et al. Biocompatible Zr-based nanoscale MOFs coated with modified poly(ε-caprolactone) as anticancer drug carriers. Int J Pharm. 2016;509(1):208-18.
20. McKinlay AC, Morris RE, Horcajada P, Férey G, Gref R, Couvreur P, et al. BioMOFs: Metal–Organic Frameworks for Biological and Medical Applications. Angew Chem Int Ed. 2010;49(36):6260-6.
21. Akpinar I, Yazaydin AO. Adsorption of Atrazine from Water in Metal–Organic Framework Materials. Journal of Chemical & Engineering Data. 2018.
22. Hu Z, Chen Y, Jiang J. Zeolitic imidazolate framework-8 as a reverse osmosis membrane for water desalination: Insight from molecular simulation. J Chem Phys. 2011;134(13):134705.
23. Canepa P, Arter CA, Conwill EM, Johnson DH, Shoemaker BA, Soliman KZ, et al. High-throughput screening of small-molecule adsorption in MOF. J Mater Chem A. 2013;1(43):13597-604.
24. Tan K, Zuluaga S, Wang H, Canepa P, Soliman K, Cure J, et al. Interaction of Acid Gases SO2 and NO2 with Coordinatively Unsaturated Metal Organic Frameworks: M-MOF-74 (M = Zn, Mg, Ni, Co). Chem Mater. 2017;29(10):4227-35.
25. Khay I, Chaplais G, Nouali H, Ortiz G, Marichal C, Patarin J. Assessment of the energetic performances of various ZIFs with SOD or RHO topology using high pressure water intrusion-extrusion experiments. Dalton Transactions. 2016;45(10):4392-400.
26. Ortiz G, Nouali H, Marichal C, Chaplais G, Patarin J. Energetic Performances of "ZIF-71–Aqueous Solution" Systems: A Perfect Shock-Absorber with Water. J Phys Chem C. 2014;118(37):21316-22.
27. Ortiz G, Nouali H, Marichal C, Chaplais G, Patarin J. Energetic performances of the metal-organic framework ZIF-8 obtained using high pressure water intrusion-extrusion experiments. Phys Chem Chem Phys. 2013;15(14):4888-91.
28. Yot PG, Boudene Z, Macia J, Granier D, Vanduyfhuys L, Verstraelen T, et al. Metal-organic frameworks as potential shock absorbers: the case of the highly flexible MIL-53(Al). Chem Commun. 2014;50(67):9462-4.
29. Moghadam PZ, Li A, Wiggin SB, Tao A, Maloney AGP, Wood PA, et al. Development of a Cambridge Structural Database Subset: A Collection of Metal–Organic Frameworks for Past, Present, and Future. Chem Mater. 2017;29(7):2618-25.
30. Park J, Howe JD, Sholl DS. How Reproducible Are Isotherm Measurements in Metal–Organic Frameworks? Chem Mater. 2017;29(24):10487-95.
31. Broom DP, Hirscher M. Irreproducibility in hydrogen storage material research. Energy & Environmental Science. 2016;9(11):3368-80.
32. Yu D, Yazaydin AO, Lane JR, Dietzel PDC, Snurr RQ. A combined experimental and quantum chemical study of CO2 adsorption in the metal-organic framework CPO-27 with different metals. Chem Sci. 2013;4(9):3544-56.
33. Fairen-Jimenez D, Galvelis R, Torrisi A, Gellan AD, Wharmby MT, Wright PA, et al. Flexibility and swing effect on the adsorption of energy-related gases on ZIF-8: combined experimental and simulation study. Dalton Transactions. 2012;41(35):10752-62.
34. Guo H-c, Shi F, Ma Z-f, Liu X-q. Molecular Simulation for Adsorption and Separation of CH4/H2 in Zeolitic Imidazolate Frameworks. J Phys Chem C. 2010;114(28):12158-65.
35. Hobday CL, Woodall CH, Lennox MJ, Frost M, Kamenev K, Düren T, et al. Understanding the adsorption process in ZIF-8 using high pressure crystallography and computational modelling. Nature Communications. 2018;9(1):1429.

36. Snurr RQ, Bell AT, Theodorou DN. Prediction of adsorption of aromatic hydrocarbons in silicalite from grand canonical Monte Carlo simulations with biased insertions. The Journal of Physical Chemistry. 1993;97(51):13742-52.
37. Zhang H, Snurr RQ. Computational Study of Water Adsorption in the Hydrophobic Metal–Organic Framework ZIF-8: Adsorption Mechanism and Acceleration of the Simulations. J Phys Chem C. 2017;121(43):24000-10.
38. Hyeon S, Kim Y-C, Kim J. Computational prediction of high methane storage capacity in V-MOF-74. Phys Chem Chem Phys. 2017;19(31):21132-9.
39. Jiao Y, Morelock CR, Burtch NC, Mounfield WP, Hungerford JT, Walton KS. Tuning the Kinetic Water Stability and Adsorption Interactions of Mg-MOF-74 by Partial Substitution with Co or Ni. Industrial & Engineering Chemistry Research. 2015;54(49):12408-14.
40. Kim H, Park J, Jung Y. The binding nature of light hydrocarbons on Fe/MOF-74 for gas separation. Phys Chem Chem Phys. 2013;15(45):19644-50.
41. Kuppler RJ, Timmons DJ, Fang Q-R, Li J-R, Makal TA, Young MD, et al. Potential applications of metal-organic frameworks. Coord Chem Rev. 2009;253(23–24):3042-66.
42. Babaei H, McGaughey AJH, Wilmer CE. Effect of pore size and shape on the thermal conductivity of metal-organic frameworks. Chem Sci. 2017;8(1):583-9.
43. Susumu K, Mitsuru K. Functional Micropore Chemistry of Crystalline Metal Complex-Assembled Compounds. Bull Chem Soc Jpn. 1998;71(8):1739-53.
44. Serre C, Millange F, Thouvenot C, Noguès M, Marsolier G, Louër D, et al. Very Large Breathing Effect in the First Nanoporous Chromium(III)-Based Solids: MIL-53 or CrIII(OH)·{O2C−C6H4−CO2}·{HO2C−C6H4−CO2H}x·H2Oy. J Am Chem Soc. 2002;124(45):13519-26.
45. Ferey G, Serre C. Large breathing effects in three-dimensional porous hybrid matter: facts, analyses, rules and consequences. Chem Soc Rev. 2009;38(5):1380-99.
46. Chuan-De W, Wenbin L. Highly Porous, Homochiral Metal–Organic Frameworks: Solvent-Exchange-Induced Single-Crystal to Single-Crystal Transformations. Angew Chem Int Ed. 2005;44(13):1958-61.
47. Ania CO, García-Pérez E, Haro M, Gutiérrez-Sevillano JJ, Valdés-Solís T, Parra JB, et al. Understanding Gas-Induced Structural Deformation of ZIF-8. J Phys Chem Lett. 2012;3(9):1159-64.
48. Armaroli N, Balzani V, Collin J-P, Gaviña P, Sauvage J-P, Ventura B. Rotaxanes incorporating two different coordinating units in their thread: synthesis and electrochemically and photochemically induced molecular motions. J Am Chem Soc. 1999;121(18):4397-408.
49. Neal EA, Goldup SM. Chemical consequences of mechanical bonding in catenanes and rotaxanes: isomerism, modification, catalysis and molecular machines for synthesis. Chem Commun. 2014;50(40):5128-42.
50. Vignon SA, Jarrosson T, Iijima T, Tseng H-R, Sanders JK, Stoddart JF. Switchable neutral bistable rotaxanes. J Am Chem Soc. 2004;126(32):9884-5.
51. Chen Q, Sun J, Li P, Hod I, Moghadam PZ, Kean ZS, et al. A Redox-Active Bistable Molecular Switch Mounted inside a Metal–Organic Framework. J Am Chem Soc. 2016;138(43):14242-5.
52. Silvi S, Venturi M, Credi A. Light operated molecular machines. Chem Commun. 2011;47(9):2483-9.
53. Feringa B, Koumura N, Van Delden R, Ter Wiel M. Light-driven molecular switches and motors. Applied Physics A: Materials Science & Processing. 2002;75(2):301-8.

54. Pollard MM, ter Wiel MKJ, van Delden RA, Vicario J, Koumura N, van den Brom CR, et al. Light-Driven Rotary Molecular Motors on Gold Nanoparticles. Chem Eur J. 2008;14(36):11610-22.
55. Hess H, Clemmens J, Qin D, Howard J, Vogel V. Light-Controlled Molecular Shuttles Made from Motor Proteins Carrying Cargo on Engineered Surfaces. Nano Lett. 2001;1(5):235-9.
56. Koumura N, Zijlstra RWJ, van Delden RA, Harada N, Feringa BL. Light-driven monodirectional molecular rotor. Nature. 1999;401(6749):152-5.
57. Shirai Y, Morin J-F, Sasaki T, Guerrero JM, Tour JM. Recent progress on nanovehicles. Chem Soc Rev. 2006;35(11):1043-55.
58. Seldenthuis JS, Prins F, Thijssen JM, van der Zant HSJ. An All-Electric Single-Molecule Motor. ACS Nano. 2010;4(11):6681-6.
59. Kudernac T, Ruangsupapichat N, Parschau M, Macia B, Katsonis N, Harutyunyan SR, et al. Electrically driven directional motion of a four-wheeled molecule on a metal surface. Nature. 2011;479(7372):208-11.
60. van Dijk L, Tilby MJ, Szpera R, Smith OA, Bunce HAP, Fletcher SP. Molecular machines for catalysis. Nature Reviews Chemistry. 2018;2:0117.
61. Lavigne JJ, Anslyn EV. Sensing A Paradigm Shift in the Field of Molecular Recognition: From Selective to Differential Receptors. Angew Chem Int Ed. 2001;40(17):3118-30.
62. Dietrich-Buchecker CO, Sauvage JP, Kintzinger JP. Une nouvelle famille de molecules : les metallo-catenanes. Tetrahedron Lett. 1983;24(46):5095-8.
63. Anelli PL, Spencer N, Stoddart JF. A molecular shuttle. J Am Chem Soc. 1991;113(13):5131-3.
64. Eelkema R, Pollard MM, Vicario J, Katsonis N, Ramon BS, Bastiaansen CWM, et al. Molecular machines: Nanomotor rotates microscale objects. Nature. 2006;440(7081):163-.
65. Akimov AV, Kolomeisky AB. Unidirectional Rolling Motion of Nanocars Induced by Electric Field. J Phys Chem C. 2012;116(42):22595-601.
66. Lindqvist M, Borre K, Axenov K, Kótai B, Nieger M, Leskelä M, et al. Chiral Molecular Tweezers: Synthesis and Reactivity in Asymmetric Hydrogenation. J Am Chem Soc. 2015;137(12):4038-41.
67. Dahl BJ, Branchaud BP. Synthesis and characterization of a functionalized chiral biaryl capable of exhibiting unidirectional bond rotation. Tetrahedron Lett. 2004;45(52):9599-602.
68. van Delden RA, ter Wiel MKJ, Pollard MM, Vicario J, Koumura N, Feringa BL. Unidirectional molecular motor on a gold surface. Nature. 2005;437(7063):1337-40.
69. Ruangsupapichat N, Pollard MM, Harutyunyan SR, Feringa BL. Reversing the direction in a light-driven rotary molecular motor. Nat Chem. 2011;3(1):53-60.
70. McGonigal PR, Deria P, Hod I, Moghadam PZ, Avestro A-J, Horwitz NE, et al. Electrochemically addressable trisradical rotaxanes organized within a metal–organic framework. Proc Natl Acad Sci USA. 2015;112(36):11161-8.
71. Loeb SJ. Metal-organic rotaxane frameworks; MORFs. Chem Commun. 2005(12):1511-8.
72. Hoffart DJ, Loeb SJ. Metal–Organic Rotaxane Frameworks: Three-Dimensional Polyrotaxanes from Lanthanide-Ion Nodes, Pyridinium N-Oxide Axles, and Crown-Ether Wheels. Angew Chem. 2005;117(6):923-6.
73. Li L, Tang S, Wang C, Lv X, Jiang M, Wu H, et al. High gas storage capacities and stepwise adsorption in a UiO type metal-organic framework incorporating Lewis basic bipyridyl sites. Chem Commun. 2014;50(18):2304-7.

74. Ackley MW, Rege SU, Saxena H. Application of natural zeolites in the purification and separation of gases. Microporous and Mesoporous Materials. 2003;61(1):25-42.
75. Czaja AU, Trukhan N, Muller U. Industrial applications of metal-organic frameworks. Chem Soc Rev. 2009;38(5):1284-93.
76. Kootteri PT, Ho HD, Paik SM. High Gas Sorption and Metal-Ion Exchange of Microporous Metal–Organic Frameworks with Incorporated Imide Groups. Chem Eur J. 2010;16(47):14043-50.
77. Calleja G, Botas JA, Sánchez-Sánchez M, Orcajo MG. Hydrogen adsorption over Zeolite-like MOF materials modified by ion exchange. Int J Hydrogen Energy. 2010;35(18):9916-23.
78. Desai AV, Roy A, Samanta P, Manna B, Ghosh SK. Base-Resistant Ionic Metal-Organic Framework as a Porous Ion-Exchange Sorbent. iScience. 2018;3:21-30.
79. Kusakabe K, Kuroda T, Morooka S. Separation of carbon dioxide from nitrogen using ion-exchanged faujasite-type zeolite membranes formed on porous support tubes. Journal of Membrane Science. 1998;148(1):13-23.
80. Zhan Y, Shen L, Xu C, Zhao W, Cao Y, Jiang L. MOF-derived porous Fe2O3 with controllable shapes and improved catalytic activities in H2S selective oxidation. CrystEngComm. 2018;20(25):3449-54.
81. Lee J, Farha OK, Roberts J, Scheidt KA, Nguyen ST, Hupp JT. Metal-organic framework materials as catalysts. Chem Soc Rev. 2009;38(5):1450-9.
82. Majewski MB, Howarth AJ, Li P, Wasielewski MR, Hupp JT, Farha OK. Enzyme encapsulation in metal-organic frameworks for applications in catalysis. CrystEngComm. 2017;19(29):4082-91.
83. Parlett CMA, Wilson K, Lee AF. Hierarchical porous materials: catalytic applications. Chem Soc Rev. 2013;42(9):3876-93.
84. Barea E, Montoro C, Navarro JAR. Toxic gas removal - metal-organic frameworks for the capture and degradation of toxic gases and vapours. Chem Soc Rev. 2014;43(16):5419-30.
85. Bobbitt NS, Mendonca ML, Howarth AJ, Islamoglu T, Hupp JT, Farha OK, et al. Metal-organic frameworks for the removal of toxic industrial chemicals and chemical warfare agents. Chem Soc Rev. 2017;46(11):3357-85.
86. Grant Glover T, Peterson GW, Schindler BJ, Britt D, Yaghi O. MOF-74 building unit has a direct impact on toxic gas adsorption. Chem Eng Sci. 2011;66(2):163-70.
87. Ruyra À, Yazdi A, Espín J, Carné-Sánchez A, Roher N, Lorenzo J, et al. Synthesis, Culture Medium Stability, and In Vitro and In Vivo Zebrafish Embryo Toxicity of Metal–Organic Framework Nanoparticles. Chem Eur J. 2015;21(6):2508-18.
88. Kurniawan TA, Chan GYS, Lo W-h, Babel S. Comparisons of low-cost adsorbents for treating wastewaters laden with heavy metals. Sci Total Environ. 2006;366(2):409-26.
89. McCusker L, Liebau F, Engelhardt G. Nomenclature of structural and compositional characteristics of ordered microporous and mesoporous materials with inorganic hosts (IUPAC Recommendations 2001). Pure Appl Chem. 2001;73(2):381-94.
90. Davis ME, Lobo RF. Zeolite and molecular sieve synthesis. Chem Mater. 1992;4(4):756-68.
91. Breck DW. Zeolite molecular sieves: structure, chemistry and use: Krieger; 1984.
92. Mohan D, Pittman CU. Activated carbons and low cost adsorbents for remediation of tri- and hexavalent chromium from water. J Hazard Mater. 2006;137(2):762-811.
93. Horcajada P, Gref R, Baati T, Allan PK, Maurin G, Couvreur P, et al. Metal–Organic Frameworks in Biomedicine. Chem Rev. 2012;112(2):1232-68.

94. Li H, Eddaoudi M, O'Keeffe M, Yaghi OM. Design and synthesis of an exceptionally stable and highly porous metal-organic framework. Nature. 1999;402:276.
95. Frost H, Düren T, Snurr RQ. Effects of Surface Area, Free Volume, and Heat of Adsorption on Hydrogen Uptake in Metal−Organic Frameworks. J Phys Chem B. 2006;110(19):9565-70.
96. Farha OK, Eryazici I, Jeong NC, Hauser BG, Wilmer CE, Sarjeant AA, et al. Metal–Organic Framework Materials with Ultrahigh Surface Areas: Is the Sky the Limit? J Am Chem Soc. 2012;134(36):15016-21.
97. Park KS, Ni Z, Côté AP, Choi JY, Huang R, Uribe-Romo FJ, et al. Exceptional chemical and thermal stability of zeolitic imidazolate frameworks. Proc Natl Acad Sci USA. 2006;103(27):10186-91.
98. Phan A, Doonan CJ, Uribe-Romo FJ, Knobler CB, O'Keeffe M, Yaghi OM. Synthesis, Structure, and Carbon Dioxide Capture Properties of Zeolitic Imidazolate Frameworks. Acc Chem Res. 2010;43(1):58-67.
99. Shekhah O, Liu J, Fischer RA, Woll C. MOF thin films: existing and future applications. Chem Soc Rev. 2011;40(2):1081-106.
100. Pan Y, Lai Z. Sharp separation of C2/C3 hydrocarbon mixtures by zeolitic imidazolate framework-8 (ZIF-8) membranes synthesized in aqueous solutions. Chem Commun. 2011;47(37):10275-7.
101. Garcia-Garcia P, Muller M, Corma A. MOF catalysis in relation to their homogeneous counterparts and conventional solid catalysts. Chem Sci. 2014;5(8):2979-3007.
102. Aisheng H, Jürgen C. Covalent Post-Functionalization of Zeolitic Imidazolate Framework ZIF-90 Membrane for Enhanced Hydrogen Selectivity. Angew Chem Int Ed. 2011;50(21):4979-82.
103. Kitagawa S, Kitaura R, Noro S-i. Functional Porous Coordination Polymers. Angew Chem Int Ed. 2004;43(18):2334-75.
104. Coti KK, Belowich ME, Liong M, Ambrogio MW, Lau YA, Khatib HA, et al. Mechanised nanoparticles for drug delivery. Nanoscale. 2009;1(1):16-39.
105. Fairen-Jimenez D, Moggach SA, Wharmby MT, Wright PA, Parsons S, Düren T. Opening the Gate: Framework Flexibility in ZIF-8 Explored by Experiments and Simulations. J Am Chem Soc. 2011;133(23):8900-2.
106. Seo J, Matsuda R, Sakamoto H, Bonneau C, Kitagawa S. A Pillared-Layer Coordination Polymer with a Rotatable Pillar Acting as a Molecular Gate for Guest Molecules. J Am Chem Soc. 2009;131(35):12792-800.
107. Tanaka D, Nakagawa K, Higuchi M, Horike S, Kubota Y, Kobayashi TC, et al. Kinetic Gate-Opening Process in a Flexible Porous Coordination Polymer. Angew Chem. 2008;120(21):3978-82.
108. Song Q, Nataraj SK, Roussenova MV, Tan JC, Hughes DJ, Li W, et al. Zeolitic imidazolate framework (ZIF-8) based polymer nanocomposite membranes for gas separation. Energy & Environmental Science. 2012;5(8):8359-69.
109. Wu X, Bao Z, Yuan B, Wang J, Sun Y, Luo H, et al. Microwave synthesis and characterization of MOF-74 (M = Ni, Mg) for gas separation. Microporous and Mesoporous Materials. 2013;180:114-22.
110. Wen L, Zhao J, Lv K, Wu Y, Deng K, Leng X, et al. Visible-Light-Driven Photocatalysts of Metal–Organic Frameworks Derived from Multi-Carboxylic Acid and Imidazole-Based Spacer. Cryst Growth Des. 2012;12(3):1603-12.
111. Walton IM, Cox JM, Coppin JA, Linderman CM, Patel DG, Benedict JB. Photo-responsive MOFs: light-induced switching of porous single crystals containing a photochromic diarylethene. Chem Commun. 2013;49(73):8012-4.

112. Mukhopadhyay RD, Praveen VK, Ajayaghosh A. Photoresponsive metal–organic materials: exploiting the azobenzene switch. Materials Horizons. 2014;1(6):572-6.
113. Brown JW, Henderson BL, Kiesz MD, Whalley AC, Morris W, Grunder S, et al. Photophysical pore control in an azobenzene-containing metal–organic framework. Chem Sci. 2013;4(7):2858-64.
114. Knebel A, Geppert B, Volgmann K, Kolokolov DI, Stepanov AG, Twiefel J, et al. Defibrillation of soft porous metal-organic frameworks with electric fields. Science. 2017;358(6361):347-51.
115. Dhara B, Nagarkar SS, Kumar J, Kumar V, Jha PK, Ghosh SK, et al. Increase in Electrical Conductivity of MOF to Billion-Fold upon Filling the Nanochannels with Conducting Polymer. J Phys Chem Lett. 2016;7(15):2945-50.
116. Chen L, Mowat JPS, Fairen-Jimenez D, Morrison CA, Thompson SP, Wright PA, et al. Elucidating the Breathing of the Metal–Organic Framework MIL-53(Sc) with ab Initio Molecular Dynamics Simulations and in Situ X-ray Powder Diffraction Experiments. J Am Chem Soc. 2013;135(42):15763-73.
117. Ghoufi A, Benhamed K, Boukli-Hacene L, Maurin G. Electrically Induced Breathing of the MIL-53(Cr) Metal–Organic Framework. ACS Central Science. 2017;3(5):394-8.
118. Ryder MR, Civalleri B, Bennett TD, Henke S, Rudić S, Cinque G, et al. Identifying the Role of Terahertz Vibrations in Metal-Organic Frameworks: From Gate-Opening Phenomenon to Shear-Driven Structural Destabilization. Phys Rev Lett. 2014;113(21):215502.
119. Johan vdB, Canan G, A. PE, M. HEJ, Jorge G, Freek K. Understanding the Anomalous Alkane Selectivity of ZIF-7 in the Separation of Light Alkane/Alkene Mixtures. Chem Eur J. 2011;17(32):8832-40.
120. Krokidas P, Castier M, Economou IG. Computational Study of ZIF-8 and ZIF-67 Performance for Separation of Gas Mixtures. J Phys Chem C. 2017;121(33):17999-8011.
121. Krokidas P, Castier M, Moncho S, Sredojevic DN, Brothers EN, Kwon HT, et al. ZIF-67 Framework: A Promising New Candidate for Propylene/Propane Separation. Experimental Data and Molecular Simulations. J Phys Chem C. 2016;120(15):8116-24.
122. Ortiz AU, Freitas AP, Boutin A, Fuchs AH, Coudert F-X. What makes zeolitic imidazolate frameworks hydrophobic or hydrophilic? The impact of geometry and functionalization on water adsorption. Phys Chem Chem Phys. 2014;16(21):9940-9.
123. Aguado S, Bergeret G, Titus MP, Moizan V, Nieto-Draghi C, Bats N, et al. Guest-induced gate-opening of a zeolite imidazolate framework. New J Chem. 2011;35(3):546-50.
124. Nijem N, Wu H, Canepa P, Marti A, Balkus KJ, Thonhauser T, et al. Tuning the Gate Opening Pressure of Metal–Organic Frameworks (MOFs) for the Selective Separation of Hydrocarbons. J Am Chem Soc. 2012;134(37):15201-4.
125. A. MS, D. BT, K. CA. The Effect of Pressure on ZIF-8: Increasing Pore Size with Pressure and the Formation of a High-Pressure Phase at 1.47 GPa. Angew Chem Int Ed. 2009;48(38):7087-9.
126. Yanai N, Uemura T, Inoue M, Matsuda R, Fukushima T, Tsujimoto M, et al. Guest-to-Host Transmission of Structural Changes for Stimuli-Responsive Adsorption Property. J Am Chem Soc. 2012;134(10):4501-4.
127. Fabrice S, Aziz G, Guillaume M, G. BR, Caroline M-D, Gérard F. Molecular Dynamics Simulations of Breathing MOFs: Structural Transformations of MIL-53(Cr) upon Thermal Activation and CO2 Adsorption. Angew Chem Int Ed. 2008;47(44):8487-91.

128. Liu D, Yan L, Li L, Gu X, Dai P, Yang L, et al. Impact of moderative ligand hydrolysis on morphology evolution and the morphology-dependent breathing effect performance of MIL-53(Al). CrystEngComm. 2018;20(15):2102-11.
129. Shi Y-X, Li W-X, Zhang W-H, Lang J-P. Guest-Induced Switchable Breathing Behavior in a Flexible Metal–Organic Framework with Pronounced Negative Gas Pressure. Inorg Chem. 2018.
130. Horcajada P, Salles F, Wuttke S, Devic T, Heurtaux D, Maurin G, et al. How Linker's Modification Controls Swelling Properties of Highly Flexible Iron(III) Dicarboxylates MIL-88. J Am Chem Soc. 2011;133(44):17839-47.
131. Heinen J, Dubbeldam D. On flexible force fields for metal–organic frameworks: Recent developments and future prospects. Wiley Interdisciplinary Reviews: Computational Molecular Science. 2018;8(4):e1363.
132. Ma B-Q, Mulfort KL, Hupp JT. Microporous Pillared Paddle-Wheel Frameworks Based on Mixed-Ligand Coordination of Zinc Ions. Inorg Chem. 2005;44(14):4912-4.
133. Köberl M, Cokoja M, Herrmann WA, Kühn FE. From molecules to materials: Molecular paddle-wheel synthons of macromolecules, cage compounds and metal–organic frameworks. Dalton Transactions. 2011;40(26):6834-59.
134. Seo J, Bonneau C, Matsuda R, Takata M, Kitagawa S. Soft Secondary Building Unit: Dynamic Bond Rearrangement on Multinuclear Core of Porous Coordination Polymers in Gas Media. J Am Chem Soc. 2011;133(23):9005-13.
135. Zheng B, Pan Y, Lai Z, Huang K-W. Molecular Dynamics Simulations on Gate Opening in ZIF-8: Identification of Factors for Ethane and Propane Separation. Langmuir. 2013;29(28):8865-72.
136. Tian T, Zeng Z, Vulpe D, Casco ME, Divitini G, Midgley PA, et al. A sol–gel monolithic metal–organic framework with enhanced methane uptake. Nature Materials. 2017;17:174.
137. Liu J, Benin AI, Furtado AMB, Jakubczak P, Willis RR, LeVan MD. Stability Effects on CO2 Adsorption for the DOBDC Series of Metal–Organic Frameworks. Langmuir. 2011;27(18):11451-6.
138. Lyndon R, Konstas K, Thornton AW, Seeber AJ, Ladewig BP, Hill MR. Visible Light-Triggered Capture and Release of CO2 from Stable Metal Organic Frameworks. Chem Mater. 2015;27(23):7882-8.
139. Yu K, Kiesling K, Schmidt JR. Trace Flue Gas Contaminants Poison Coordinatively Unsaturated Metal–Organic Frameworks: Implications for CO2 Adsorption and Separation. J Phys Chem C. 2012;116(38):20480-8.
140. Kadhom M, Deng B. Metal-organic frameworks (MOFs) in water filtration membranes for desalination and other applications. Applied Materials Today. 2018;11:219-30.
141. Greenlee LF, Lawler DF, Freeman BD, Marrot B, Moulin P. Reverse osmosis desalination: Water sources, technology, and today's challenges. Water Res. 2009;43(9):2317-48.
142. Horinek D, Michl J. Surface-mounted altitudinal molecular rotors in alternating electric field: Single-molecule parametric oscillator molecular dynamics. Proc Natl Acad Sci USA. 2005;102(40):14175-80.
143. Rouquerol J, Rouquerol F, Llewellyn P, Maurin G, Sing KS. Adsorption by powders and porous solids: principles, methodology and applications: Academic press; 2013.
144. Wu H, Chua YS, Krungleviciute V, Tyagi M, Chen P, Yildirim T, et al. Unusual and highly tunable missing-linker defects in zirconium metal–organic framework UiO-66 and their important effects on gas adsorption. J Am Chem Soc. 2013;135(28):10525-32.

145. Petkov PS, Vayssilov GN, Liu J, Shekhah O, Wang Y, Wöll C, et al. Defects in MOFs: A Thorough Characterization. ChemPhysChem. 2012;13(8):2025-9.
146. Canivet J, Fateeva A, Guo Y, Coasne B, Farrusseng D. Water adsorption in MOFs: fundamentals and applications. Chem Soc Rev. 2014;43(16):5594-617.
147. Brenner H. Adsorption Calculations and Modelling: Elsevier; 2013.
148. Fang Z, Bueken B, Vos DED, Fischer RA. Defect-Engineered Metal–Organic Frameworks. Angew Chem Int Ed. 2015;54(25):7234-54.
149. Xydias P, Spanopoulos I, Klontzas E, Froudakis GE, Trikalitis PN. Drastic Enhancement of the CO2 Adsorption Properties in Sulfone-Functionalized Zr- and Hf-UiO-67 MOFs with Hierarchical Mesopores. Inorg Chem. 2014;53(2):679-81.
150. Fang Q-R, Makal T, D. Young M, Zhou H-C. Recent advances in the study of mesoporous metal-organic frameworks2010.
151. Brunauer S, Emmett PH, Teller E. Adsorption of Gases in Multimolecular Layers. J Am Chem Soc. 1938;60(2):309-19.
152. Yot PG, Ma Q, Haines J, Yang Q, Ghoufi A, Devic T, et al. Large breathing of the MOF MIL-47(VIV) under mechanical pressure: a joint experimental–modelling exploration. Chem Sci. 2012;3(4):1100-4.
153. Horike S, Shimomura S, Kitagawa S. Soft porous crystals. Nature Chemistry. 2009;1:695.
154. Thomas A. Functional Materials: From Hard to Soft Porous Frameworks. Angew Chem Int Ed. 2010;49(45):8328-44.
155. Neimark AV, Coudert F-X, Boutin A, Fuchs AH. Stress-Based Model for the Breathing of Metal−Organic Frameworks. J Phys Chem Lett. 2010;1(1):445-9.
156. Boutin A, Coudert F-X, Springuel-Huet M-A, Neimark AV, Férey G, Fuchs AH. The Behavior of Flexible MIL-53(Al) upon CH4 and CO2 Adsorption. J Phys Chem C. 2010;114(50):22237-44.
157. Llewellyn PL, Horcajada P, Maurin G, Devic T, Rosenbach N, Bourrelly S, et al. Complex Adsorption of Short Linear Alkanes in the Flexible Metal-Organic-Framework MIL-53(Fe). J Am Chem Soc. 2009;131(36):13002-8.
158. Férey G, Latroche M, Serre C, Millange F, Loiseau T, Percheron-Guégan A. Hydrogen adsorption in the nanoporous metal-benzenedicarboxylate M(OH)(O2C–C6H4–CO2) (M = Al3+, Cr3+), MIL-53. Chem Commun. 2003(24):2976-7.
159. Neimark AV, Coudert F-X, Triguero C, Boutin A, Fuchs AH, Beurroies I, et al. Structural Transitions in MIL-53 (Cr): View from Outside and Inside. Langmuir. 2011;27(8):4734-41.
160. Llewellyn PL, Bourrelly S, Serre C, Filinchuk Y, Férey G. How Hydration Drastically Improves Adsorption Selectivity for CO2 over CH4 in the Flexible Chromium Terephthalate MIL-53. Angew Chem Int Ed. 2006;45(46):7751-4.
161. Bousquet D, Coudert F-X, Boutin A. Free energy landscapes for the thermodynamic understanding of adsorption-induced deformations and structural transitions in porous materials. J Chem Phys. 2012;137(4):044118.
162. Munusamy K, Sethia G, Patil DV, Somayajulu Rallapalli PB, Somani RS, Bajaj HC. Sorption of carbon dioxide, methane, nitrogen and carbon monoxide on MIL-101(Cr): Volumetric measurements and dynamic adsorption studies. Chem Eng J. 2012;195-196:359-68.
163. Alhamami M, Doan H, Cheng C-H. A Review on Breathing Behaviors of Metal-Organic-Frameworks (MOFs) for Gas Adsorption. Materials. 2014;7(4):3198.
164. Férey G, Serre C. Large breathing effects in three-dimensional porous hybrid matter: facts, analyses, rules and consequences. Chem Soc Rev. 2009;38(5):1380-99.

165. Pan Y, Liu Y, Zeng G, Zhao L, Lai Z. Rapid synthesis of zeolitic imidazolate framework-8 (ZIF-8) nanocrystals in an aqueous system. Chem Commun. 2011;47(7):2071-3.
166. Zhang L, Hu Z, Jiang J. Sorption-Induced Structural Transition of Zeolitic Imidazolate Framework-8: A Hybrid Molecular Simulation Study. J Am Chem Soc. 2013;135(9):3722-8.
167. Coudert F-X, Jeffroy M, Fuchs AH, Boutin A, Mellot-Draznieks C. Thermodynamics of Guest-Induced Structural Transitions in Hybrid Organic−Inorganic Frameworks. J Am Chem Soc. 2008;130(43):14294-302.
168. Zang J, Nair S, Sholl DS. Osmotic ensemble methods for predicting adsorption-induced structural transitions in nanoporous materials using molecular simulations. J Chem Phys. 2011;134(18):184103.
169. Dunne LJ, Manos G. Exact matrix treatment of an osmotic ensemble model of adsorption and pressure induced structural transitions in metal organic frameworks. Dalton Transactions. 2016;45(10):4213-7.
170. Dunne LJ, Manos G. Statistical mechanics of binary mixture adsorption in metal organic frameworks in the osmotic ensemble. Philosophical Transactions of the Royal Society A: Mathematical, Physical and Engineering Sciences. 2018;376(2115):20170151.
171. Posch HA, Hoover WG, Vesely FJ. Canonical dynamics of the Nose oscillator: Stability, order, and chaos. Physical Review A. 1986;33(6):4253-65.
172. Berendsen HJC, Postma JPM, van Gunsteren WF, DiNola A, Haak JR. Molecular dynamics with coupling to an external bath. J Chem Phys. 1984;81(8):3684-90.
173. Tanaka H, Nakanishi K, Watanabe N. Constant temperature molecular dynamics calculation on Lennard-Jones fluid and its application to watera). J Chem Phys. 1983;78(5):2626-34.
174. Parrinello M, Rahman A. Crystal Structure and Pair Potentials: A Molecular-Dynamics Study. Phys Rev Lett. 1980;45(14):1196-9.
175. Parrinello M, Rahman A. Polymorphic transitions in single crystals: A new molecular dynamics method. J Appl Phys. 1981;52(12):7182-90.
176. Casewit CJ, Colwell KS, Rappe AK. Application of a universal force field to organic molecules. J Am Chem Soc. 1992;114(25):10035-46.
177. Wang J, Wolf RM, Caldwell JW, Kollman PA, Case DA. Development and testing of a general amber force field. J Comput Chem. 2004;25(9):1157-74.
178. Mayo SL, Olafson BD, Goddard WA. DREIDING: a generic force field for molecular simulations. The Journal of Physical Chemistry. 1990;94(26):8897-909.
179. Vanommeslaeghe K, Hatcher E, Acharya C, Kundu S, Zhong S, Shim J, et al. CHARMM general force field: A force field for drug-like molecules compatible with the CHARMM all-atom additive biological force fields. J Comput Chem. 2010;31(4):671-90.
180. Coupry DE, Addicoat MA, Heine T. Extension of the Universal Force Field for Metal–Organic Frameworks. J Chem Theory Comput. 2016;12(10):5215-25.
181. Bristow JK, Tiana D, Walsh A. Transferable Force Field for Metal–Organic Frameworks from First-Principles: BTW-FF. J Chem Theory Comput. 2014;10(10):4644-52.
182. Tafipolsky M, Schmid R. Systematic First Principles Parameterization of Force Fields for Metal−Organic Frameworks using a Genetic Algorithm Approach. J Phys Chem B. 2009;113(5):1341-52.
183. Perdew JP, Burke K, Ernzerhof M. Generalized Gradient Approximation Made Simple. Phys Rev Lett. 1996;77(18):3865-8.
184. Browne WR, Feringa BL. Making molecular machines work. Nat Nano. 2006;1(1):25-35.

185. Cao J, Fyfe MCT, Stoddart JF, Cousins GRL, Glink PT. Molecular Shuttles by the Protecting Group Approach. J Org Chem. 2000;65(7):1937-46.
186. Conyard J, Addison K, Heisler IA, Cnossen A, Browne WR, Feringa BL, et al. Ultrafast dynamics in the power stroke of a molecular rotary motor. Nat Chem. 2012;4(7):547-51.
187. Muramatsu S, Kinbara K, Taguchi H, Ishii N, Aida T. Semibiological Molecular Machine with an Implemented “AND” Logic Gate for Regulation of Protein Folding. J Am Chem Soc. 2006;128(11):3764-9.
188. Badjić JD, Balzani V, Credi A, Silvi S, Stoddart JF. A Molecular Elevator. Science. 2004;303(5665):1845.
189. Badjic JD, Ronconi CM, Stoddart JF, Balzani V, Silvi S, Credi A. Operating Molecular Elevators. J Am Chem Soc. 2006;128(5):1489-99.
190. Erbas-Cakmak S, Leigh DA, McTernan CT, Nussbaumer AL. Artificial Molecular Machines. Chem Rev. 2015;115(18):10081-206.
191. Kay ER, Leigh DA, Zerbetto F. Synthetic Molecular Motors and Mechanical Machines. Angew Chem Int Ed. 2007;46(1-2):72-191.
192. Bedard TC, Moore JS. Design and synthesis of molecular turnstiles. J Am Chem Soc. 1995;117(43):10662-71.
193. Zheng X, Mulcahy ME, Horinek D, Galeotti F, Magnera TF, Michl J. Dipolar and Nonpolar Altitudinal Molecular Rotors Mounted on an Au(111) Surface. J Am Chem Soc. 2004;126(14):4540-2.
194. Hsu L-Y, Li EY, Rabitz H. Single-Molecule Electric Revolving Door. Nano Lett. 2013;13(11):5020-5.
195. Li H, Eddaoudi M, O'Keeffe M, Yaghi OM. Design and synthesis of an exceptionally stable and highly porous metal-organic framework. Nature. 1999;402(6759):276-9.
196. Zhou H-C, Kitagawa S. Metal-Organic Frameworks (MOFs). Chem Soc Rev. 2014;43:5415 - 8.
197. Long JR, Yaghi OM. The pervasive chemistry of metal-organic frameworks. Chem Soc Rev. 2009;38(5):1213-4.
198. Wang Z, Cohen SM. Postsynthetic modification of metal-organic frameworks. Chem Soc Rev. 2009;38(5):1315-29.
199. Deng H, Grunder S, Cordova KE, Valente C, Furukawa H, Hmadeh M, et al. Large-Pore Apertures in a Series of Metal-Organic Frameworks. Science. 2012;336(6084):1018-23.
200. Qiu S, Xue M, Zhu G. Metal-organic framework membranes: from synthesis to separation application. Chem Soc Rev. 2014;43(16):6116-40.
201. Zhuang J, Kuo C-H, Chou L-Y, Liu D-Y, Weerapana E, Tsung C-K. Optimized Metal–Organic-Framework Nanospheres for Drug Delivery: Evaluation of Small-Molecule Encapsulation. ACS Nano. 2014;8(3):2812-9.
202. Kundu T, Mitra S, Patra P, Goswami A, Díaz Díaz D, Banerjee R. Mechanical Downsizing of a Gadolinium(III)-based Metal–Organic Framework for Anticancer Drug Delivery. Chem Eur J. 2014;20(33):10514-8.
203. Ma D, Li B, Zhou X, Zhou Q, Liu K, Zeng G, et al. A dual functional MOF as a luminescent sensor for quantitatively detecting the concentration of nitrobenzene and temperature. Chem Commun. 2013;49(79):8964-6.
204. Dong M-J, Zhao M, Ou S, Zou C, Wu C-D. A Luminescent Dye@MOF Platform: Emission Fingerprint Relationships of Volatile Organic Molecules. Angew Chem Int Ed. 2014;53(6):1575-9.

205. Herbst A, Khutia A, Janiak C. Brønsted Instead of Lewis Acidity in Functionalized MIL-101Cr MOFs for Efficient Heterogeneous (nano-MOF) Catalysis in the Condensation Reaction of Aldehydes with Alcohols. Inorg Chem. 2014;53(14):7319-33.
206. Dhakshinamoorthy A, Garcia H. Metal-organic frameworks as solid catalysts for the synthesis of nitrogen-containing heterocycles. Chem Soc Rev. 2014;43(16):5750-65.
207. Wang Z, Cohen SM. Tandem Modification of Metal–Organic Frameworks by a Postsynthetic Approach. Angew Chem. 2008;120(25):4777-80.
208. Li B, Zhang Y, Ma D, Li L, Li G, Li G, et al. A strategy toward constructing a bifunctionalized MOF catalyst: post-synthetic modification of MOFs on organic ligands and coordinatively unsaturated metal sites. Chem Commun. 2012;48(49):6151-3.
209. McDonald TM, D'Alessandro DM, Krishna R, Long JR. Enhanced carbon dioxide capture upon incorporation of N,N[prime or minute]-dimethylethylenediamine in the metal-organic framework CuBTTri. Chem Sci. 2011;2(10):2022-8.
210. Yazaydın AÖ, Benin AI, Faheem SA, Jakubczak P, Low JJ, Willis RR, et al. Enhanced CO2 Adsorption in Metal-Organic Frameworks via Occupation of Open-Metal Sites by Coordinated Water Molecules. Chem Mater. 2009;21(8):1425-30.
211. Zheng S-T, Zhao X, Lau S, Fuhr A, Feng P, Bu X. Entrapment of Metal Clusters in Metal–Organic Framework Channels by Extended Hooks Anchored at Open Metal Sites. J Am Chem Soc. 2013;135(28):10270-3.
212. Fu Y-Y, Yang C-X, Yan X-P. Control of the Coordination Status of the Open Metal Sites in Metal–Organic Frameworks for High Performance Separation of Polar Compounds. Langmuir. 2012;28(17):6794-802.
213. Hwang YK, Hong D-Y, Chang J-S, Jhung SH, Seo Y-K, Kim J, et al. Amine Grafting on Coordinatively Unsaturated Metal Centers of MOFs: Consequences for Catalysis and Metal Encapsulation. Angew Chem Int Ed. 2008;47(22):4144-8.
214. Torrisi A, Bell RG, Mellot-Draznieks C. Functionalized MOFs for Enhanced CO2 Capture. Cryst Growth Des. 2010;10(7):2839-41.
215. Zlotea C, Phanon D, Mazaj M, Heurtaux D, Guillerm V, Serre C, et al. Effect of NH2 and CF3 functionalization on the hydrogen sorption properties of MOFs. Dalton Transactions. 2011;40(18):4879-81.
216. Bloch ED, Queen WL, Krishna R, Zadrozny JM, Brown CM, Long JR. Hydrocarbon Separations in a Metal-Organic Framework with Open Iron(II) Coordination Sites. Science. 2012;335(6076):1606-10.
217. Zhou W, Wu H, Yildirim T. Enhanced H2 Adsorption in Isostructural Metal−Organic Frameworks with Open Metal Sites: Strong Dependence of the Binding Strength on Metal Ions. J Am Chem Soc. 2008;130(46):15268-9.
218. Wu H, Zhou W, Yildirim T. High-Capacity Methane Storage in Metal−Organic Frameworks M2(dhtp): The Important Role of Open Metal Sites. J Am Chem Soc. 2009;131(13):4995-5000.
219. Pham T, Forrest KA, Eckert J, Space B. Dramatic Effect of the Electrostatic Parameters on H2 Sorption in an M-MOF-74 Analogue. Cryst Growth Des. 2016;16(2):867-74.
220. Pham T, Forrest KA, McLaughlin K, Eckert J, Space B. Capturing the H2–Metal Interaction in Mg-MOF-74 Using Classical Polarization. J Phys Chem C. 2014;118(39):22683-90.
221. Dzubak AL, Lin L-C, Kim J, Swisher JA, Poloni R, Maximoff SN, et al. Ab initio carbon capture in open-site metal–organic frameworks. Nat Chem. 2012;4(10):810-6.
222. Verma P, Xu X, Truhlar DG. Adsorption on Fe-MOF-74 for C1–C3 Hydrocarbon Separation. J Phys Chem C. 2013;117(24):12648-60.
223. Chavan SM, Shearer GC, Bloch E, Bordiga S. Acetylene Adsorption on CPO-27-M Metal–Organic Frameworks (M=Fe, Co and Ni). ChemPhysChem. 2012;13(2):445-8.

224. Moss GP. Nomenclature of fused and bridged fused ring systems (IUPAC Recommendations 1998). Pure Appl Chem1998. p. 143.
225. Rosi NL, Kim J, Eddaoudi M, Chen B, O'Keeffe M, Yaghi OM. Rod Packings and Metal−Organic Frameworks Constructed from Rod-Shaped Secondary Building Units. J Am Chem Soc. 2005;127(5):1504-18.
226. Silva P, Vilela SMF, Tome JPC, Almeida Paz FA. Multifunctional metal-organic frameworks: from academia to industrial applications. Chem Soc Rev. 2015;44(19):6774-803.
227. Bae Y-S, Lee CY, Kim KC, Farha OK, Nickias P, Hupp JT, et al. High Propene/Propane Selectivity in Isostructural Metal–Organic Frameworks with High Densities of Open Metal Sites. Angew Chem Int Ed. 2012;51(8):1857-60.
228. Britt D, Tranchemontagne D, Yaghi OM. Metal-organic frameworks with high capacity and selectivity for harmful gases. Proc Natl Acad Sci USA. 2008;105(33):11623-7.
229. Li L, Lin R-B, Krishna R, Wang X, Li B, Wu H, et al. Efficient separation of ethylene from acetylene/ethylene mixtures by a flexible-robust metal-organic framework. J Mater Chem A. 2017.
230. Oh H, Maurer S, Balderas-Xicohtencatl R, Arnold L, Magdysyuk OV, Schütz G, et al. Efficient synthesis for large-scale production and characterization for hydrogen storage of ligand exchanged MOF-74/174/184-M (M=Mg2+, Ni2+). Int J Hydrogen Energy. 2017;42(2):1027-35.
231. Liu J, Thallapally PK, McGrail BP, Brown DR, Liu J. Progress in adsorption-based CO2 capture by metal-organic frameworks. Chem Soc Rev. 2012;41(6):2308-22.
232. Tan K, Zuluaga S, Gong Q, Canepa P, Wang H, Li J, et al. Water Reaction Mechanism in Metal Organic Frameworks with Coordinatively Unsaturated Metal Ions: MOF-74. Chem Mater. 2014;26(23):6886-95.
233. Botas JA, Calleja G, Sánchez-Sánchez M, Orcajo MG. Effect of Zn/Co ratio in MOF-74 type materials containing exposed metal sites on their hydrogen adsorption behaviour and on their band gap energy. Int J Hydrogen Energy. 2011;36(17):10834-44.
234. Zhuang J, Young AP, Tsung C-K. Integration of Biomolecules with Metal–Organic Frameworks. Small. 2017;13(32):1700880-n/a.
235. Bae Y-S, Snurr RQ. Development and Evaluation of Porous Materials for Carbon Dioxide Separation and Capture. Angew Chem Int Ed. 2011;50(49):11586-96.
236. Yang D-A, Cho H-Y, Kim J, Yang S-T, Ahn W-S. CO2 capture and conversion using Mg-MOF-74 prepared by a sonochemical method. Energy & Environmental Science. 2012;5(4):6465-73.
237. Simmons JM, Wu H, Zhou W, Yildirim T. Carbon capture in metal-organic frameworks-a comparative study. Energy & Environmental Science. 2011;4(6):2177-85.
238. Park J, Kim H, Han SS, Jung Y. Tuning Metal–Organic Frameworks with Open-Metal Sites and Its Origin for Enhancing CO2 Affinity by Metal Substitution. J Phys Chem Lett. 2012;3(7):826-9.
239. DeCoste JB, Peterson GW, Schindler BJ, Killops KL, Browe MA, Mahle JJ. The effect of water adsorption on the structure of the carboxylate containing metal-organic frameworks Cu-BTC, Mg-MOF-74, and UiO-66. J Mater Chem A. 2013;1(38):11922-32.
240. Valenzano L, Civalleri B, Chavan S, Palomino GT, Areán CO, Bordiga S. Computational and Experimental Studies on the Adsorption of CO, N2, and CO2 on Mg-MOF-74. J Phys Chem C. 2010;114(25):11185-91.
241. Yu J, Balbuena PB. Water Effects on Postcombustion CO2 Capture in Mg-MOF-74. J Phys Chem C. 2013;117(7):3383-8.

242. Cornell WD, Cieplak P, Bayly CI, Gould IR, Merz KM, Ferguson DM, et al. A Second Generation Force Field for the Simulation of Proteins, Nucleic Acids, and Organic Molecules. J Am Chem Soc. 1995;117(19):5179-97.
243. Klok M, Boyle N, Pryce MT, Meetsma A, Browne WR, Feringa BL. MHz unidirectional rotation of molecular rotary motors. J Am Chem Soc. 2008;130(32):10484-5.
244. Feringa BL. In control of motion: from molecular switches to molecular motors. Acc Chem Res. 2001;34(6):504-13.
245. Faucheux LP, Bourdieu L, Kaplan P, Libchaber AJ. Optical thermal ratchet. Phys Rev Lett. 1995;74(9):1504.
246. Astumian RD. Thermodynamics and kinetics of a Brownian motor. science. 1997;276(5314):917-22.
247. Kelly TR, De Silva H, Silva RA. Unidirectional rotary motion in a molecular system. Nature. 1999;401(6749):150.
248. Coulston RJ, Onagi H, Lincoln SF, Easton CJ. Harnessing the energy of molecular recognition in a nanomachine having a photochemical on/off switch. J Am Chem Soc. 2006;128(46):14750-1.
249. Wang B, Vuković L, Král P. Nanoscale rotary motors driven by electron tunneling. Phys Rev Lett. 2008;101(18):186808.
250. Porto M. Molecular motor based entirely on the Coulomb interaction. Physical Review E. 2001;63(3):030102.
251. Li J, Wang X, Zhao L, Gao X, Zhao Y, Zhou R. Rotation Motion of Designed Nano-Turbine. Scientific Reports. 2014;4:5846.
252. Soong RK, Bachand GD, Neves HP, Olkhovets AG, Craighead HG, Montemagno CD. Powering an Inorganic Nanodevice with a Biomolecular Motor. Science. 2000;290(5496):1555-8.
253. Walker JE. ATP synthesis by rotary catalysis. Chemistry, 1996-2000. 2003:146.
254. Astumian RD, Bier M. Mechanochemical coupling of the motion of molecular motors to ATP hydrolysis. Biophysical journal. 1996;70(2):637-53.
255. Zhou H-X. Chemically driven motility of Brownian particles. Phys Rev Lett. 1996;77(1):194.
256. Tsong TY. Na,K-ATPase as A Brownian Motor: Electric Field-InducedConformational Fluctuation Leads to Uphill Pumping of Cation inthe Absence of ATP. Journal of Biological Physics. 2002;28(2):309-25.
257. Magnasco MO. Forced thermal ratchets. Phys Rev Lett. 1993;71(10):1477.
258. Alemani M, Peters MV, Hecht S, Rieder K-H, Moresco F, Grill L. Electric field-induced isomerization of azobenzene by STM. J Am Chem Soc. 2006;128(45):14446-7.
259. Astumian RD, Bier M. Fluctuation driven ratchets: molecular motors. Phys Rev Lett. 1994;72(11):1766.
260. Kelly TR. Progress toward a rationally designed molecular motor. Acc Chem Res. 2001;34(6):514-22.
261. Malanoski AP, Johnson BJ, Erickson JS, Sun CK, Scoggins CS, Nasir M, et al. Nanoparticle-Surface Interactions in Geometrical Separation Devices. Chromatography. 2015;2(3):567-79.
262. Padgett M, Di Leonardo R. Holographic optical tweezers and their relevance to lab on chip devices. Lab on a Chip. 2011;11(7):1196-205.
263. Kelly TR, Tellitu I, Sestelo JP. Auf der Suche nach molekularen Sperrädern. Angew Chem. 1997;109(17):1969-72.
264. Fletcher SP, Dumur F, Pollard MM, Feringa BL. A reversible, unidirectional molecular rotary motor driven by chemical energy. Science. 2005;310(5745):80-2.

265. Greb L, Lehn J-M. Light-driven molecular motors: imines as four-step or two-step unidirectional rotors. J Am Chem Soc. 2014;136(38):13114-7.
266. Glass TE. Cooperative Chemical Sensing with Bis-tritylacetylenes: Pinwheel Receptors with Metal Ion Recognition Properties. J Am Chem Soc. 2000;122(18):4522-3.
267. Raker J, Glass TE. Selectivity via Cooperative Interactions: Detection of Dicarboxylates in Water by a Pinwheel Chemosensor. J Org Chem. 2002;67(17):6113-6.
268. Ichimura K, Oh S-K, Nakagawa M. Light-Driven Motion of Liquids on a Photoresponsive Surface. Science. 2000;288(5471):1624.
269. Lee E, Kim J, Heo J, Whang D, Kim K. A Two-Dimensional Polyrotaxane with Large Cavities and Channels: A Novel Approach to Metal–Organic Open-Frameworks by Using Supramolecular Building Blocks. Angew Chem Int Ed. 2001;40(2):399-402.
270. Zhu K, O'Keefe CA, Vukotic VN, Schurko RW, Loeb SJ. A molecular shuttle that operates inside a metal–organic framework. Nat Chem. 2015;7(6):514-9.
271. Panda T, Pachfule P, Chen Y, Jiang J, Banerjee R. Amino functionalized zeolitic tetrazolate framework (ZTF) with high capacity for storage of carbon dioxide. Chem Commun. 2011;47(7):2011-3.
272. Zhang Z, Zhao Y, Gong Q, Li Z, Li J. MOFs for CO2 capture and separation from flue gas mixtures: the effect of multifunctional sites on their adsorption capacity and selectivity. Chem Commun. 2013;49(7):653-61.
273. Mondloch JE, Bury W, Fairen-Jimenez D, Kwon S, DeMarco EJ, Weston MH, et al. Vapor-Phase Metalation by Atomic Layer Deposition in a Metal–Organic Framework. J Am Chem Soc. 2013;135(28):10294-7.
274. Deria P, Bury W, Hupp JT, Farha OK. Versatile functionalization of the NU-1000 platform by solvent-assisted ligand incorporation. Chem Commun. 2014;50(16):1965-8.
275. Queen WL, Hudson MR, Bloch ED, Mason JA, Gonzalez MI, Lee JS, et al. Comprehensive study of carbon dioxide adsorption in the metal-organic frameworks M2(dobdc) (M = Mg, Mn, Fe, Co, Ni, Cu, Zn). Chem Sci. 2014;5(12):4569-81.
276. Clark Stewart J, Segall Matthew D, Pickard Chris J, Hasnip Phil J, Probert Matt IJ, Refson K, et al. First principles methods using CASTEP. Zeitschrift für Kristallographie - Crystalline Materials2005. p. 567.
277. Tkatchenko A, Scheffler M. Accurate Molecular Van Der Waals Interactions from Ground-State Electron Density and Free-Atom Reference Data. Phys Rev Lett. 2009;102(7):073005.
278. Abraham MJ, Murtola T, Schulz R, Páll S, Smith JC, Hess B, et al. GROMACS: High performance molecular simulations through multi-level parallelism from laptops to supercomputers. SoftwareX. 2015;1–2:19-25.
279. Potoff JJ, Siepmann JI. Vapor–liquid equilibria of mixtures containing alkanes, carbon dioxide, and nitrogen. AlChE J. 2001;47(7):1676-82.
280. Campañá C, Mussard B, Woo TK. Electrostatic Potential Derived Atomic Charges for Periodic Systems Using a Modified Error Functional. J Chem Theory Comput. 2009;5(10):2866-78.
281. Swope WC, Andersen HC, Berens PH, Wilson KR. A computer simulation method for the calculation of equilibrium constants for the formation of physical clusters of molecules: Application to small water clusters. J Chem Phys. 1982;76(1):637-49.
282. Bradbury K. Energy storage technology review. Duke University. 2010:1-34.
283. Lewis NS. Toward Cost-Effective Solar Energy Use. Science. 2007;315(5813):798-801.
284. Ferey G. Hybrid porous solids: past, present, future. Chem Soc Rev. 2008;37(1):191-214.

285. Xiao-Chun H, Yan-Yong L, Jie-Peng Z, Xiao-Ming C. Ligand-Directed Strategy for Zeolite-Type Metal–Organic Frameworks: Zinc(II) Imidazolates with Unusual Zeolitic Topologies. Angew Chem Int Ed. 2006;45(10):1557-9.
286. Lewis DW, Ruiz-Salvador AR, Gomez A, Rodriguez-Albelo LM, Coudert F-X, Slater B, et al. Zeolitic imidazole frameworks: structural and energetics trends compared with their zeolite analogues. CrystEngComm. 2009;11(11):2272-6.
287. Küsgens P, Rose M, Senkovska I, Fröde H, Henschel A, Siegle S, et al. Characterization of metal-organic frameworks by water adsorption. Microporous and Mesoporous Materials. 2009;120(3):325-30.
288. Zielkiewicz J. Structural properties of water: Comparison of the SPC, SPCE, TIP4P, and TIP5P models of water. J Chem Phys. 2005;123(10):104501.
289. Horn HW, Swope WC, Pitera JW, Madura JD, Dick TJ, Hura GL, et al. Development of an improved four-site water model for biomolecular simulations: TIP4P-Ew. J Chem Phys. 2004;120(20):9665-78.
290. Abascal JLF, Vega C. A general purpose model for the condensed phases of water: TIP4P/2005. J Chem Phys. 2005;123(23):234505.
291. Paranthaman S, Coudert F-X, Fuchs AH. Water adsorption in hydrophobic MOF channels. Phys Chem Chem Phys. 2010;12(28):8124-30.
292. Peng X, Lin L-C, Sun W, Smit B. Water adsorption in metal–organic frameworks with open-metal sites. AlChE J. 2015;61(2):677-87.
293. Hertäg L, Bux H, Caro J, Chmelik C, Remsungnen T, Knauth M, et al. Diffusion of CH4 and H2 in ZIF-8. Journal of Membrane Science. 2011;377(1):36-41.
294. Krokidas P, Castier M, Moncho S, Brothers E, Economou IG. Molecular Simulation Studies of the Diffusion of Methane, Ethane, Propane, and Propylene in ZIF-8. J Phys Chem C. 2015;119(48):27028-37.
295. Zheng B, Sant M, Demontis P, Suffritti GB. Force Field for Molecular Dynamics Computations in Flexible ZIF-8 Framework. J Phys Chem C. 2012;116(1):933-8.
296. Wu X, Huang J, Cai W, Jaroniec M. Force field for ZIF-8 flexible frameworks: atomistic simulation of adsorption, diffusion of pure gases as CH4, H2, CO2 and N2. RSC Advances. 2014;4(32):16503-11.
297. Kusalik PG, Svishchev IM. The Spatial Structure in Liquid Water. Science. 1994;265(5176):1219-21.
298. Pantatosaki E, Pazzona FG, Megariotis G, Papadopoulos GK. Atomistic Simulation Studies on the Dynamics and Thermodynamics of Nonpolar Molecules within the Zeolite Imidazolate Framework-8. J Phys Chem B. 2010;114(7):2493-503.
299. Tanaka H, Ohsaki S, Hiraide S, Yamamoto D, Watanabe S, Miyahara MT. Adsorption-Induced Structural Transition of ZIF-8: A Combined Experimental and Simulation Study. J Phys Chem C. 2014;118(16):8445-54.
300. Dubbeldam D, Calero S, Ellis DE, Snurr RQ. RASPA: molecular simulation software for adsorption and diffusion in flexible nanoporous materials. Molecular Simulation. 2016;42(2):81-101.
301. Çağin T, Pettitt BM. Molecular dynamics with a variable number of molecules. Mol Phys. 1991;72(1):169-75.
302. Vega C, Abascal JLF. Simulating water with rigid non-polarizable models: a general perspective. Phys Chem Chem Phys. 2011;13(44):19663-88.
303. Ding L, Yazaydin AO. Hydrogen and methane storage in ultrahigh surface area Metal–Organic Frameworks. Microporous and Mesoporous Materials. 2013;182:185-90.
304. Zheng B, Zhu Y, Fu F, Wang LL, Wang J, Du H. Theoretical prediction of the mechanical properties of zeolitic imidazolate frameworks (ZIFs). RSC Advances. 2017;7(66):41499-503.

305. Chen L, Chen X, Liu H, Li Y. Encapsulation of Mono- or Bimetal Nanoparticles Inside Metal–Organic Frameworks via In situ Incorporation of Metal Precursors. Small. 2015;11(22):2642-8.
306. Teplensky MH, Fantham M, Li P, Wang TC, Mehta JP, Young LJ, et al. Temperature Treatment of Highly Porous Zirconium-Containing Metal–Organic Frameworks Extends Drug Delivery Release. J Am Chem Soc. 2017;139(22):7522-32.
307. Greathouse JA, Allendorf MD. The Interaction of Water with MOF-5 Simulated by Molecular Dynamics. J Am Chem Soc. 2006;128(33):10678-9.
308. Liu X, Demir NK, Wu Z, Li K. Highly Water-Stable Zirconium Metal–Organic Framework UiO-66 Membranes Supported on Alumina Hollow Fibers for Desalination. J Am Chem Soc. 2015;137(22):6999-7002.
309. Zhang R, Ji S, Wang N, Wang L, Zhang G, Li J-R. Coordination-Driven In Situ Self-Assembly Strategy for the Preparation of Metal–Organic Framework Hybrid Membranes. Angew Chem Int Ed. 2014;53(37):9775-9.
310. Ghosh P, Kim KC, Snurr RQ. Modeling Water and Ammonia Adsorption in Hydrophobic Metal–Organic Frameworks: Single Components and Mixtures. J Phys Chem C. 2014;118(2):1102-10.
311. Fine RA, Millero FJ. Compressibility of water as a function of temperature and pressure. J Chem Phys. 1973;59(10):5529-36.
312. Akhavan M, Schofield J, Jalili S. Water transport and desalination through double-layer graphyne membranes. Phys Chem Chem Phys. 2018;20(19):13607-15.
313. Wang L, Dumont RS, Dickson JM. Nonequilibrium molecular dynamics simulation of water transport through carbon nanotube membranes at low pressure. J Chem Phys. 2012;137(4):044102.
314. Gupta KM, Qiao Z, Zhang K, Jiang J. Seawater Pervaporation through Zeolitic Imidazolate Framework Membranes: Atomistic Simulation Study. ACS Applied Materials & Interfaces. 2016;8(21):13392-9.
315. Gupta KM, Zhang K, Jiang J. Water Desalination through Zeolitic Imidazolate Framework Membranes: Significant Role of Functional Groups. Langmuir. 2015;31(48):13230-7.
316. Heiranian M, Farimani AB, Aluru NR. Water desalination with a single-layer MoS2 nanopore. Nature Communications. 2015;6:8616.
317. Shen M, Keten S, Lueptow RM. Dynamics of water and solute transport in polymeric reverse osmosis membranes via molecular dynamics simulations. Journal of Membrane Science. 2016;506:95-108.
318. Ruiz L, Wu Y, Keten S. Tailoring the water structure and transport in nanotubes with tunable interiors. Nanoscale. 2015;7(1):121-32.
319. Semino R, Ramsahye NA, Ghoufi A, Maurin G. Microscopic Model of the Metal–Organic Framework/Polymer Interface: A First Step toward Understanding the Compatibility in Mixed Matrix Membranes. ACS Applied Materials & Interfaces. 2016;8(1):809-19.
320. Yeh I-C, Berkowitz ML. Ewald summation for systems with slab geometry. J Chem Phys. 1999;111(7):3155-62.
321. Vega C, Abascal JLF. Relation between the melting temperature and the temperature of maximum density for the most common models of water. J Chem Phys. 2005;123(14):144504.
322. Coudert F-X. Molecular Mechanism of Swing Effect in Zeolitic Imidazolate Framework ZIF-8: Continuous Deformation upon Adsorption. ChemPhysChem. 2017;18(19):2732-8.